NASA Contractor Report 172169

AN EVALUATION OF THE EFFECTS OF STACKING
SEQUENCE AND THICKNESS ON THE FATIGUE LIFE
OF QUASI-ISOTROPIC GRAPHITE/EPOXY LAMINATES

C. E. Harris and D. H. Morris

VIRGINIA POLYTECHNIC INSTITUTE AND STATE UNIVERSITY
Blacksburg, Virginia 24061

NF02526

NASA

National Aeronautics and
Space Administration

Langley Research Center
Hampton, Virginia 23665

FOREWORD

This work was supported by NASA Grant NAG1-264 from the Fatigue and Fracture Branch of NASA-Langley. Sincere appreciation is extended to E. P. Phillips of NASA-Langley for designing the compression test fixture and for his encouragement and helpful discussions.

The authors wish to thank Dr. C. T. Herakovich for providing discussion, consultation, and information concerning the computation and interpretation of interlaminar stresses.

The invaluable assistance and consultation provided by the following laboratory and shop personnel is gratefully acknowledged: Ken McCauley, Archie Montgomery, Bob Davis, and George Lough.

All Blank Pages

Intentionally Left Blank

To Keep Document Continuity

SUMMARY

A test program has been conducted in which the effect of specimen thickness on the fatigue lives of quasi-isotropic, graphite/epoxy laminates was investigated. Notched and unnotched geometries at 16, 32 and 64 ply thicknesses of a $[90/45/0/-45]_{ns}$ laminate and a $[45/0/-45/90]_{ns}$ laminate were tested in compression-compression fatigue. The fatigue life and the initiation, type and progression of damage was determined in each test. Specially designed antibuckling fixtures were utilized to prevent specimen out-of-plane motion. Interlaminar stresses were generated at straight, free edges of axially loaded laminates; these stresses were used to interpret the test results.

The fatigue lives of the notched specimens did not appear to be a strong function of laminate stacking sequence or specimen thickness. The stress concentration at the hole dominated over the interlaminar stresses at the straight free edge. The unnotched specimens of the $[90/45/0/-45]_{ns}$ laminate with tensile interlaminar normal stresses delaminated more readily than did the $[45/0/-45/90]_{ns}$ laminate with compressive interlaminar normal stress. The life of the 16 ply unnotched specimens was lower than was the life of the 32 and 64 ply specimens. Delaminations were located at the interface where the maximum τ_{xz} shear stress occurred regardless of the sense or magnitude of the interlaminar normal stress. Finally, the antibuckling fixture was found to be effective in preventing out-of-plane motion without overconstraining the specimen.

All Blank Pages

Intentionally Left Blank

To Keep Document Continuity

TABLE OF CONTENTS

All Blank Pages

Intentionally Left Blank

To Keep Document Continuity

LIST OF FIGURES

All Blank Pages

Intentionally Left Blank

To Keep Document Continuity

LIST OF TABLES

All Blank Pages

Intentionally Left Blank

To Keep Document Continuity

1.0 INTRODUCTION

The role of the interlaminar stresses at the free edges of laminated composites in the delamination of laminates has been previously explored by a number of investigations. In fatigue, macroscopic damage of certain laminate types begins with delaminations forming at the free edges. The magnitude of these interlaminar stresses have been shown to be a function of laminate thickness [1]. Furthermore, the boundary layer at the laminate edge over which these stresses exist have also been shown to be approximately equal to the laminate thicknesses [1]. It is therefore of interest to explore the role of laminate thickness on the fatigue life and mode of damage formation in composite laminates.

1.1 PROGRAM OBJECTIVES

The objectives of the fatigue program described herein are as follows:

1. Determine the fatigue life of notched and unnotched laminates as a function of laminate thickness.

2. Determine the location of the initiation of fatigue damage.

3. Determine the types of damage and the progression of damage throughout the fatigue life.

4. Compute the interlaminar stresses of the unnotched specimen geometry and utilize these stresses along with existing analyses, to interpret the fatigue results.

The method of accomplishing these objectives is briefly described in the following section.

1.2 PROGRAM DESCRIPTION (OVERVIEW)

Experimental data was obtained for compression-compression fatigue tests of notched and unnotched specimens of two laminate stacking sequences and three laminate thicknesses. Quasi-isotropic laminates were prepared of T300/5208 graphite-epoxy using $[90/45/0/-45]_{ns}$ and $[45/90/-45/0]_{ns}$ stacking sequences, where ns means multiple layers of the stacking sequence symmetric about the midplane. The two laminate types were selected because the $[90/45/0/-45]_{ns}$ laminate has high tensile interlaminar normal stresses under compressive loading and the other laminate has high compressive interlaminar normal stresses. Laminates were prepared with thicknesses of 16 plies, 32 plies, and 64 plies. The notched specimen had a 0.25 in. (6.35 mm) center circular hole. Three replicate tests were conducted at each test condition.

The fatigue tests were compression-compression fatigue at an R value of 10 and a frequency of 10 Hz. All specimens of a specific "laminate-specimen type" combination were tested at the same stress range. The stress ranges were determined from a series of preliminary tests. The fatigue specimens were loaded with direct compressive bearing loads on the specimen ends. The test fixture included anti-buckling guides to minimize out-of-plane motion.

Nondestructive examinations were performed in order to locate the initiation of damage and to monitor and record the progression and mode of damage. These examinations consisted of a combination of enhanced X-ray radiography, edge replication, and visual observations.

The final phase of the fatigue project was an analysis of the interlaminar stresses at the straight free edges of the subject laminates. The Pipes-Pagano approximation [1] was used to determine the interlaminar normal stress, σ_z. This analysis was supplemented by other analyses results in the literature [2] for the determination of the shear stress distributions.

2.0 DESCRIPTION OF TEST PROGRAM

This section provides a more detailed description of the test program to supplement the overview given in section 1.2.

2.1 DESCRIPTION OF SPECIMENS

Fatigue tests were conducted using two basic specimen types. The unnotched specimen was a straight coupon with a 1.0 in. (25.4 mm) width and 8.0 in. (203 mm) length (Figure 1a). Specimen thicknesses were 16 plies (typically 0.083", 2.11 mm), 32 plies (0.165 in., 4.19 mm) and 64 plies (0.333 in., 8.46 mm). The notched specimen, Figure 1b, was a straight coupon 2.0 in. (50.8 mm) wide and 8.0 in. (203 mm) in length with a 0.25 in. (6.35 mm) diameter center, circular hole. The thicknesses of the notched and unnotched specimens were the same.

All specimens of a specific thickness were cut from the same laminate. The $[90/45/0/-45]_{ns}$ specimens were cut at a 90° orientation to the 0° outer ply fiber direction. The $[45/0/-45/90]_{ns}$ specimens were cut at a 45° orientation to the 0° outer ply fiber direction (Figure 2).

2.2 DESCRIPTION OF NOTCHED SPECIMEN TEST FIXTURE

The notched specimens were loaded in direct compressive bearing on the specimen ends. Special flat plates with end supports constrained the specimen ends and contacted the flat surfaces of the test machine cross-heads (Figure 3). Further discussion is given in Section 3.0. Anti-buckling suppports prevented out-of-plane motion of the specimens by contact-supporting both faces of the specimen along the full length and width of the specimen with the exception of the "test section." Dry

lubrication was used to minimize friction between the specimen and the supports. A test fixture "test section" was formed by cutting 1 5/8 in. x 1 5/8 in. (41.3 mm x 41.3 mm) windows out of the buckling supports surrounding the central region of the specimen where the hole is located. The size of this window was optimized by a previous test program conducted by Phillips [3] at the NASA Langley Research Center. The contacting surfaces of the buckling supports were machined to insure a close fit along the specimen length.

It was found during the initial preliminary tests (see section 4.1) that additional end constraints were necessary to preclude early specimen failures by end brooming and crushing. The C-clamps shown in Figure 3 were used for this purpose. This constraint arrangement resulted in all test failures occurring in the fixture "test section."

The fixture was also equipped with adjustable guides that supported and aligned the anti-buckling supports. This allowed for precise positioning of the specimen vertically to minimize misalignment-induced bending. Strain gages in the test section were used to check the alignment. The gages were mounted across the width and on opposite faces to check in-plane and through-the-thickness bending.

2.3 DESCRIPTION OF UNNOTCHED SPECIMEN TEST FIXTURE

The unnotched test fixture is shown in Figure 4. This fixture also loads the specimen in direct compressive bearing at the specimen ends. As with the notched specimen fixture, the specimen ends are constrained by flat plates with specimen end constraints. These flat plates contact the flat surfaces of the test fixture cross-heads. Anti-buckling supports contact the full length of the specimen faces to prevent out-of-

plane motion. Dry lubrication is used to minimize friction. The contact surfaces of the anti-buckling supports are machined to maximize the contact with the specimen as well as to provide a vertical alignment for the specimen. The width of the specimen contacted by the anti-buckling support is 0.25 in. (6.35 mm) and the fixture has positioning guides to insure that the specimen centerline and support contact centerline coincide.

The unnotched specimens were instrumented with a number of strain gages to check the alignment and the load variation along the specimen length. Strain gages mounted across the specimen width and on opposite faces provided in-plane bending and through the thickness bending alignment information. Gages mounted along the length of the specimen provided information on the difference in axial strain due to friction between the specimen and anti-buckling support.

During preliminary testing of the unnotched specimens (see section 4.1) it was found that additional constraint at both specimen ends was necessary to prevent premature failures by end effects such as brooming, crushing, or the formation of full length delamination splits that originated at the ends. The C-clamps shown in Figure 4 provided a sufficient constraint so that all subsequent test failures occurred in the central region of the specimen away from the ends.

2.4 TEST CONDITIONS

2.4.1 INITIAL PRELIMINARY TESTS

A series of preliminary tests were conducted in order to evaluate the efffectiveness of the test fixture, identify problem areas in conducting the fatigue tests and to determine the appropriate stress levels

for the "production" fatigue tests. At least two specimens at each thickness, stacking sequence, and geometry were tested to failure, and the nondestructive examination procedures were checked during this phase of the testing.

Several important factors concerning the test fixture were evaluated. First, the specimen alignment must be as true as possible to minimize bending. This was evaluated by visual means (machinist square, level, etc.) and by the use of strain gages. The strain gages were located along the specimen length, across the wide, and on opposite faces. The second factor was the effectiveness of the anti-buckling guides. The effects of gaps that might be present due to specimen thickness variability was assessed. Various ways of lubricating the contacting surfaces were also evaluated. The final factor was whether or not the specimen behaved as expected and desired in the fixture. The modes of damage, progression of damage, mode of failure and life of failure were closely monitored during the preliminary tests. Where possible the test results were compared to data in the literature from other test programs. The results of these tests and evaluations were used to identify and make modifications to the test fixtures.

The procedures and techniques for conducting nondestructive examinations were also evaluated during these initial tests. The method of applying enhancer (zinc iodide) to the specimen for x-rays was checked. This included applying the enhancer to the specimen under load and unloaded. X-ray exposure times were also established. Trial specimens were polished and the edge replication technique was also evaluated.

The final objective of these tests was to establish the alternating stress range for conducting the "production" tests. It was desirable to

choose a stress range for each geometry type that would produce a fatigue life on the order of 100,000 cycles. A literature review established target maximum stress levels for the notched and unnotched geometry. Numerous tests were conducted to determine the life in the vicinity of these target stress levels.

2.4.2 PRODUCTION TESTS

"Production tests" refers to those tests conducted for the purpose of carrying out the program objectives, i.e. assess damage growth and the thickness effect. At each test condition--a specific laminate stacking sequence, thickness, and geometry type--three replicate tests were conducted. As previously discussed the objective of the preliminary tests was to identify the production test stress range that would yield fatigue lives in the 100,000 cycle range. (See Section 4.1 for the preliminary test results.) Provided below is a listing of the Production Test conditions.

Type of
Alternating Stress: Compression-Compression

R Value: 10

Frequency: 10 Hz

Maximum Nominal
Stress $(\frac{P}{A})$:

All Notched	- 38 ksi (262 MPa)
Unnotched, $[45/0/-45/90]_{ns}$	- 60 ksi (414 MPa)
Unnotched, $[90/45/0/-45]_{ns}$	- 48 ksi (331 MPa)

The specific tasks conducted during each Production Test was to periodically nondestructively examine the specimen to determine the location of the initiation of damage, document the progression of damage, document the type and location of final failure, and to determine the

number of cycles at final failure. Continuous observations of the specimen during the test were necessary to appropriately document the major damage accumulation "events" during the specimen life.

2.5 PROGRESSION OF DAMAGE BY NONDESTRUCTIVE EXAMINATIONS

The initiation, growth, and type of damage was documented during each production test by nondestructive examinations. These examinations were a combination of visual observations, enhanced x-rays, and edge replication. Visual observations were good for describing the general damage state and the overall damage progression, but could not be relied upon to determine the initiation of damage. Through-the-thickness x-rays were used to determine the initiation of damage and the growth of damage. The test was stopped periodically very early in life for x-rays. Once the damage was obvious by visual inspections the periods between x-rays were determined by the occurrence of damage growth events. Once the first test at a given test condition was complete, the x-rays were evaluated and the periods of time for the x-rays of the subsequent replicate tests were established. X-rays were usually taken at the same number of cycles along with additional inspections for comparison purposes. Through-the-width (edge view) x-rays were also taken along with through-the-thickness x-rays.

For the unnotched specimens edge replicas were taken in addition to the x-rays. The edge replicas provided a better documentation of through-the-thickness damage formation at the laminate edges than did the x-rays. Edge replicas were typically taken whenever a major observable damage event occurred such as the formation of a second or third interior split at the edge. These damage events were typically associa-

ted with an audible acoustic emission. Because the tests were continuously monitored this allowed for a complete documentation of all damage events.

3.0 EXPERIMENTAL PROCEDURES

This section describes the detailed procedures followed for conducting the various tasks of the test program. Also provided is a brief description of the test equipment used.

3.1 FATIGUE TEST PROCEDURE

The fatigue tests were conducted on a closed-loop electro-hydraulic MTS testing machine. The initial setup of the MTS test machine included removing the hydraulic grips, installing the compression-compression fatigue fixture, calibrating the load cell and checking the frequency generator. A model 8000A Fluke digital voltmeter was connected to read the static and mean load voltage and a model 5113 Textronic Oscilloscope was connected to read the dynamic voltage signal.

The average of five thickness readings were used to compute the alternating load range and the corresponding voltages. A test specimen was then installed and aligned in the test fixture. The alignment was checked using the strain gages. If the alignment was acceptable the fatigue test would then proceed. First the voltage corresponding to the mean load was set on the digital voltmeter. The specimen was then visually checked in the fixture for any problems. Next the maximum compressive load was set statically and the stroke limit was set just above the stroke position at the maximum static load. (The stroke limit automatically shut off the machine, including the counter, whenever catastrophic failure occurred.) After setting the stroke limit the mean load was reset. The minimum peak detector was set at the voltage corresponding to the maximum compressive load and the maximum peak detector was set at

the voltage equivalent to the minimum compressive load. The frequency generator was set for a sine function at 10 Hz. The counter was reset to zero with an x10 multiplier. The maximum span control was set to zero (half the total span for test restarts) and the Program Control and Record function was started. The span was increased toward the max/min setting, slowly for initial test startups, more rapidly for test re-starts. When the span control was in the vicinity of the max/min volt-age the oscilloscope was monitored closely. When the maximum/minimum voltages were achieved the oscilloscope signal would grow "wings" indi-cating one or both of the max/min limits had been exceeded. The span control was lowered to the point where the signal "wings" ceased to ap-pear on the scope. Then throughout the test the max/min range was checked to insure the proper position of the span control. (The span setting ± the mean voltage was almost equal to the maximum and minimum voltage settings but not exactly. Therefore, monitoring the signal on the scope was essential.) Interruption of the fatigue tests could be achieved by stopping the Program and Record function which stopped the cyclic load and returned the specimen to the mean static load. Edge replicas could then be taken or the specimen could be completely unload-ed and removed for x-rays. Test restarts took place more rapidly than the initial startups. This was to minimize the number of cycles at a much lower than desired load range. Usually restarts and return to the desired load range took 100-150 cycles (10-15 seconds). When cata-strophic failure occurred the specimen was crushed thus allowing the stroke position to move upward exceeding the position at the maximum load. Then the Stroke Limit interlock failsafe system automatically shut down the hydraulic system and stopped the counter.

3.2 ENHANCED X-RAY PROCEDURE

A Hewlett-Packard Faxitron, Model 43805N, x-ray system was used for all x-ray examinations. Damaged areas of the specimen were enhanced by the use of zinc iodide which penetrates the regions of matrix cracks and delaminations. The zinc iodide retards the penetration of the x-rays thus enhancing the damage regions. The specimens were typically subjected to the zinc iodide under the static mean load for a period of not less than one minute. The specimen was then removed from the fixture and the surfaces were cleaned with acetone to remove any excess zinc iodide. The specimen was then placed directly on the film (type M double emulsion) and onto the sensor assembly shelf. The sensor assembly shelf was positioned in the bottom shelf position in the x-ray cabinet. The voltage and time exposures are listed below:

Face View:	16 plies	0.9 mins.	20 kvp
	32 plies	1.8 mins.	20 kvp
	64 plies	3.6 mins.	20 kvp
Edge View:	Notched	2.0 mins.	40 kvp
	Unnotched	1.0 min.	40 kvp

3.3 EDGE REPLICA PROCEDURE

The edge replica technique, developed at Virginia Tech by W. W. Stinchcomb, et al., [4] provides very detailed information at the edge of a specimen. An edge replica taken of a well polished edge provides the identification of each individual ply of the laminate and the location of matrix cracks and delamination splits.

The first step toward edge replication is the preparation of the specimen edge. Sanding and polishing is necessary to remove extraneous markings such as scratches or saw blade marks. The 64 ply fatigue spec-

imens had especially bad saw marks and required considerable sanding. The general edge polishing procedure is as follows. First, the edges were sanded with a very rough sandpaper. Next a rough, 400 CP1 sandpaper was used. Each edge was polished 100 back-and-forth strokes. This was followed by the exact same application of a 220A sandpaper. The fourth step was to polish each edge using 5 micron jeweler's powder. Again 100 back-and-forth strokes were used. The final process was polishing with a 3 micron jeweler's powder for 200 back-and-forth strokes. A reference edge replica was taken to check the quality of each polished edge.

An edge replication is taken by using specially prepared acetate replicating tape. The tape is loosely attached to the specimen edge by using standard adhesive tape. Acetone is injected between the acetate tape and specimen edge by a hypodermic needle. The acetate tape is then pressed against the specimen edge by running a finger down the length of the tape. After about 45 seconds to a minute the tape is peeled off the specimen. Care must be taken not to let the acetate tape slip or to allow the formation of a bubble under the tape. If either occurs the process is simply repeated with a new piece of tape.

During the fatigue tests edge replicas were taken to document and examine each major damage event such as the formation of a new delamination split. Usually edge replicas were taken under load. While this was not essential, a better definition of the splits was obtained.

4.0 EXPERIMENTAL RESULTS

4.1 PRELIMINARY TEST RESULTS

Thirty-three specimens (12 notched, 21 unnotched) were tested to failure during the initial test phase of the program. The purpose of these tests was to learn about the characteristics of the test fixtures and the specimens so that meaningful "production tests" could be conducted. The test results are presented in Tables 1 and 2. There were three fundamental results obtained from these tests. First, it was found that the specimen alignment in the test fixture was critical but adequate alignment could be achieved with both fixtures. Second, it was found that substantial constraints along the specimen faces at the specimen ends was essential. With only minimal constraint it was found that premature failures occurred at the ends such as brooming, crushing or excessive splitting. Finally, the stress levels for each specific laminate stacking sequence and geometry were established. Each of these results are discussed in more detail in the following paragraphs.

The anti-buckling face plates of the notched specimen test fixture provided some constraint against end failures, as does the top loading plate. However, it was found that during the test the face plates would gradually rise off of the bottom loading plate thus leaving an unconstrained end. In this situation, end crushing occurred. This situation was eliminated by the use of 1 in. (25.4 mm) cubic constraint blocks that beared against tthe bottom of the anti-buckling face plates. A large C-clamp squeezed the constraint blocks against the face plates. After making this alteration all subsequent specimens failed in the test section which was through the ligaments adjacent to the hole.

End constraints for the unnotched specimens were necessary to prevent an entirely different type of deviate failure. The unnotched test fixture provided enough constraint to prevent end crushing but delamination splits originated at either the top or bottom end. These splits progressed up or down the specimen length until a complete full width and length split occurred. This pattern of damage was consistent and occurred at a relatively low number of cycles. The use of C-clamps at the top and bottom was found to eliminate end induced damage initiation. These C-clamps "squeezed" the alignment blocks attached to the top and bottom loading plates against the specimen faces. After this modification there was no preferential location for the initiation of damage along the specimen edges. This was checked by specimen FU10 (32 plies) where a C-clamp was used at the top only. The damage initiated at the specimen bottom end where a delamination split formed near each face and fully through the width. Both splits progressed upward from the botton.

The stress range for each production test condition was established by the preliminary test results. The notched tests, see Table 2, were conducted at a maximum compressive stress of 40 ksi (276 MPa). The fatigue lives were not as high as desired, although the 64 ply specimen of the [45/0/-45/90] laminate failed at 82,500 cycles. Furthermore, 40 ksi (275.8 MPa) was marginal for the 16 ply specimens of the [90/45/0/-45] laminate. Several specimens cracked under the maximum static load before the fatigue test began and the fatigue lives were very short. Specimen F6 was tested at a maximum compressive stress of 35 ksi (241 MPa) and the life was 161,500 cycles. This was slightly higher than the target of 100,000 cycles. Therefore, an intermediate value of 38 ksi (262 MPa) was selected for all the notched production tests.

Unnotched tests were conducted at maximum compressive stresses that range from 40 ksi (276 MPa) to 60 ksi (414 (MPa). A partial "S-N" curve is shown in Figure 5. At a maximum stress of 60 ksi (414 MPa), the specimens of the $[45/0/-45/90]_{ns}$ laminate failed at fatigue lives in the 100,000 cycle range. This level of stress was selected for the $[45/0/-45/90]_{ns}$ specimens. The life of the $[90/45/0/-45]_{ns}$ specimens were considered to be two low and several 16 ply specimens failed statically in the 47 ksi (324 MPa) to 55 ksi (379 MPa) range. Two tests were run at 50 ksi (345 MPa). The 16 ply specimen, FU13, failed statically right at the max load while the 64 ply specimen, FU15, failed at 238,500 cycles. Based on these test results the maximum compressive stress of 48 ksi (331 MPa) was selected as being appropriate for the specimens of the $[90/45/0/-45]$ laminates.

Finally, the preliminary tests confirmed that the specimen could be removed from the fixture for examination and reinstalled several times without significantly influencing the fatigue life. The next section discusses how the strain gages were utilized to confirm that proper alignment could be achieved on reinstallation.

4.2 SPECIMEN STRAIN GAGE ALIGNMENT RESULTS

Electrical resistance strain gages were used to check the specimen alignment during static loading. In-plane bending was checked by gages on opposite edges of the same face and at the same elevation. Through-the-thickness bending was checked by gages on opposite faces but at the same edge and elevation. The difference in strain at different elevations due to friction between the specimen face and anti-buckling supports was checked by comparing gages at various elevations. Figures 6

and 7 show the gage locations for the notched and unnotched specimens, respectively. It should be noted that once the fatigue test began the static strain gages became loose and ceased to function. Therefore, only the initial alignment strains were available.

The unnotched specimen alignment data is summarized in Table 3. For gages of a typical specimen, plots of load versus strain are given in Figures 8 and 9. Through-the-thickness bending was the smallest bending component, typically less than 3%. The in-plane bending component was also relatively small, usually between 1% to 7%. The elevation strain variation was the largest, being typically in the 5% to 25% range. While this was larger than expected, it was not considered significant. This was because the strain gage readings were taken at a static load on the order of only 10% of the maximum dynamic load. The friction loss would obviously be more significant, percentage-wise, at the lower load. Nevertheless, to minimize this effect the specimen-fixture interface was always well lubricated during the fatigue tests.

The notched specimen alignment data is given in Table 4. For gages of a typical specimen, plots of load versus strain are shown in Figures 10, 11 and 12. There was no variation in elevation data because all gages were in the test section. However, the mean strain readings from the through-the-thickness gages compared very closely to the calculated strain, thus indicating little if any friction losses at the test section. Through-the-thickness variations were again small (2-4%), while the in-plane variation was larger (10-24%).

One reason for the in-plane variation being large was due to the ends of the specimens not being completely square. In an attempt to correct this situation two specimens (FU9, FU18) were machined to a

square condition with respect to one of the specimen side edges. The in-plane variation dropped from 16.4% to 5.7% for FU9 and from 21.4% to 7.8% for FU18. However, the machining process damaged the specimen ends considerably. The first machined specimen to be tested failed under the maximum static load by end crushing. Therefore, no further specimens were machined and all specimens were fatigue tested in their original as-delivered condition.

In order to address the question of alignment repeatability several different alignment tests were conducted. This question was pertinent because the typical specimen was removed for x-rays and reinstalled several times during the fatigue test. The first way of checking realignment was to obtain a set of strain readings, take the specimen out and reinstall it upside down and/or backwards in the fixture. These dual position readings are shown in Table 5. As can be seen, the strain gage readings are virtually the same. The other type of test was to compare the alignment strain values of a specific specimen at several days interval. During the interim the fixture alignment was altered by conducting fatigue tests on other specimens and then realigned. This data is also shown in Table 6. Again the strain readings are virtually the same. Therefore, the fatigue tests were conducted with high confidence that proper alignment could be achieved repeatedly by the use of visual tools such as the machinist square and level.

4.3 NOTCHED SPECIMEN TEST RESULTS

Three replica fatigue tests were conducted at each laminate and thickness condition. Data for the $[45/0/-45/90]_{ns}$ laminate tests are tabulated in Table 7 while the data for the $[90/45/0/-45]_{ns}$ laminate

tests are tabulated in Table 8. The data are also plotted in Figure 13. All tests were conducted under the same test conditions. Except for specimens F1, F2 and F22, the progression of damage was documented by visual observations and enhanced x-rays.

The progression of damage was, in general, similar and the failure modes were the same for all specimens, regardless of thickness and laminate type, except for specimen F1. Specimen F1 is a 16 ply specimen of the $[45/0/-45/90]_{ns}$ laminate. This specimen cracked while under the maximum static load when the stroke limit interlock was being set. Since the specimen did not fail, i.e. it still supported the maximum load, it was fatigue loaded and failed at 1040 cycles. (This represented about 400 cycles at the desired load range.)

The ranges of the fatigue life for each test condition (specific thickness and laminate type) overlap, see Figure 13. With the exception of deviate test F1, the 16 ply and 32 ply data for both laminates are essentially indistinguishable. However, the highest fatigue lives belonged to the 64 ply specimens. As with the other two thicknesses there is little difference between the two laminates at 64 plies. The $[90/45/0/-45]_{ns}$ specimens exhibited the greater data scatter.

Damage in the typical specimen became visible in the 3000 to 8000 cycle range and was directly adjacent to the hole. X-ray examinations taken early in life (3500 cycles, 4000 cycles or 5000 cycles) typically revealed small damage adjacent to the hole prior to the damage being visually observed. The damage then progressed at a moderate rate until it was on both faces and at both edges of the hole. The damage was usually about one hole diameter wide. Damage then slowed considerably as if a damage plateau had been reached. Towards the end of life (85%-

90%) damage began to progress rapidly. Frequently the damage "jumped" (with an associated "audible sound" perhaps to half the ligament on either side of the hole). Near the end of life the damage would "jump" completely across the ligament to one side of the hole, then do the same on the other side. This usually occurred on both faces. This was accompanied by considerable audible cracking sounds and almost immediate failure.

The photographs of Figure 14 present typical enhanced x-ray examinations showing damage in the $[90/45/0/-45]_{ns}$ laminate, and Figure 15 shows typical x-ray photographs of damage in the $[45/0/-45/90]_{ns}$ laminate. Furthermore, Figure 14 compares the progression of damage in two specimens, F20 and F21, that had essentially the same life, 31,360 cycles and 30,850 cycles, respectively. Finally, Figure 15 constrasts the progression of damage in three specimens, F8, F9 and F7, that had different lives, 25,110 cycles, 44,120 cycles, and 90,850 cycles, respectively. (It should be noted that since the damage is localized around the hole and across the width adjacent to the hole, there does not appear to be any influence from the antibuckling guides on the formation of damage.)

Comparing Figures 14 and 15 it is evident that the gross damage surrounding the hole is similar for both laminates. Damage consists of a fairly broad, circular delaminated region in which numerous 0°, 45°, and 90° matrix cracks are visible. The 90° matrix cracks dominate the view in the $[90/45/0/-45]$ laminate while 45° cracks dominate in the $[45/0/-45/90]$ laminate. This is not surprising since the edge view x-rays, shown in Figures 16 and 17, illustrate that the damage is predominantly confined to the first couple of plies from the face. The

damage in specimens F20 and F21 at 90% of life doesn't appear to be nearly as substantial as the corresponding damage in F7, F8 or F9 at 90% of life. The test chronologies indicate that this distinction may be typical. Figure 18 shows the damage in the [90/45/0/-45] specimen F17 at 98.8% of life and as can be seen the damage does not extend fully across the specimen width as it does at 90% of life for specimens F7, F8 and F9.

The progression of damage of specimens F20 and F21 shown in Figure 14 is typical of specimens failing at essentially the same life. As can be seen, there is no appreciable difference in the magnitude or appearance of the damage in these two specimens. Damage progresses steadily to about 35-40% of life, progresses less rapidly to 80% and at 90% is only about half-way across the specimen width. From this point damage progression is much more rapid.

On the other hand Figure 15 illustrates the progression-of-damage in 3 specimens where the range of life was a factor of 4. It is quite obvious that the damage appears nearly identical in the three specimens, the difference being the rate at which the damage developed. The final photograph in each sequence shows massive damage at 92% of life (F8), 95% of life (F9) and 88% of life (F7). The damage in F9 is slightly more than F8 which is slightly more than F7, as the percentages might indicate. However, the total number of cycles is about half the other in each case. All three specimens show about the same damage at 5000 cycles but at 10,000 cycles F8 (failure at 25,110 cycles) is now showing about twice as much damage as the other two. It is also interesting to note that specimen F9 is showing about the same damage at 25,000 cycles (57% of Life) as does F7 at 25,000 cycles (28% of Life). This may be

because both specimens are probably on the damage plateau where damage accumulates more slowly than at the beginning or end of life.

There was no appreciable difference in the type or appearance of failed specimens. Figures 19 through 22 show the appearance of failed specimens. The damage is generally confined to the region immediately adjacent to the hole. However, long axial delamination splits, clearly visible in Figures 20 and 22, did typically accompany the catastrophic failure in the test section. These major splits were never visible in x-rays so they were thought to occur at catastrophic failure as opposed to preceding or precipitating failure.

4.4   UNNOTCHED SPECIMEN TEST RESULTS

Three replicate fatigue tests were conducted at each test condition. The data for the $[45/0/-45/90]_{ns}$ laminate is tabulated in Table 9 and is displayed graphically in Figure 23. These tests were conducted at a maximum stress of -60 ksi (-414 MPa). The data for the $[90/45/0/-45]_{ns}$ laminate is tabulated in Table 10 and displayed graphically in Figure 24. These tests were conducted at a maximum stress of -48 ksi (-331 MPa). Except for the maximum load, all tests were conducted at the same test conditions. Tables 9 and 10 list the progression-of-damage studies that were conducted.

The progression of damage and mode of failure was similar for all tests except for specimens FU6 (16 plies, Table 9) and FU19 (16 plies, Table 10). The deviate failure of specimen FU6 was brought about by operator error. Specimen FU6 was accidentally overloaded by about 20% due to misreading the max/min peaks of a temporary replacement oscilloscope. (This was the only test for which the temporary scope was used.) This

test does not represent a valid test, so the results have only been included on Table 9. It is not included on the associated plot, Figure 23.

The 16 ply specimen FU19 also failed in a deviate manner. This specimen cracked while loaded statically at the maximum load. Since it would still support load it was cyclically loaded. The desired load range was achieved at about 500 cycles. The specimen failed at 1320 cycles. An edge replica was taken after the initial static crack. The location of the crack was identical to the location of the first delamination split for its counterpart, specimen FU17.

The test data shown in Figures 23 and 24 clearly points out the differences in fatigue lives of the two laminates. The interlaminar normal stress, σ_z, is tensile in the $[90/45/0/-45]_{ns}$ laminate and compressive in the $[45/0/-45/90]_{ns}$ laminate, with the magnitude being about the same. (Refer to Chapter 5 for the interlaminar stress distribution.) The fatigue lives of the $[90/45/0/-45]_{ns}$ laminate are somewhat higher than the $[45/0/-45/90]_{ns}$ laminate. (The maximum stress level was 20% lower.) Any thickness effect trends brought about by differences in the magnitude of the interlaminar normal stress are not so obvious. The range of fatigue lives for the $[45/0/-45/90]_{ns}$ laminates overlap and there is very little difference between the 16 ply and 32 ply data. The 64 ply data is slightly higher but overlaps the 32 ply data. This is somewhat opposite to the trend shown by the other laminate. The $[90/45/0/-45]_{ns}$ laminate, with tensile interlaminar normal stress, shows no difference in the lives of the 32 ply and 64 ply specimens. However, the lives of the 16 ply specimens are an order of magnitude lower than those of the 32 and 64 ply specimens. In fact there is a tendency for

the 16 ply specimens to crack statically in the vicinity of the maximum
test load. Finally, as with the notched specimens, the $[90/45/0/-45]_{ns}$
specimens exhibit less data scatter than do the $[45/0/-45/90]_{ns}$ speci-
mens, if one excludes specimen FU19 which cracked statically before
failing at 1320 cycles.

In spite of the differences in the fatigue lives of the unnotched
specimens there was virtually no difference in the initiation, type and
progression of damage, as well as the type of final catastropic failure.
Damage initiated at some random location along the specimen length in
the form of a small delamination at the free edge. Tables 11 and 12
give the ply interface location of these delaminations as determined
from edge replicas. In general the delaminations occurred at the 0/-45
interface, plies 2 and 3 for [45/0/-45/90] and plies 3 and 4 for
[90/45/0/-45]. From this initiation the delaminations extended along
the specimen length until it was more or less full length. (Edge repli-
cas verify the delaminations to be at the same interface along the
specimen length and on both edges.) The delamination then worked
through the width and finally along the opposite edge lengthwise. (The
test fixture end constraints prevented the cracks from extending to the
specimen ends. In addition, the antibuckling constraint did not prevent
damage formation across the specimen width.) The process is illustrated
by the x-ray photographs shown in Figure 25. Frequently while the first
delamination was progressing a delamination at the same location from
the opposite face would initiate in a similar manner as the first.
These splits are also listed in Tables 11 and 12. As these outside de-
laminations extended, the outer plies that were split from the laminate
buckled under the compressive load and caused the formation of the ma-

trix cracks that are visible in the x-rays of Figure 25. The next major damage event was the initiation of a second interior split. Sometimes but not always the second interior split opened at the same elevation location as the initiation of the first split. These interior splits opened at a 0/-45 interface but 4 plies inward from the initial 0/-45 split. The location of the initiation of second interior split was usually the location of the final catastrophic failure. However, catastrophic failure did not occur until the second interior split extended lengthwise and through the width. Usually a third and sometimes a fourth interior split would initiate. These multiple interior splits normally initiated at the elevation location of the second interior split. Multiple interior splits may have formed relative to both faces before final failure. The third and fourth splits did not extend along the specimen length nor through the width. One distinction in thickness is that only two interior splits opened in the 16 ply specimens before failure and multiple splits (3 or 4) may open in the 32 and 64 ply specimens. In addition, delaminations of the 16 ply specimens don't extend lengthwise and through the width as did the 32 and 64 ply specimens.

Typical edge replicas are shown in Figures 26 through 31. These photographs clearly show the delamination splits and with careful examination individual plies are visible. Much larger magnifications were used for actually counting plies to locate the delamination splits. The location of splits relative to the laminate midplane are listed in Tables 11 and 12. It should be noted that many splits form at the 0/45 interface rather than the -45/0 interface. Also delaminations frequently change interfaces as is shown in Figure 27, 28, 30 and 31. Frequently secondary splits form after the primary or first split. One such

secondary split is shown on the right edge of the laminate in Figure 29. (Interface changes and secondary splits will be discussed further in Section 5.3.) Finally, the broken plies visible in all the figures, are due to the buckling of the outer plies after splitting away from the laminate.

Photographs of typical failed specimens are shown in Figures 32 and 33. Each broken specimen exhibits a localized region of massive damage where the catastrophic failure occurred. This location normally coincided with the formation of multiple interior splits prior to failure. The 32 and 64 ply specimens exhibit the extensive delaminations that were typical of all specimens except the 16 ply specimens. Load redistribution may be an explanation for the difference between the 16 ply and 32, 64 ply specimens. When a delamination forms between the second and third plies, inward from a face, the redistributed load to the undamaged laminate is much higher for a 16 ply specimen than is the case for the 32 and 64 ply laminates with the same split. The formation of only two interior splits was typical of the 16 ply specimens and catastrophic failure closely followed the formation of the second split.

5.0   INTERLAMINAR STRESSES AT LAMINATE FREE EDGES

As a result of the mismatch of Poisson's ratio $\left(\nu_{xy} = - \varepsilon_y/\varepsilon_x\right)$ be-
tween adjacent layers and the mismatch of the coefficient of mutual in-
fluence $\left(\eta_{xy,x} = \gamma_{xy}/\varepsilon_x\right)$, interlaminar stresses are necessary at the
free edges of laminates for equilibrium [5]. These interlaminar stres-
ses can be defined with the aid of the diagrams shown in Figure 34. For
a uniaxial force in the x-direction the normal stresses in the y-direc-
tion, σ_y vary in magnitude and direction from one ply to the next, refer
to Figure 34a. These σ_y stresses produce a moment about the x-axis. To
counterbalance this moment, the interlaminar stress σ_z, must be present.
(The interlaminar stress τ_{zy} is necessary for equilibrium of y-direction
forces between plies.) Since the moment produced by σ_y is a function of
its distance, z, from the midplane, it will vary with laminate and ply
thickness and so must the interlaminar normal stress, σ_z. There is also
a moment produced by the in-plane shear stress τ_{xy}, at the free edges of
laminates where τ_{xy} must be zero. Referring to Figure 34b we see that
the moment due to τ_{xy} is about the z-axis. Therefore, it must be coun-
terbalanced by the presence of the interlaminar shear stress τ_{xz} at the
free edges. Since this moment is about the z-axis, the interlaminar
shear stress, τ_{xz}, is not a function of distance, z, from the midplane,
i.e. τ_{xz} is not a function of laminate thickness or ply location within
the laminate. (Also, τ_{zy} is not a function of laminate thickness or ply
location since it is only required to balance forces between plies.)

5.1 STRESS ANALYSIS OF THE UNNOTCHED GEOMETRY

There have been many studies concerning the computation of inter-laminar stresses. Finite difference schemes, the finite element methods, and other approximations have been developed. Herein, the inter-laminar normal stress, σ_z, will be calculated using the approximation method proposed by Pipes and Pagano [1]. The interlaminar shear stress distributions will be obtained from a finite element analysis by Herakovich, et al. [2]. Because of the thickness effect the interlaminar normal stress distributions must be generated for the specific laminates and thicknesses of this study. Since the shear stess analyses are not a function of thickness, the existing analyses of Herakovich, et al. [2] for the $[45/0/-45/90]_s$ and $[90/45/0/-45]_s$ graphite/epoxy laminates are valid for the 16, 32, and 64 ply cases studied herein. (Analyses will be performed for only the unnotched geometry.)

Pipes and Pagano [1] developed a method for approximating the interlaminar normal stress, σ_z. A stress distribution approximation was devised that matched the essential features of the interlaminar stress field. A schematic of their model is shown in Figure 35. The essential model assumptions are that the normal stress is constant or varies linearly, as shown, and that the normal stress is confined to a boundary layer region at the free edge that is equal to the laminate thickness. Since the resultant of the σ_z stress distribution is a pure couple, the relationship between σ_m and σ_m' (refer to Figure 35) is [1]

$$\sigma_m' = \frac{\sigma_m}{5}$$

where σ_m is given by the expression

$$\sigma_m = \sigma_m(z) = 45M(z)/14h^2$$

where: h   = half the laminate thickness

$$M(z) = \int_z^h \sigma_y(\xi)d\xi$$

and: $\sigma_y(z) = Q_{yj}(\epsilon_j - \alpha_j T)$, j = 1,2,6

In addition: Q_{yj} = reduced stiffness constants

α_j = coefficients of thermal expansion

ϵ_j = engineering strain components

and   T   = constant temperature change.

Normal stress distributions were computed for the laminates and thicknesses of the unnotched fatigue specimens for applied loads and residual thermal stresses due to curing cooldown. Stresses were calculated for the $[45/0/-45/90]_{ns}$ laminate at 16, 32 and 64 plies for a static load corresponding to an applied laminate stress, σ_x, of -60 ksi (-414 MPa). The stresses are plotted for each thickness in Figure 36. Stresses in the $[90/45/0/-45]_{ns}$ laminate at 16, 32 and 64 plies were computed for a static load corresponding to an applied laminate stress, σ_x, of -48 ksi (-331 MPa). These stresses are plotted in Figure 37. (The applied laminate stresses, -60 ksi (414 MPa) and -48 ksi (331 MPa), correspond to the peak fatigue load for the $[45/0/-45/90]_{ns}$ and $[90/45/0/-45]_{ns}$ laminates, respectively.) Note that in Figure 36 the σ_z stresses in the $[45/0/-45/90]_{ns}$ laminate are compressive while those

in the $[90/45/0/-45]_{ns}$ laminate are tensile under the applied compressive load.

It is interesting to note that as the laminate thickness increases the magnitude of σ_z decreases. In fact, doubling the thickness halves the σ_z stress. A review of the Pipes and Pagano model [1] reveals why this is the case. When a stack of $[90/45/0/-45]_s$ plies are added to the laminate the moment is increased. Since the forces due to the individual ply stresses σ_y, add to zero, a pure couple, independent of location from the midplane, is added. Therefore, doubling the thickness and doubling the applied load results in a doubled moment $M(z)$. However, doubling the laminate thickness doubles the region, 2h, over which the interlaminar stress, $\sigma_m(z)$, exists. Since $\sigma_m(z)$ is an inverse function of the thickness squared, h^2, the stress is then halved.

The shear stresses, τ_{yz} and τ_{xz}, have been generated by a finite element analysis [2]. The analysis was quasi three-dimensional, generalized plane strain. The elements were constant strain elements with a high concentration of small elements in the boundary layer along the free edge. The laminate cross-section was represented by a two-dimensional grid where individual plies were treated as homogeneous orthotropic with properties of unidirectional (which can be off axis) fibrous composites. The nondimensional shear stress distributions for the $[90/45/0/-45]_s$ graphite-epoxy laminate are shown in Figure 38 and those for the $[45/0/-45/90]_s$ graphite-epoxy laminate are shown in Figure 39. (Note that the interlaminar stresss have been normalized by dividing by the applied laminate stress.) The stress distributions shown are equally applicable to the 16, 32, and 64 ply cases of this study since τ_{yz} and τ_{xz} are not functions of the laminate thickness. The distribution shown

is simply the same for each repeated stack of four plies. The normalized stress scale is included only for the purpose of comparing the relative magnitude of the stresses. The finite element results show the shear stress, τ_{xz}, to be the largest in magnitude of the three interlaminar stresses for these two laminates.

5.2 RELATIONSHIP BETWEEN INTERLAMINAR STRESSES AND THE FATIGUE TEST RESULTS

The sketches shown in Figure 40 illustrate the types of damage that can be produced by each interlaminar stress component. In each case, the damage is most likely to be a delamination. When the normal stress, σ_z, is tensile all three interlaminar stress components are working together to produce a delamination. When σ_z is compressive the two shear stresses still work together to produce a delamination. The interfacial location of the delamination may be determined by the peak stress location of one dominant stress such as σ_z or τ_{xz} or it may be determined by a combination of the stresses working together.

The notched geometry fatigue tests were all conducted at the same load ranges with the maximum applied nominal stress being -38 ksi (262 MPa). There is very little difference in the fatigue lives when comparing specimen thickness or laminate type (see Figure 13). Furthermore, the damage begins at the hole and progresses across the width, adjacent to the hole, with substantial matrix cracking accompanying the delaminations. In spite of the dramatic differences in the interlaminar normal stresses of these two laminates, the dominant factor affecting damage and failure is the stress concentration at the hole and not the interlaminar stress.

Recalling Figures 23 and 24, we see that the unnotched specimens do exhibit different fatigue lives when comparing the two laminates. This is evident by the fact that the $[45/0/-45/90]_{ns}$ laminate specimens, with compressive interlaminar normal stresses, had fatigue lives in the same decade at -60 ksi (414 MPa) as did the $[90/45/0/-45]_{ns}$ laminate, with tensile interlaminar normal stresses, and a stress of -48 ksi (331 MPa). However, differences in the fatigue lives as a function of thickness are not so evident. Since the interlaminar normal stress varies by a factor of two between 16 and 32 plies and another factor of two between 32 and 64 plies, it seems unlikely that the interlaminar normal stress is the sole or dominant contributor toward damage and failure. It is more likely that damage is brought about by the combination of the tensile or compressive normal stress, and the relatively high interlaminar shear stress τ_{xz}. This will be more fully explored in the following paragraphs by examining the location, initiation, and progression of damage.

It is evident from the nondestructive examinations that the interlaminar stresses are the dominant factor in the damage development in the unnotched specimens. Comparing the x-rays of the two geometries, it is evident that matrix cracking is much more prevalent in the notched specimens. In fact the damage around the holes may begin as matrix cracks, see Figures 14 and 15. On the other hand the damage in the unnotched specimens is predominantly delaminations. There are far fewer matrix cracks and those that are present are associated with the large out-of-plane buckling of the plies that are split from the remaining undamaged laminate. This large, localized out-of-plane displacement is illustrated best by the edge replicas which were taken under the mean static load. Figure 30 shows a delamination on the right face that runs

the full length of the replica but exhibits large displacements at two locations and there is, in effect, a buckling mode nodal point in the center. Broken fibers are quite common in the large displacement region as illustrated on the opposite face of the replica in Figure 30. Finally the sequence of x-rays shown in Figure 25 demonstrates that the initiation and progression of damage is an edge effect. The delamination begins at the edge and runs along the length of the specimen in the region where the interlaminar stresses are located before penetrating through the specimen width.

Now that delaminations have been established as the primary type of damage, (as would be expected when relatively high interlaminar stresses are present), the relationship between the interlaminar stress distribution and the interfacial location of the delaminations will be examined. The location of delaminations have been determined from edge replicas and are tabulated in Table 11 for the $[45/0/-45/90]_{ns}$ laminate and Table 12 for the $[90/45/0/-45]_{ns}$ laminate. A cursive review of these tables quickly establishes the -45/0 interface (plies located from laminate midplane) as the most common location of delaminations regardless of laminate type. Also the adjacent interface, 0/45, is the location of almost all other delaminations. A review of the interlaminar stress distributions, Figures 36-39, provides an explanation for the preference of these two interfaces for delaminations. The interlaminar shear stress, τ_{xz}, is a maximum value at these two interfaces for both laminate types. It is also of comparable magnitude and algebraic sign for both laminate types and thicknesses. In the case of the $[90/45/0/-45]_{ns}$ laminate the interlaminar normal stress is slightly more tensile at the -45/0 interface than at the 0/45. This would make the -45/0 interface

slightly more preferential than the 0/45 as is supported by the data in Table 12. One might expect just the opposite to be the case for the $[45/0/-45/90]_{ns}$ laminate because the -45/0 interface has a higher compressive normal stress. However, the data in Table 11 still indicates the -45/0 interface to be preferential. Perhaps this is because at the first, or outermost delaminations the magnitude of the interlaminar normal stress is small relative to the τ_{xz} shear stress so it may have little to do with the formation of the delamination. Moving inward to the second or third interior split, the interlaminar normal stress is higher; substantially so for the 16 and 32 ply laminates. Again one sees from the tables that the preference is still at the -45/0 or 0/45 interfaces, with the -45/0 being more preferential than 0/45 for both laminate types. The τ_{xz} shear stress has the same distribution and magnitude in interior stacks of [90/45/0/-45] plies as it does in the outer plies. Therefore, since the delaminations are forming at the interfaces of maximum shear stress regardless of laminate type, i.e. without regard to $+\sigma_z$ or $-\sigma_z$, it appears that the location of maximum interlaminar shear stress, τ_{xz}, determines the preference for delamination locations.

Delamination interface changes also appear to be consistent with the interlaminar shear stress distribution. In some instances a delamination at the 90/-45 interface changed to the more preferential -45/0 interface. Also in one instance an interface change between the -45/0 and 0/45 occurred. This might be expected since they have equal τ_{xz} shear stresses. Furthermore in those instances where a delamination occurred at the 90/-45 or 45/90 interface, they always appeared to be associated with an interface change to the more preferential -45/0 interface.

6.0 <u>DISCUSSION</u>

This chapter presents a discussion of the compression test fixture as well as the test results. For discussion and interpretive purposes, various aspects of this test program are compared to results from similar studies reported in the literature.

6.1 <u>DISCUSSION OF TEST RESULTS</u>

There have been a number of fatigue studies in which quasi-isotropic graphite-epoxy laminates were tested and studies in which the role of interlaminar stresses of the free edges in the damage development process have been investigated. However, none of these studies examine the laminate thickness effect and none are for the specific laminate stacking sequences studied herein. In order to put the test results of this study in perspective some comparisons are nonetheless available and will be cited below.

The lives of the notched geometry specimens were in the 10^3-10^5 cycle range at a maximum stress of -38 ksi (262 MPa) with most data in the 10^4-10^5 range. There was little distinguishable difference in the lives of the two laminates. Black and Stinchcomb [6] conducted compression-compression fatigue test on a 48 ply quasi-isotropic laminate using center notched specimens and found fatigue lives in the same range. At a maximum stress of -40 ksi (276 MPa) the lives were in the 10^3-10^5 cycle range and at -35 ksi (241 MPa) they were in the 10^5-10^6 cycle range. They also reported damage development similar to that reported herein. Large delaminations developed adjacent to the hole and at interfaces closest to the surface. These results are in general agreement

with those of this study. Furthermore, Whitney and Kim [7] studied the static fracture of $[90/0/\pm45]_s$ and $[\pm45/0/90]_s$ laminats which have high tensile and high compressive interlaminar normal stresses at straight free edges. They found the tensile strength of unnotched specimens to be reduced by tensile interlaminar normal stress, but found no difference in the strength of notched specimens of the two different laminates provided the geometry was such that damage began at the notch rather than the straight free edge. Again this is consistent with the reported results herein where there was no difference in the fatigue lives of the two notched laminates.

The range of fatigue lives of the unnotched specimens are similar to those of Ryder and Lauraitis [8] who studied a $[0/45/90/-45_2/90/45/0]_s$ graphite-epoxy laminate. This laminate has very low compressive interlaminar normal stresses (about 10% of σ_z of the subject laminate) under a compressive applied load. At $R = -\infty$, the fatigue lives for maximum stresses of -30 ksi (207 MPa) to -50 ksi (345 MPa) are similar to those of the $[90/45/0/-45]_{ns}$ laminate of the subject study.

The damage development in the unnotched specimens of the subject tests are strongly related to the τ_{xz} interlaminar shear stress distribution. Delaminations occurred where the τ_{xz} stress is maximum regardless of the magnitude and algebraic sign of the interlaminar normal stress. There are similar results in the literature. Stalnaker and Stinchcomb [9] studied $[0/\pm45/90]_s$ and $[0/90/\pm45]_s$ laminates and found that the first laminate formed delaminations primarily produced by tensile interlaminar normal stresses. In both laminates they reported branch delaminations at the interfaces where high τ_{xz} shear stresses existed even when the interlaminar normal stress is compressive.

Herakovich, et al. [5] performed an analytical study using a tensor polynomial failure criterion in which quasi-isotropic graphite-epoxy laminates were included and found that the interlaminar normal stress was never the dominant stress for initiation of failure. Failure was either due to τ_{xz} or a combination of τ_{xz} and tensile σ_z. Finally, Whitcomb [10] studied graphite-epoxy quasi-isotropic laminates experimentally and with a finite element analysis. His analysis results and experimental results compared well and he reported that delaminations were more likely to occur in areas where the interlaminar normal stress is high tensile and the τ_{xz} shear stress is high. Whitcomb [10] further reported that delaminations were found and predicted to occur in regions where the τ_{xz} stress is high but the interlaminar normal stress is compressive.

6.2 DISCUSSION OF ANTIBUCKLING TEST FIXTURE

The prevention of specimen buckling under compression fatigue loading has been treated in several different ways. (Buckling may be an unacceptable specimen failure mode when addressing large structural components that do not buckle under compressive loads.) Stinchcomb and Black [6] tested specimens with low slenderness ratios that did not buckle under the fatigue load. Others have used reinforcement tabs that limit the size of the specimen "test section" thus lowering the slenderness ratio so that buckling does not occur. Ryder and Lauraitis [8] utilized an antibuckling guide to minimize buckling. In the subject study specially designed antibuckling guides were also employed to prevent or minimize out-of-plane displacements.

The antibuckling fixture utilized by Ryder and Lauraitis is shown in Figure 41. Rollers contact the specimen at opposite faces spaced along the specimen length to form six bays and to approximate fixed grips at the ends. The fixture was subjected to a test evaluation and it was found that the specimen out-of-plane deflection in any one bay was no greater than 0.001" (0.025 mm) and less than this value in all other bays. However, Ryder and Lauraitis reported compression fatigue failure (the inability of coupon to sustain further load) was due to local buckling.

The antibuckling fixtures (originally designed by Phillips [3] and refined by the writer) employed in the subject study have been described in detail in sections 2.2 and 2.3 of this report. The unnotched fixture provided full length continuous constraint against out-of-plane motion. Some specimens exhibited variations in thickness which produced "light gaps" extending over small longitudinal distances on the order of 0.5" (12.7 mm) to 1" (25.4 mm) long. Feeler gages were used to approximately measure these gaps under the maximum static load. Gaps were always on the order of 0.001" (0.025 mm). When gaps occurred with the 16 ply specimens, out-of-plane vibrations were observed at the local areas where the gaps existed. However, there was no coincidence between the location of a "light gap" and the formation of the first delamination or of catastrophic failure. Therefore, buckling may have had little if anything to do with the failure of the 16 ply specimens. It should be noted, though, that the 16 ply specimens did not exhibit the substantial delamination splitting as did the 32 and 64 ply specimens. Finally, the antibuckling constraints did not prevent delaminations from growing through the specimen width. So the specimens were apparently not over-constrained.

The antibuckling guides for the notched geometry provided full face constraint except at the test section where windows were located. The size of these windows were optimized in a previous study by Phillips [3]. The specimen damage was confined to the test section and did not extend into the region where the face plates were in contact with the specimen. Therefore, the antibuckling guide did not interfere with the normal damage development of the specimens. Only the 16 ply specimens exhibited out-of-plane motion in the test section region. This vibratory deflection was obvious to the touch and visible by light reflection off the smooth face. It was observably small in magnitude but no attempt was made to actually measure the magnitude. This probably did not effect the test results because the fatigue lives of the 16 ply specimens were essentially the same as the 32 ply specimens where no out-of-plane motion was observed.

7.0 SUMMARY AND CONCLUSIONS

A test program has been conducted in which the effect of specimen thickness on the fatigue lives of quasi-isotropic, graphite-epoxy laminates was investigated. Three replicate specimens for each notched and unnotched geometry at 16, 32 and 64 ply thicknesses of a $[90/45/0/-45]_{ns}$ laminate and a $[45/0/-45/90]_{ns}$ laminate were tested in compression-compression fatigue. The fatigue life and the initiation, type and progression of damage was determined in each test. The damage was determined by enhanced x-rays, edge replication, and visual observations. Specially designed antibuckling fixtures prevented out-of-plane motion. The interlaminar stress distributions at the straight, free edge of both unnotched laminate types were utilized to interpret the test results. The interlaminar normal stress, σ_z, was a function of the laminate thickness. The Pipes and Pagano approximation [1] was used to compute the interlaminar normal stress at each thickness. The interlaminar normal stress was halved when the laminate thickness was doubled by doubling the number of multiples of the repeated stacking sequence and also doubling the applied load. The maximum stress occurred at the laminate midplane. The $[90/45/0/-45]_{ns}$ laminate had tensile interlaminar normal stresses while the $[45/0/-45/90]_{ns}$ laminate had compressive stresses under an applied compressive load. The τ_{xz} and τ_{yz} shear stress distributions were generated by a quasi-three dimensional finite element analysis. The τ_{xz} shear stress was the largest in magnitude of the three stress components and had the same magnitude and algebraic sign for both laminates. Neither shear stress was a function of the laminate thickness. Provided below is a list of the test results and conclusions:

1. NOTCHED SPECIMEN TEST RESULTS:

   (a) At a maximum stress of -38 ksi (262 MPa), R = 10, the notched specimen lines were between 5×10^3 and 1×10^5 cycles.

   (b) There was essentially no difference in the fatigue lives of the two laminates.

   (c) There was no strong thickness effect although the highest lives belonged to the 64 ply specimens and the lowest lives belonged to the 16 ply specimens.

   (d) The damage was localized around the hole and spread out across the specimen width adjacent to the hole. Damage tended to accumulate near the surface of both faces.

   (e) The stress concentration effect at the hole dominates over the interlaminar stresses in precipitating damage and failure.

2. UNNOTCHED SPECIMEN TEST RESULTS:

   (a) The $[90/45/0/-45]_{ns}$ laminate was tested at a maximum stress of -48 ksi (331 MPa), R = 10. The 32 ply and 64 ply specimens exhibited lives between 5×10^5 cycles and 1×10^6 cycles. The 16 ply specimen lives were between 1×10^3 and 2×10^4 cycles.

   (b) The $[45/0/-45/90]_{ns}$ laminate was tested at a maximum stress of -60 ksi (414 ksi), R = 10. The 16 ply and 32 ply specimens exhibited lives between 1.5×10^4 and 1.7×10^5 cycles while the 64 ply specimens exhibited lives between 1.4×10^5 cycles and 3.1×10^5 cycles.

   (c) The damage was predominantly delaminations which began at the edge, progressed along the specimen length, then through the width and along the adjacent edge. Multiple interior delaminations, always at similar interfaces, also opened and grew in a

similar manner to the outermost delamination which opened first.

(d) There was a strong correlation between the interlaminar stress distributions and the formation of delaminations. The τ_{xz} shear stress was found to be the dominant interlaminar stress. Delaminations formed at the interface where τ_{xz} was a maximum. Delaminations form more easily when the interlaminar normal stress is high tensile ($[90/45/0/-45]_{ns}$ laminate) and the τ_{xz} shear stress is high, but delaminations also form when the τ_{xz} shear stress is high and the interlaminar normal stress is compressive ($[45/0/-45/90]_{ns}$ laminate).

3. The antibuckling fixtures for both specimen types were effective in preventing specimen buckling. In neither case did the fixture over-constrain the specimen and interfere or influence the formation and progression of damage.

4. Removal of the specimen from the test fixture for examination and reinstallation does not appear to influence the test results.

5. Enhanced x-ray and edge replication form a good nondestructive examination team for defining fatigue damage when edge effects dominate. Specimen sectioning is probably necessary to define through-the-thickness damage of notched specimens, although edge x-rays are helpful.

REFERENCES

1. Pagano, N. J. and Pipes, R. B., "Interlaminar Stresses in Composite Laminates Under Uniform Axial Extension," Journal of Composite Materials, Vol. 4, 1970, pp. 538-548.

2. Rooney, M. and Herakovich, C. T., "An Approximate Method for Optimizing Stacking Sequence in the Presence of Edge Effects," Technical Report VPI-E-83-32, Virginia Polytechnic Institute and State University, Blacksburg, VA. (To be published.)

3. Phillips, E. P., "Effects of Truncation of a Predominantly Compression Load Spectrum on the Life of a Notched Graphite/Epoxy Laminate," NASA Technical Memorandum 80114, Hampton, VA, 1979.

4. Stalnaker, D. O. and Stinchcomb, W. W., "An Investigation of Edge Damage Development in Quasi-Isotropic Graphite Epoxy Laminates," Technical Report VPI-E-77-24, Virginia Polytechnic Institute and State University, Blacksburg, VA, Sept. 1977.

5. Herakovich, C. T., Nagarkar, A., and O'Brien, D. A., "Failure Analysis of Composite Laminates with Free Edges," in Modern Developments in Composite Materials and Structures, J. R. Vinson, Ed., The American Society of Mechanical Engineers, Dec. 1979, pp. 53-66.

6. Black, N. F. and Stinchcomb, W. W., "Compression Fatigue Damage in Thick, Notched Graphite Epoxy Laminates," presented at the Conference on Long-Term Behavior of Composites, Williamsburg, VA, American Society for Testing and Materials, March 1982.

7. Whitney, J. M. and Kim, R. Y., "Effect of Stacking Sequence on the Notched Strength of Laminated Composites," in Composite Materials: Testing and Design (Fourth Conference), ASTM STP 617, American Society for Testing and Materials, 1977, pp. 229-242.

8. Ryder, J. T. and Lauraitis, K. N., "Effect of Load History on Fatigue Life," Air Force Wright Aeronautical Laboratories Report, AFWAL-TR-81-4155, 1981.

9. Stalnaker, D. O. and Stinchcomb, W. W., "Load History-Edge Damage Studies in Two Quasi-Isotropic Graphite Epoxy Laminates," in Composite Materials: Testing and Design (Fifth Conference), ASTM STP 647, American Society for Testing and Materials, 1979, pp. 620-641.

10. Whitcomb, J. D., "Experimental and Analytical Study of Fatigue Damage in Notched Graphite/Epoxy Laminates," NASA Technical Memorandum 80121, Hampton, VA, 1979.

TABLE 1. UNNOTCHED SPECIMEN PRELIMINARY TEST RESULTS

SPEC. ID	OUTER PLY ANGLE	NUMBER OF PLIES	AVERAGE THICKNESS in.(mm)	MAX NOMINAL STRESS ksi(MPa)	CYCLES AT FAILURE x1000	REMARKS
FU2	45	64	0.333 (8.458)	60.0 (414)	143.4	No End Effects[1]
FU22	90	64	0.334 (8.484)	60.0 (414)	15.0	No End Effects
FU15	90	64	0.335 (8.509)	50.0 (345)	238.5	No End Effects
FU5	45	64	0.336 (8.534)	59.6 (411)	2.0	Failure End Generated
FU14	90	64	0.335 (8.509)	59.7 (412)	1.7	Failure End Generated
FU3	45	64	0.336 (8.534)	53.7 (370)	9.0	Failure End Generated
FU21	90	64	0.333 (8.458)	45.0 (310)	90	Failure End Generated
FU4	45	32	0.165 (4.191)	60.0 (414)	173.0	
FU2	45	32	0.165 (4.191)	40.0 (276)	100 DNF	Major Delaminations Both Ends
FU14	90	32	0.163 (4.140)	40.0 (276)	100 DNF	Major Delaminations Both Ends
FU19	90	32	0.164 (4.166)	45.0 (310)	0.8	Top End Crushed
FU10	45	32	0.165 (4.191)	45.0 (310)	150 DNF	C-Clamp Top, Del. at Bottom Only
FU4	45	32	0.165 (4.191)	48.0 (331)	150 DNF	No End Effects
FU4	45	32	0.165 (4.191)	55.0 (379)	160 DNF	No End Effects
FU?	90	16	0.0827 (2.101)	60.0 (414)	-----	Static Failure at 60 ksi
FU18	90	16	0.084 (2.134)	60.0 (414)	-----	Static Failure at 49 ksi
FU6	45	16	0.0822 (2.088)	55.0 (379)	157 DNF	No End Effects
				60.0 (414)	18.7	No End Effects
FU4	45	16	0.0833 (2.116)	60.0 (414)	42.2	No End Effects
FU10	45	16	0.0827 (2.101)	60.0 (414)	133.0	No End Effects
FU12	90	16	0.0831 (2.111)	55.0 (379)	1.7	Cracked Under Static Load
FU22	90	16	0.0824 (2.093)	55.0 (379)	1.4	Failure at Max Load Range
FU13	90	16	0.0823 (2.090)	50.0 (345)	2.8	Cracked at Static Load (47 ksi)

NOTES: [1]No End Effects means both ends are constrained by C-clamps and delaminations occur away from the ends.

TABLE 2. NOTCHED SPECIMEN PRELIMINARY TEST RESULTS

SPEC ID	OUTER PLY ANGLE	NUMBER OF PLIES	AVERAGE THICKNESS in.(mm)	MAX NOMINAL STRESS ksi(MPa)	CYCLES AT FAILURE x1000	REMARKS
F3	45	64	0.325 (8.255)	39.8 (274)	82.5	Failure in Test Section
F5	45	64	0.331 (8.407)	39.4 (272)	25.0	Bottom End Crushed
F14	90	64	0.338 (8.585)	38.4 (265)	102.7	Bottom End Crushed
F21	90	64	0.335 (8.509)	40.0 (276)	27.8	Failure in Test Section
F2	45	32	0.163 (4.140)	39.8 (274)	40.4	Bottom End Crushed
F10	45	32	0.165 (4.191)	39.3 (271)	26.8	Bottom End Crushed
F14	90	32	0.1645 (4.178)	40.0 (276)	22.1	Failure in Test Section
F19	90	32	0.164 (4.166)	40.0 (276)	28.3	Failure in Test Section
F4	45	16	0.0826 (2.098)	40.0 (276)	2.33	Failure in Test Section
F6	45	16	0.0823 (2.090)	35.0 (241)	161.5	Failure in Test Section
F11	90	16	0.0824 (2.093)	40.0 (276)	7.58	Failure in Test Section
F18	90	16	0.0831 (2.111)	40.0 (276)	0.87	Failure at Max Load

TABLE 3. UNNOTCHED SPECIMEN STRAIN GAGE
ALIGNMENT DATA[1,2]

SPECIMEN ID	NUMBER PLY THICKNESS	MEAN STRAIN $(-1389\mu)^2$	% IN-PLANE VAR	% THICKNESS VAR	% ELEVATION VAR
FU?	64	-1480	3.2	2.6	11.2
FU8	64	-1374	6.6	2.3	6.6
FU9	64	-1509	5.7	1.9	14.4
FU17	64	-1349	3.8	1.7	38.0
FU19	64	-1530	1.9	2.6	12.7
FU18	64	-1424	7.6	1.8	19.2
FU17	32	-1252	11.7	1.0	25.4
FU18	32	-1528	6.8	1.5	1.4
FU16	32	-1422	8.3	1.2	26.5
FU7	32	-1364	14.5	3.4	11.4
FU9	32	-1553	3.1	2.2	18.3
FU?	32	-1598	0.5	1.8	25.8
FU19	16	-1489	9.9	9.5	2.0
FU17	16	-1341	6.4	7.0	11.0
FU16	16	-1331	1.7	3.3	4.9
FU9	16	-1391	19.1	2.5	19.0
FU6	16	-1195	4.7	0.3	13.0
FU7	16	-1432	15.0	2.5	24.5

NOTE: [1]Gages are 350 Ohms ±0.3% with a gage factor of 2.075 ±0.5%.

[2]Percentages are calculated at the load equivalent to (-1389μ), i.e. 3500 lbs (15.57 KN) for 64 plies, 1750 lbs (7.78 KN) for 32 plies and 875 lbs (3.89 KN) for 16 plies.

TABLE 4.   NOTCHED SPECIMEN STRAIN GAGE
ALIGNMENT DATA[1,2]

SPECIMEN ID	NUMBER OF PLIES	MEAN[2] (-1389μ)	% IN-PLANE VARIATION	% THICKNESS VARIATION
F7	64	-1430	18.0	0.3
F8	64	-1510	21.0	3.9
F9	64	-1460	18.2	2.5
F17	64	-1516	12.5	0.8
F18	64	-1420	16.5	N.A.
F19	64	-1409	11.7	2.4
F7	32	-1450	24.2	1.6
F8	32	-1469	19.2	1.5
F9	32	-1442	11.8	2.1
F17	32	-1459	16.4	8.0
F16	32	-1570	N.A.	20.0
F18	32	-1585	14.2	0.0
F8	16	-1261	15.8	N.A.
F?	16	-1282	N.A.	N.A.
F??	16	-1486	13.1	N.A.
F16	16	-1401	23.0	N.A.

N.A. => Not Available, gages did not function properly.

NOTES: [1]Gages are 350 Ohms ±0.3% with a gage factor of 2.085 ±0.5%.

[2]Percentages are calculated at the load equivalent to -1389 μ,
i.e., 7000 lbs (31.1 KN) for 64 plies, 3500 lbs (15.57 KN) for
32 plies and 1750 lbs (7.78 KN) for 16 plies.

TABLE 5. STRAIN GAGE ALIGNMENT VALUES FOR
SPECIMENS IN DUAL POSITIONS

SPECIMEN ID	MEAN STRAIN[1] (-1389μ)	% IN-PLANE VARIATION	% THICKNESS VARIATION	% ELEVATION VARIATION
FU19	-1530	1.9	2.6	12.7
	-1549	10.2	1.5	11.8
FU9	-1325	12.8	1.9	27.5
	-1335	6.7	0.8	23.8
FU8	-1327	1.9	1.2	8.5
	-1374	6.6	2.3	6.6
FU?	-1480	3.2	2.6	11.2
	-1500	1.7	4.0	12.2
FU9	-1509	5.7	1.9	14.4
	-1343	6.4	1.9	19.4
FU18	-1433	21.4	2.5	30.0
	-1332	6.0	0.9	24.3

NOTE: [1]The mean strain and percent variations are calculated at the load
corresponding to -1389 μ, i.e., 3500 lbs (15.57 KN) for 64 plies,
1750 lbs (7.78 KN) for 32 plies and 875 lbs (3.89 KN) for 16
plies.

TABLE 6. STRAIN GAGE ALIGNMENT VALUES TAKEN
AT SEVERAL DAYS INTERVALS

SPECIMEN ID	MEAN STRAIN[1] (-1389μ)	% IN-PLANE VARIATION	% THICKNESS VARIATION	% ELEVATION VARIATION
F7	-1450	24.2	1.6	N.A.[2]
	-1412	19.4	1.7	N.A.
F8	-1469	19.2	1.5	N.A.
	-1440	19.0	1.6	N.A.
FU8	-1374	6.6	2.3	6.6
	-1434	4.4	2.2	2.0
FU18	-1433	21.4	2.5	30.0
	-1387	20.0	1.2	18.7

NOTES: [1]The mean strain and percent variations are calculated at the
load corresponding to -1389 μ, i.e for unnotched: 3500 lbs
(15.57 KN) for 64 plies, 1750 lbs (7.78 KN) for 32 plies, and
875 lbs (3.89 KN) for 16 plies; notched: 7000 lbs (31.1 KN) for
64 plies, 3500 lbs (15.57 KN) for 32 plies, and 1750 lbs (7.78
KN) for 16 plies.

[2]N.A. means not available.

TABLE 7. NOTCHED SPECIMEN PRODUCTION TEST DATA
FOR THE $[45/0/-45/90]_{ns}$ LAMINATE

SPEC. ID	NUMBER OF PLIES	AVERAGE THICKNESS in.(mm)	CYCLES AT FAILURE	REMARKS
F2	16	0.0827 (2.10)	28,600	No x-ray Examination
F8	16	0.0827 (2.10)	5,220	x-rays
F11	16	0.0825 (2.096)	1,040	Cracked at Static Load
F8	32	0.164 (4.166)	18,450	x-rays
F7	32	0.164 (4.166)	32,630	x-rays
F9	32	0.1635 (4.163)	38,350	x-rays
F7	64	0.332 (8.433)	90,850	x-rays
F9	64	0.330 (8.382)	44,120	x-rays
F8	64	0.3315 (8.446)	25,110	x-rays

NOTE: All tests were conducted at R = 10, 10 Hz and a maximum
compressive stress of 38 ksi (262 MPa).

TABLE 8. NOTCHED SPECIMEN PRODUCTION TEST DATA
FOR THE $[90/45/0/-45]_{ns}$ LAMINATE

SPEC. ID	NUMBER OF PLIES	AVERAGE THICKNESS in.(mm)	CYCLES AT FAILURE	REMARKS
F22	16	0.0827 (2.101)	37,500	No x-ray examination
F13	16	0.0822 (2.088)	17,920	x-rays
F14	16	0.0830 (2.108)	31,070	x-rays
F18	32	0.164 (4.166)	9,660	x-rays
F20	32	0.163 (4.140)	31,360	x-rays
F21	32	0.165 (4.191)	30,850	x-rays
F18	64	0.333 (8.458)	55,680	x-rays
F19	64	0.335 (8.509)	58,800	x-rays
F17	64	0.330 (8.382)	45,580	x-rays

NOTE: All tests were conducted at R = 10, 10 Hz and a maximum compressive stress of 38 ksi (262 MPa).

TABLE 9. UNNOTCHED SPECIMEN PRODUCTION TEST[1] DATA
FOR THE $[45/0/-45/90]_{ns}$ LAMINATE

SPEC. ID	NUMBER OF PLIES	AVERAGE THICKNESS in. (mm)	CYCLES AT FAILURE	REMARKS
FU4	16	0.0833 (2.116)	42,200	Originally a Setup[2] Test
FU10	16	0.0827 (2.101)	133,040	Originally a Setup Test
FU7	16	0.0831 (2.111)	23,290	x-rays, edge replica
FU6	16	0.0826 (2.098)	2,040	Failure Due to an Unintentional Overload
FU1	32	0.163 (4.140)	88,080	x-rays, edge replica
FU9	32	0.163 (4.140)	15,080	x-rays, edge replica
FU4	32	0.165 (4.191)	173,000	Originally a Setup Test
FU9	64	0.333 (8.458)	182,400	x-rays
FU8	64	0.334 (8.484)	309,150	x-rays
FU2	64	0.333 (8.458)	143,400	Originally a Setup Test

Note: [1]All tests were conducted at R = 10, 10 Hz and a maximum
compressive stress of 60 ksi (414 MPa).

[2]Setup test refers to the preliminary test, refer to section 4.1.

TABLE 10.   UNNOTCHED SPECIMEN PRODUCTION TEST DATA
FOR THE $[90/45/0/-45]_{ns}$ LAMINATE

SPEC. ID	NUMBER OF PLIES	AVERAGE THICKNESS in.(mm)	CYCLES AT FAILURE	REMARKS
FU16	16	0.0826 (2.098)	16,680	
FU17	16	0.0830 (2.108)	15,090	x-rays, edge replica
FU19	16	0.0824 (2.093)	1,320	Cracked at Max Static Load
FU16	32	0.161 (4.089)	511,750	x-rays, edge replica
FU18	32	0.163 (4.140)	944,000	x-rays, edge replica
FU17	32	0.164 (4.166)	739,410	x-rays, edge replica
FU18	64	0.332 (8.433)	578,200	Edge replica
FU19	64	0.332 (8.433)	738,660	x-rays, edge replica
FU17	64	0.334 (8.484)	634,830	x-rays, edge replica

NOTE: All tests were conducted at R = 10, 10 Hz and a maximum
compressive stress of 48 ksi (331 MPa).

TABLE 11. DELAMINATION SPLIT LOCATIONS[1] FOR THE
$[45/0/-45/90]_{ns}$ LAMINATES FROM EDGE REPLICAS

SPECIMEN ID	NUMBER OF CYCLES (1000's)	LOCATION OF REPLICA ALONG SPECIMEN	LOCATION OF DELAMINATIONS
FU7-16	19.7[2]		6/7 [-45/0]
	23.0		3/4 [0/45], 6/7 [-45/0]
	FAILURE		2/3 [-45/0], 3/4 [0/45], 6/7 [-45/0]
FU9-32	10[2]	Top	11/12 [0/45], 14/15 [-45/0]
	10[2]	Middle	14/15 [-45/0]
FU1-32	12[2]		14/15 [-45/0]
	30		14/15 [-45/0]
	35.8	Top	11/12 [0/45], 14/15 [-45/0]
	52	Bottom	11/12 [0/45], 14/15 [-45/0]
	75	Middle	10/11 [-45/0]
	81		10/11 [-45/0]

NOTES: [1]Interface locations are from the laminate midplane and are designated by giving the number of plies from the midplane followed by the ply fiber angle orientation.

[2]The first replica was taken immediately after the first delamination split was visible, i.e. at the initiation of macroscopic damage.

TABLE 12. DELAMINATION SPLIT LOCATIONS[1] FOR THE
[90/45/0/-45]$_{ns}$ LAMINATES FROM EDGE REPLICAS

SPECIMEN ID	NUMBER OF CYCLES (1000's)	LOCATION OF REPLICA ALONG SPECIMEN	LOCATION OF DELAMINATIONS
FU17-64	179[2]	Front, Middle	29/30 [-45/0], 30/31 [0/45] 29/30 [-45/0] on opposite face
	227	Top, Front	30/31 [0/45]
	385	Front, Middle	29/30 [-45/0], 30/31 [0/45] 29/30 [-45/0] on opposite face
	535	Top, Front	29/30 [-45/0], 30/31 [0/45] 29/30 [-45/0] on opposite face
	535	Bottom, Front	28/29 [90/-45] changes interface to 29/30 [-45/0]
	593	Middle, Back	27/28 [45/90], 29/30 [-45/0]
	593	Top, Front	25/26 [-45/0] other splits indistinguishable
	618	Top, Front	20/21 [90/-45] changes interface to 21/22 [-45/0] 24/25 [90/-45] changes interface to 25/26 [-45/0] 29/30 [-45/0] 29/30 [-45/0] on opposite face
FU18-64	185[2]		30/31 [0/45]
FU19-64	130[2]	Front, Top	30/31 [0/45] (right face)
	135	Front, Middle	29/30 [-45/0] and 30/31 [0/45] (right face)
	205	Front, Middle	same as above
	205	Back, Middle	same as above
	226	Back, Middle	25/26 [-45/0], 29/30 [-45/0] (right face) 29/30 [-45/0] on opposite face
	226	Back, Top	29/30 [-45/0] 29/30 [-45/0] on opposite face, 31/32 [45/90]
	342	Front, Middle	28/29 [90/-45] changes interface to 29/30 [-45/0]
	Failure		Major Delamination Between 1/2 [-45/0] which changes interface to the other 1/2 [-45/0]

NOTES: [1]Interface locations are from the laminate midplane and are
         designated by giving the number of plies from the midplane
         followed by the ply fiber angle orientation.

         [2]The first replica was taken immediately after the first
         delamination split was visible, i.e. at the initiation of
         macroscopic damage.

TABLE 12., CONTINUED

SPECIMEN ID	NUMBER OF CYCLES (1000's)	LOCATION OF REPLICA ALONG SPECIMEN	LOCATION OF DELAMINATIONS
FU17-16	15^2		4/5 [90/-45] changes interface to 5/6 [-45/0]
FU19-16	STATIC^2		4/5 [90/-45]
FU16-32	40^2		13/14 [-45/0]
	80		12/13 [90/-45] changes interface to 13/14 [-45/0]
	170		12/13 [90/-45] changes interface to 13/14 [-45/0]
	181		13/14 [-45/0], 14/15 [0/45] 12/13 [90/-45] changes interface to 13/14 [-45/0] opposite face
	196		9/10 [-45/0], 13/14 [-45/0] 13/14 [-45/0] opposite face
	420		9/10 [-45/0], 12/13 [90/-45] changes interface to 13/14 [-45/0] 14/15 [0/45] changes interface to 13/14 [-45/0] opposite face
FU17-32	25^2		12/13 [90/-45] changes interface to 13/14 [-45/0]
	36		12/13 [90/-45] changes interface to 13/14 [-45/0] 13/14 [-45/0] opposite face
	167		10/11 [0/45], 12/13 [90/-45] changes interface to 13/14 [-45/0]
	681	Front	10/11 [0/45], 13/14 [-45/0] 14/15 [0/45]
	681	Back	7/8 [45/90], 9/10 [-45/0], 10/11 [0/45] 11/12 [45/90] changes to 12/13 [90/-45] changes to 13/14 [-45/0] 14/15 [0/45] on opposite face

NOTES: [1]Interface locations are from the laminate midplane and are designated by giving the number of plies from the midplane followed by the ply fiber angle orientation.

[2]The first replica was taken immediately after the first delamination split was visible, i.e. at the initiation of macroscopic damage.

TABLE 12., CONTINUED

SPECIMEN ID	NUMBER OF CYCLES (1000's)	LOCATION OF REPLICA ALONG SPECIMEN	LOCATION OF DELAMINATIONS
FU18-32	50^2		14/15 [0/45]
	176		14/15 [0/45] on opposite face 11/12 [45/90] and 14/15 [0/45] converge to 13/14 [-45/0]
	700		10/11 [0/45], 13/14 [-45/0], 14/15 [0/45] 14/15 [0/45] on opposite face

NOTES: [1]Interface locations are from the laminate midplane and are designated by giving the number of plies from the midplane followed by the ply fiber angle orientation.

[2]The first replica was taken immediately after the first delamination split was visible, i.e. at the initiation of macroscopic damage.

1.0 in.
(25.4mm)

2.0 in.
(50.8mm)

8.0 in.
(203mm)

1/4 in.
(6.23 mm)

(a) UNNOTCHED
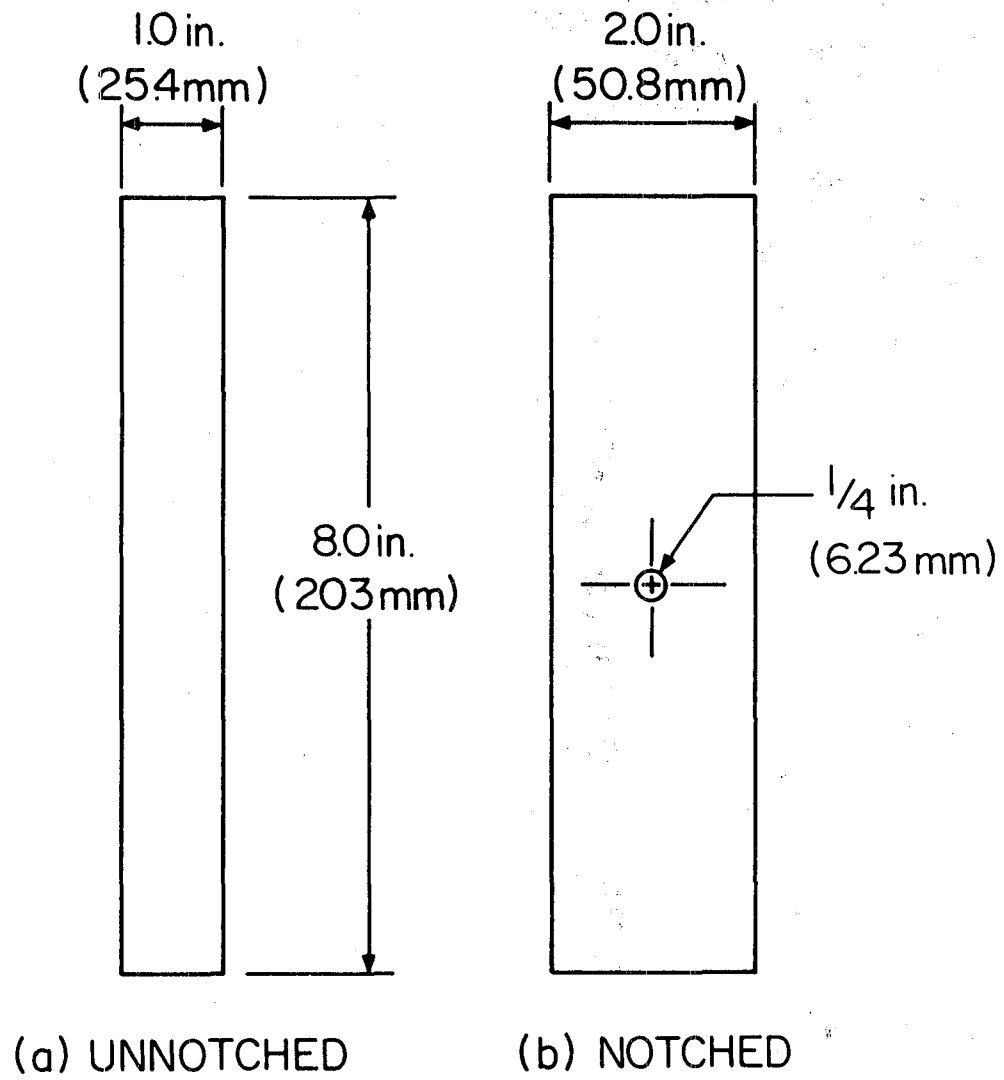
(b) NOTCHED

Figure 1 Fatigue Specimen Geometry

[45/0/-45/90]$_{ns}$
SPECIMEN
ORIENTATION

[90/45/0/-45]$_{ns}$
SPECIMEN
ORIENTATION

LAMINATE 0° FIBER DIRECTION
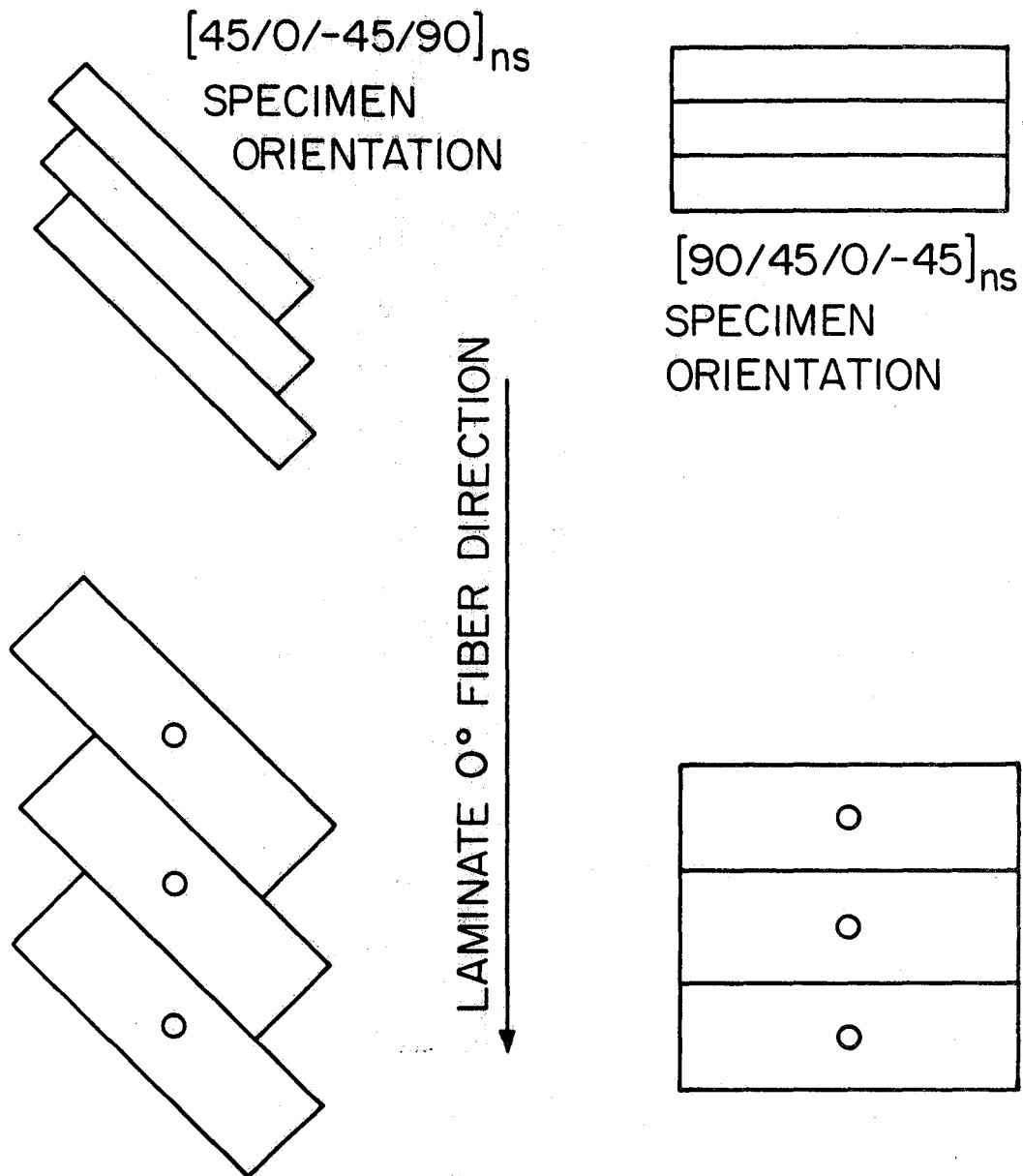
Figure 2 Laminate Schematic Showing Specimen Orientations
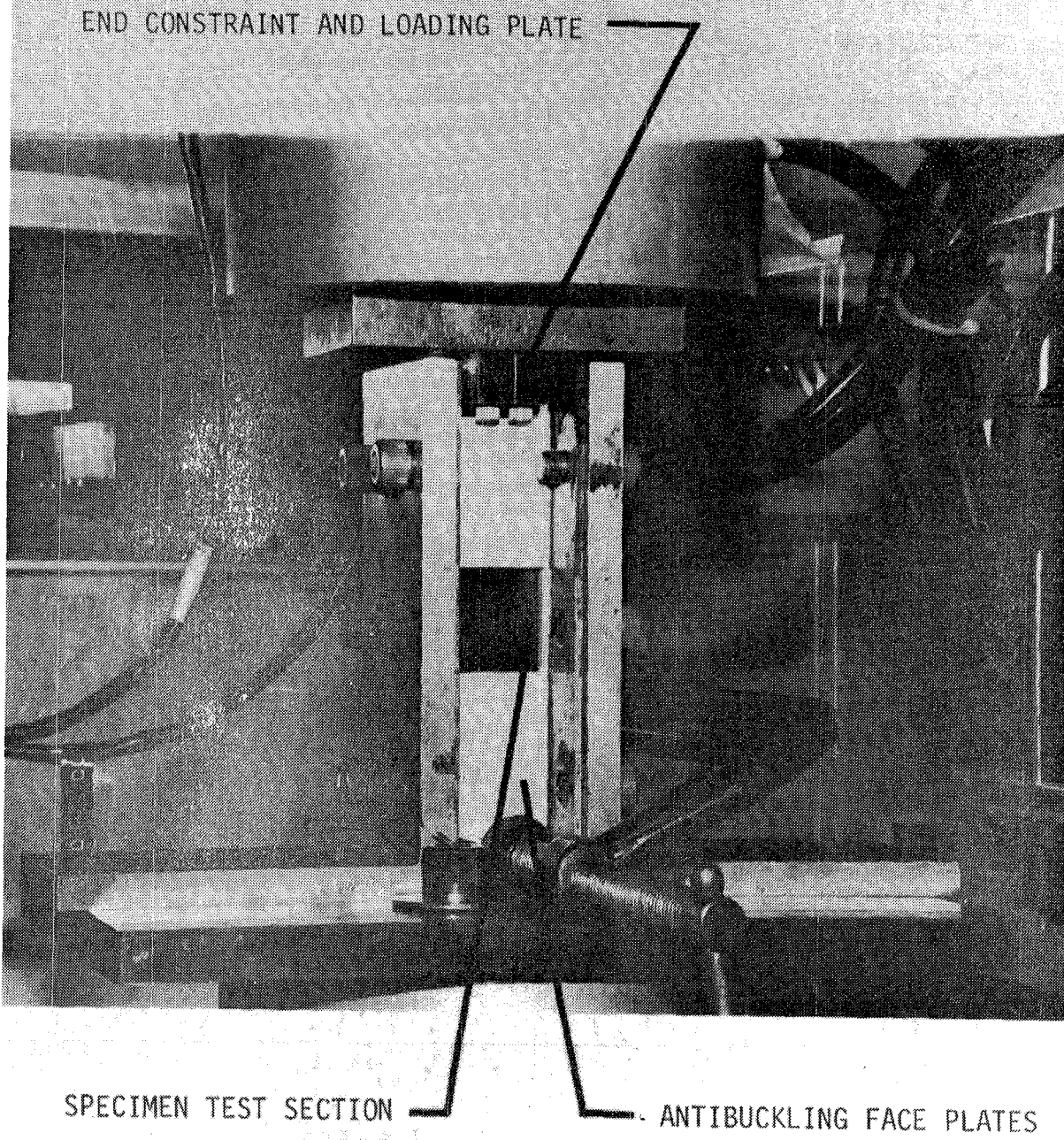
Figure 3 Notched Specimen Test Fixture
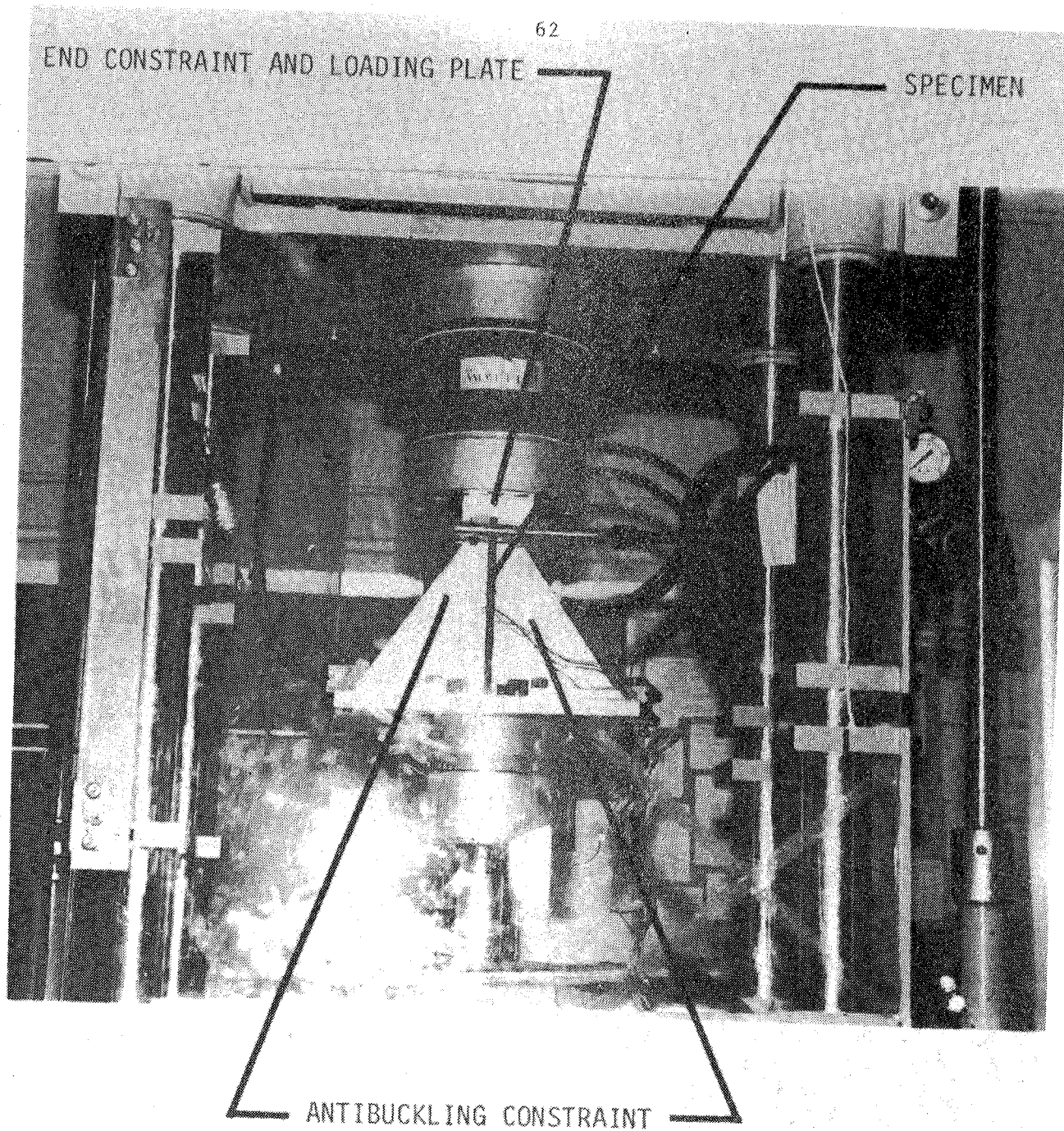
Figure 4   Unnotched Specimen Test Fixture
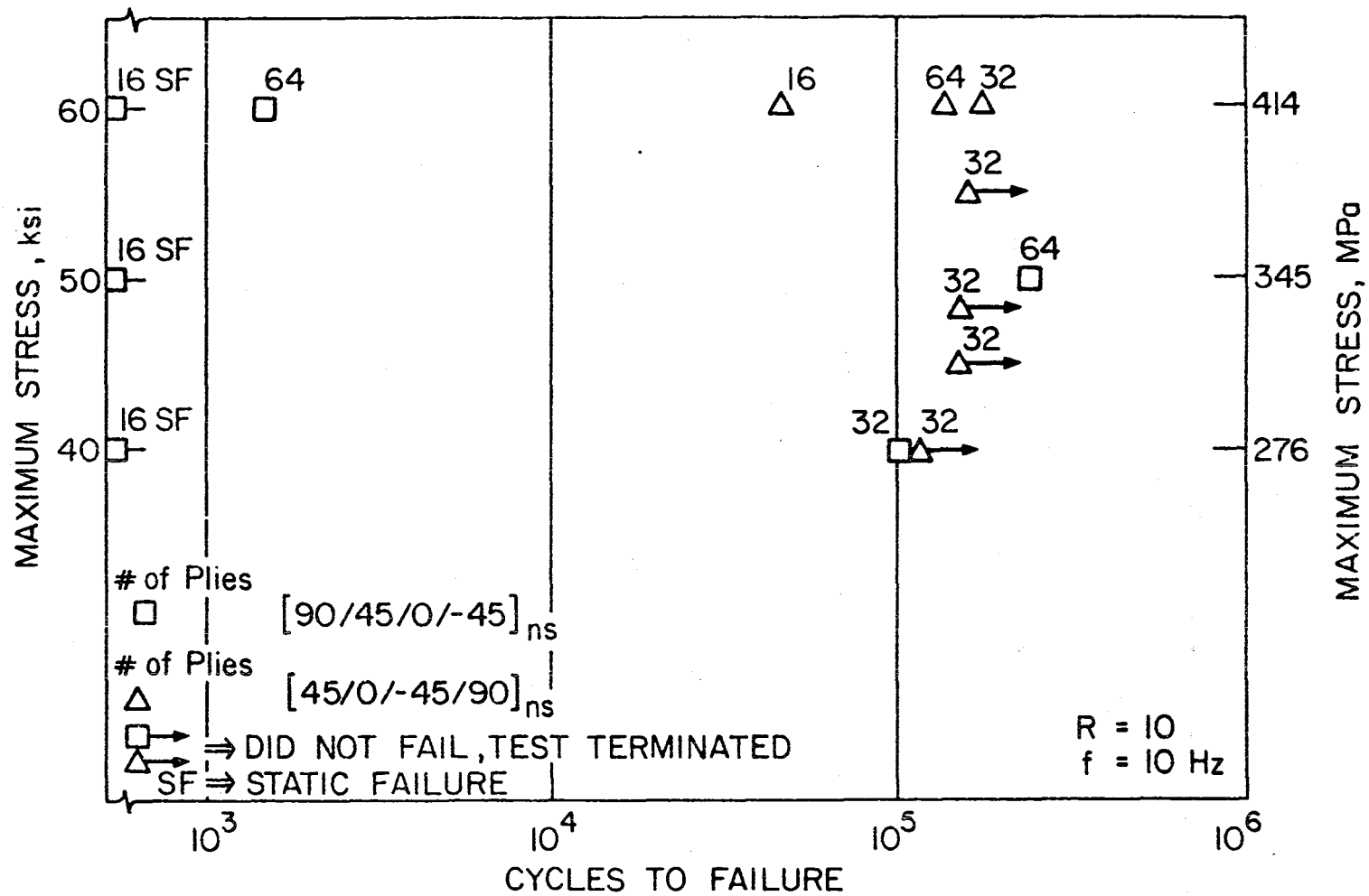
Figure 5 Partial "S-N Curves" for Unnotched
Specimens, Preliminary Test Results

FRONT SURFACE ONLY

FRONT AND BACK
SURFACE
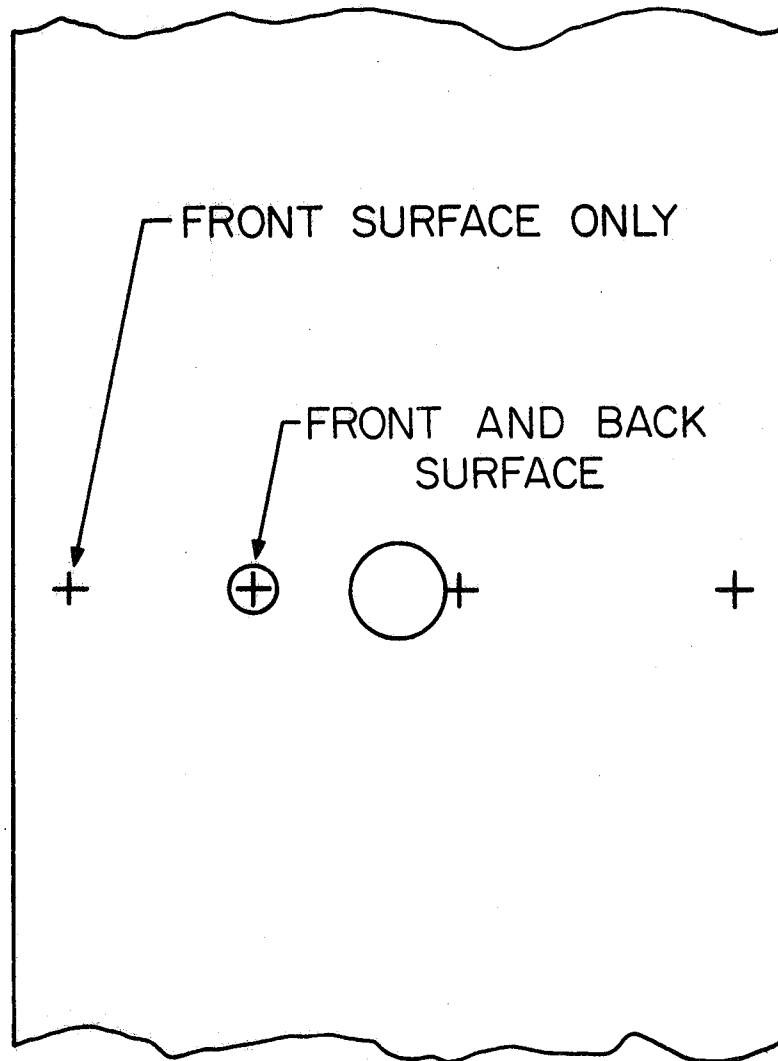
Figure 6 Notched Specimen Strain Gage Locations
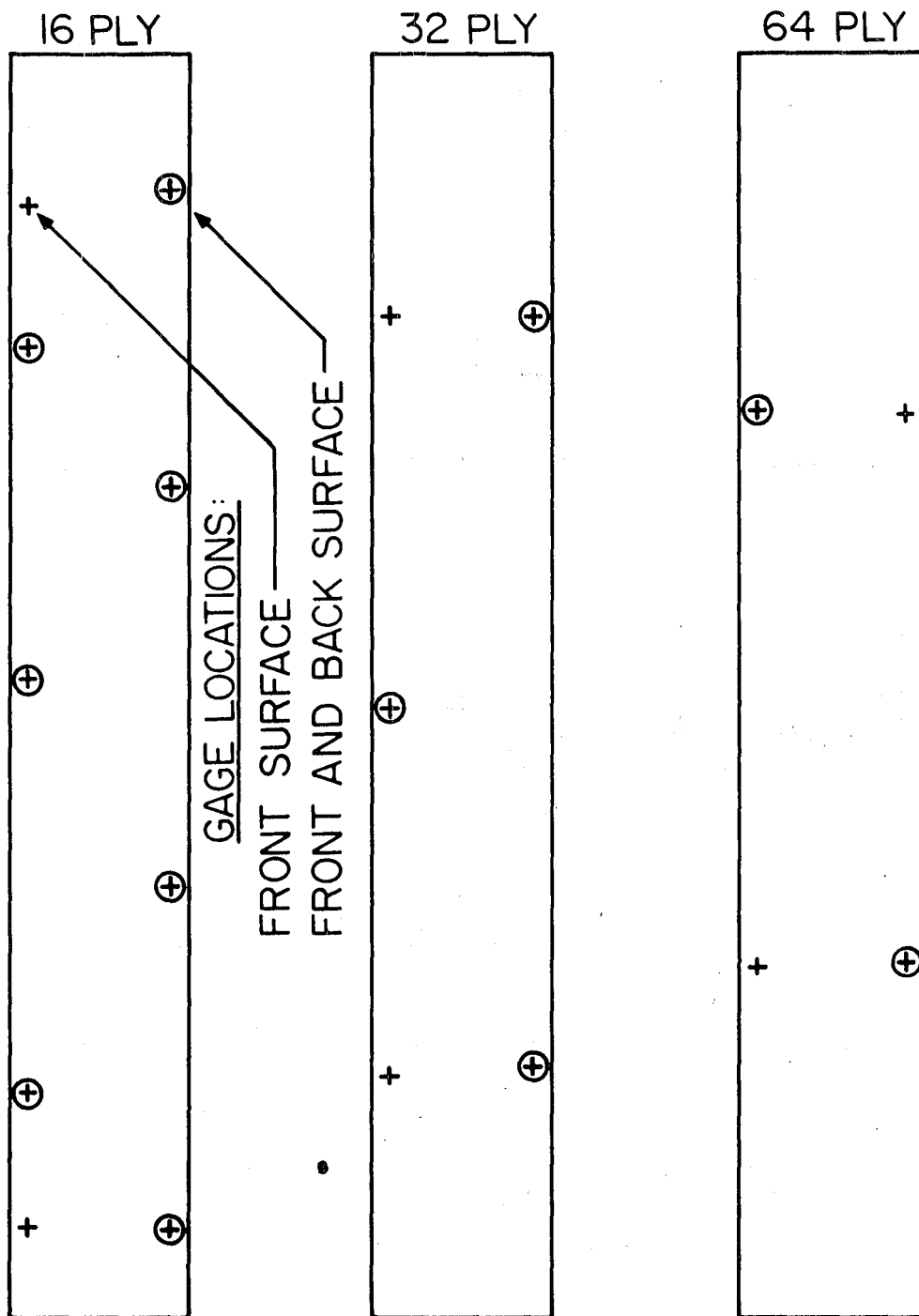
Figure 7 Unnotched Specimen Strain Gage Locations

1	4
2,3	

GAGE LOCATIONS

$E_x = 7.74 \times 10^6 \text{psi}$
(53.4 GPa)

○ GAGE 1
□ GAGE 2
△ GAGE 3 (BACK FACE)
◇ GAGE 4

COMPRESSIVE LOAD (KIPS)

COMPRESSIVE LOAD (KN)

STRAIN (MICRO in/in)
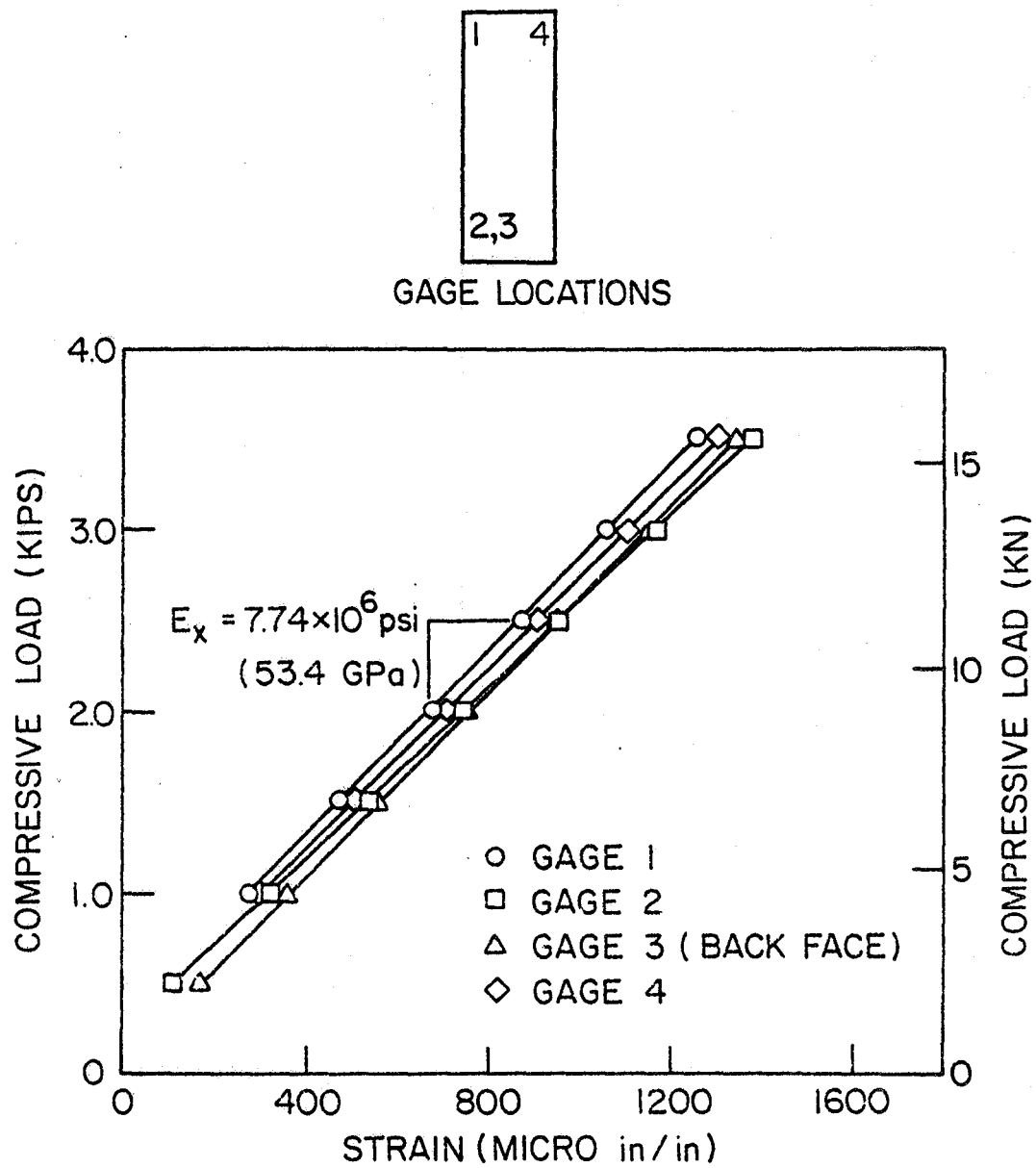
Figure 8   Typical Plot of Load Versus Strain for
an Unnotched Specimen, FU8, 64 Plies
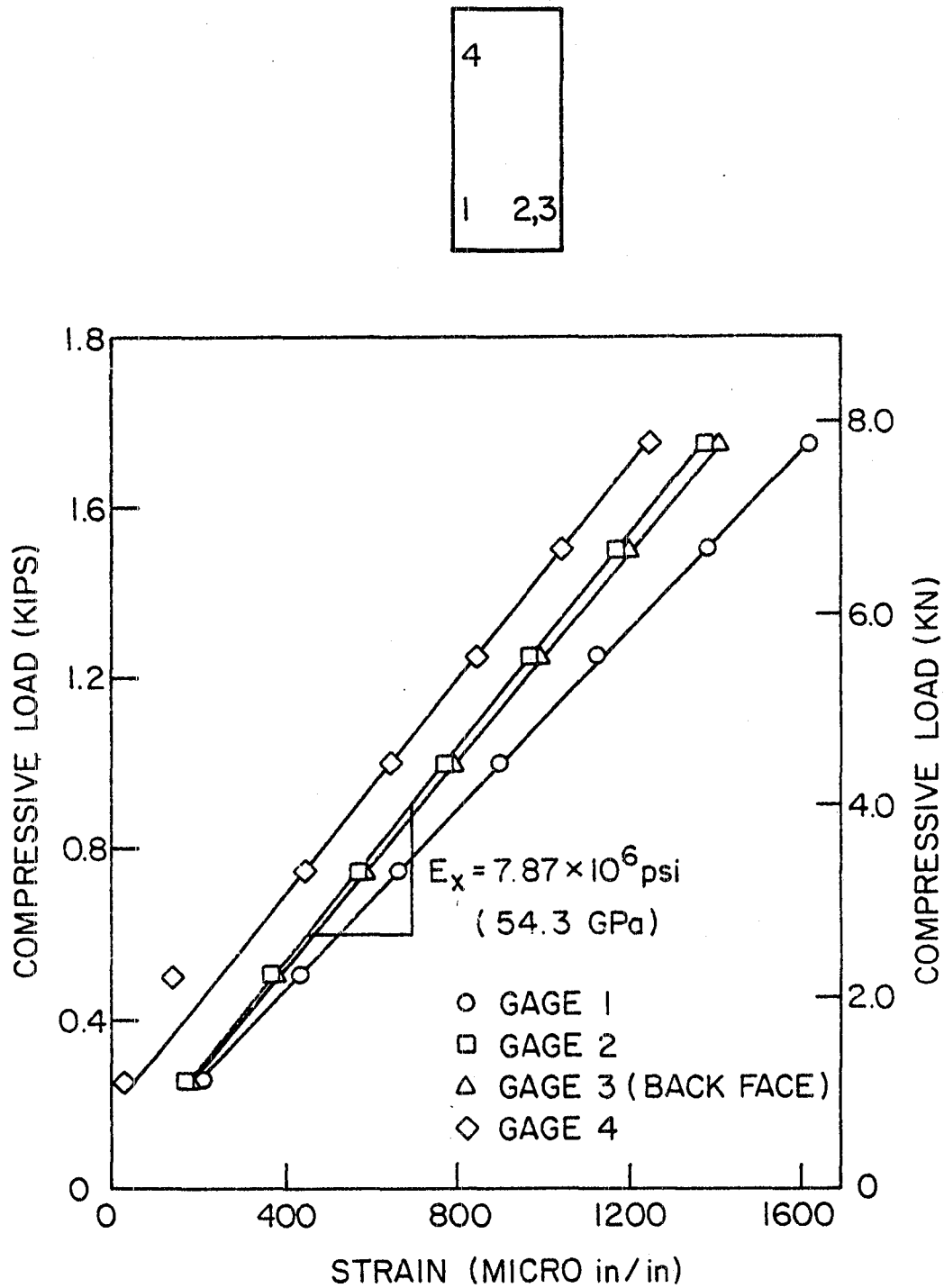
Figure 9   Typical Plot of Load Versus Strain for
an Unnotched Specimen, FU16, 32 Plies
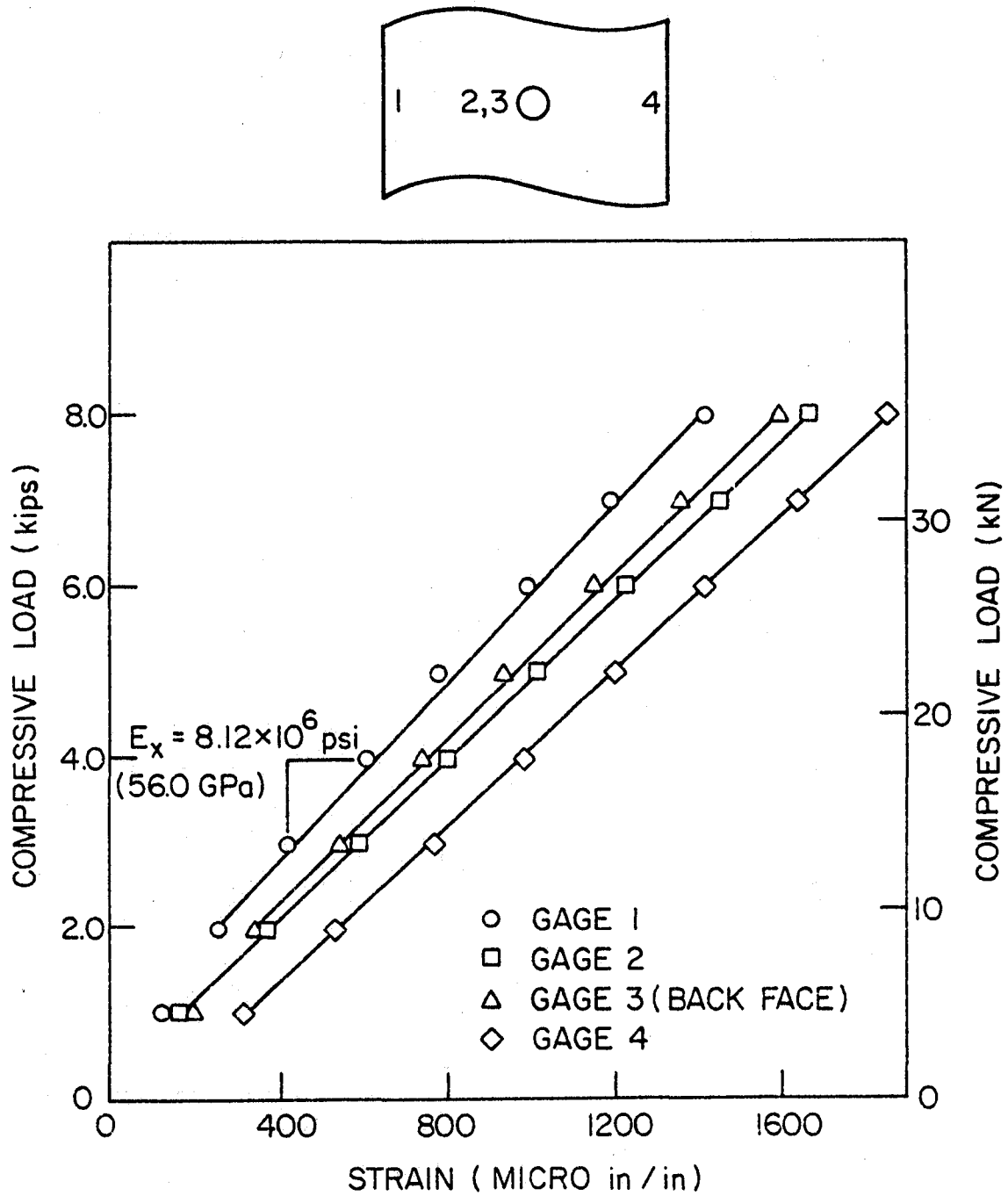
Figure 10   Typical Plot of Load Versus Strain for
a Notched Specimen, F19, 64 Plies

GAGE LOCATIONS

$E_x = 7.65 \times 10^6$ psi
(52.7 GPa)

○ GAGE 1
□ GAGE 2
△ GAGE 3
◇ GAGE 4
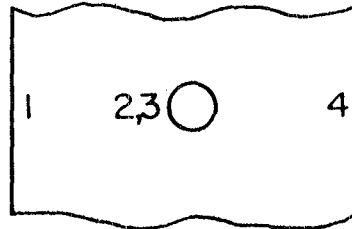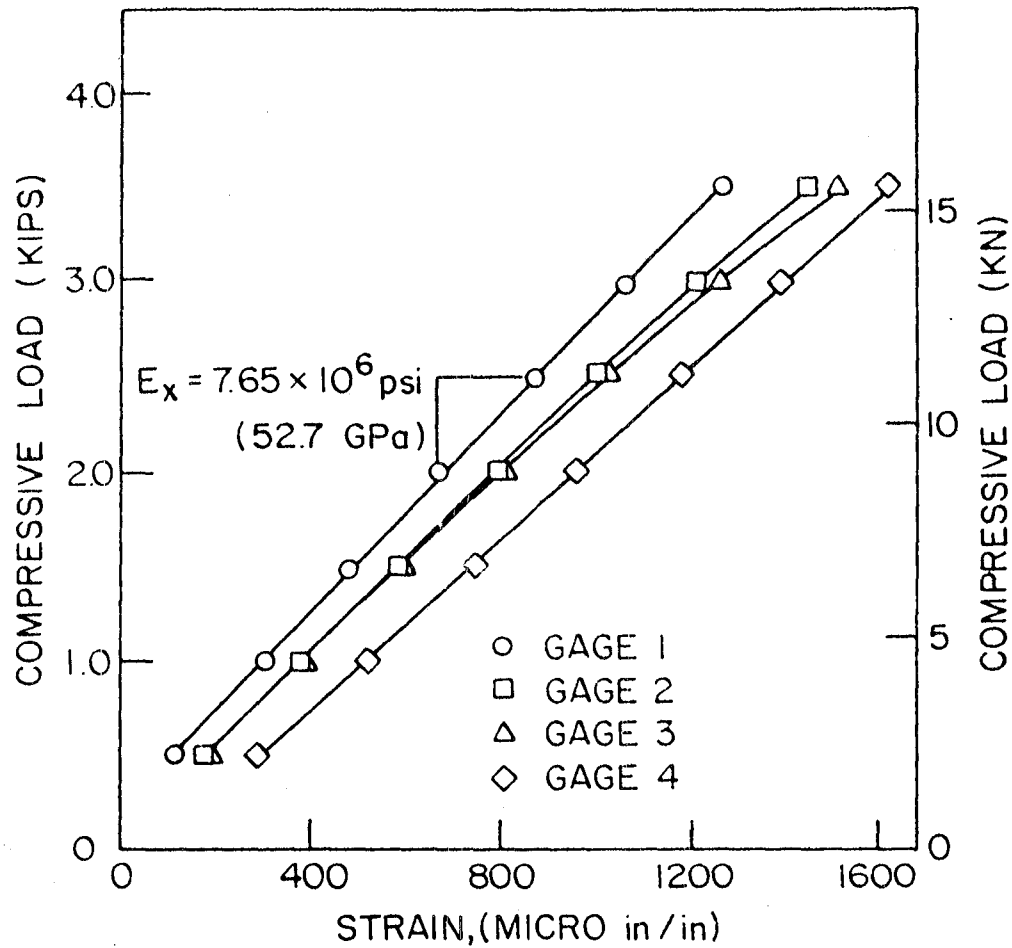
Figure 11   Typical Plot of Load Versus Strain for
a Notched Specimen, F9, 32 Plies
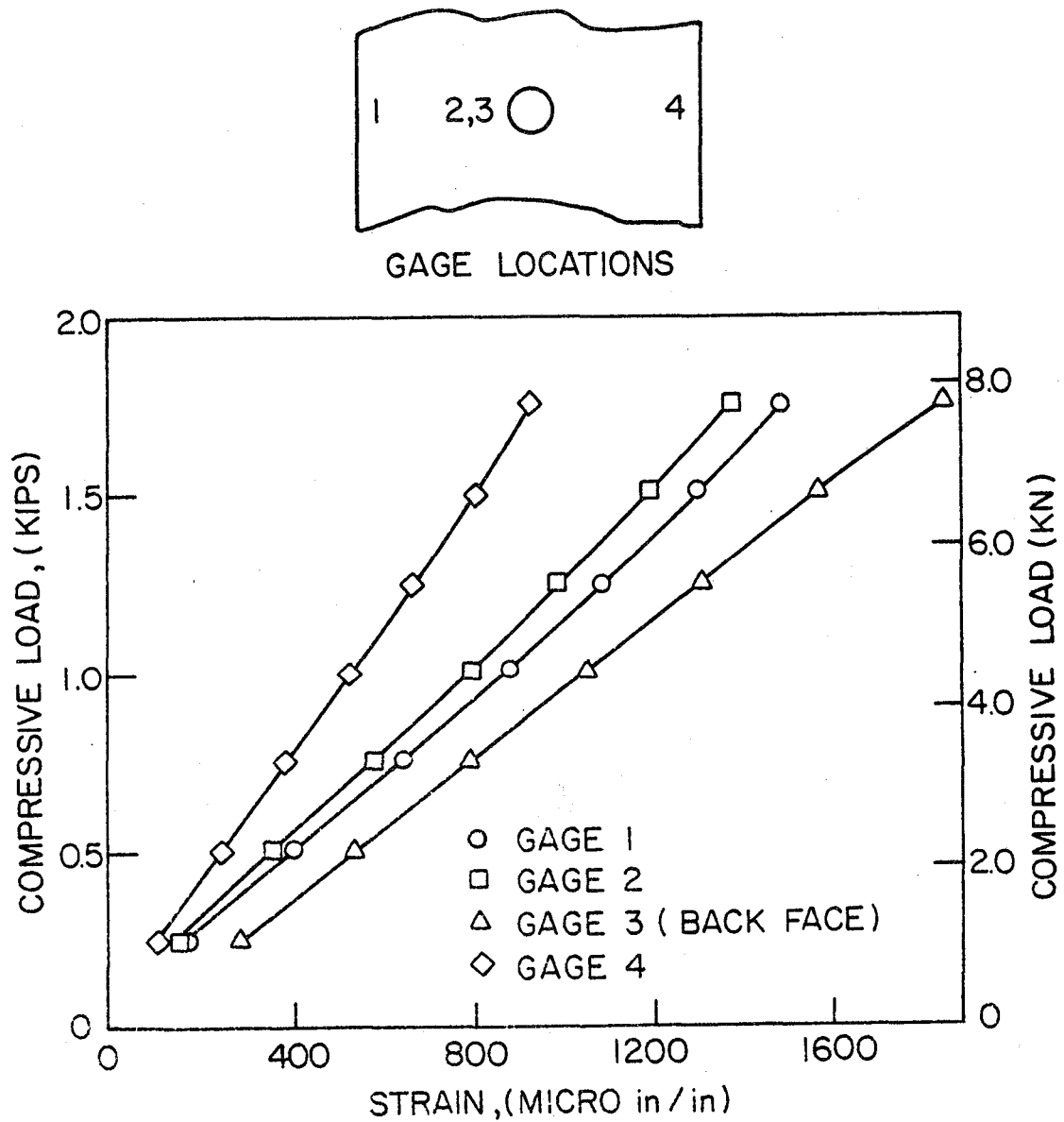
Figure 12 Plot of Load Versus Strain for
Notched Specimen F16, 16 Plies
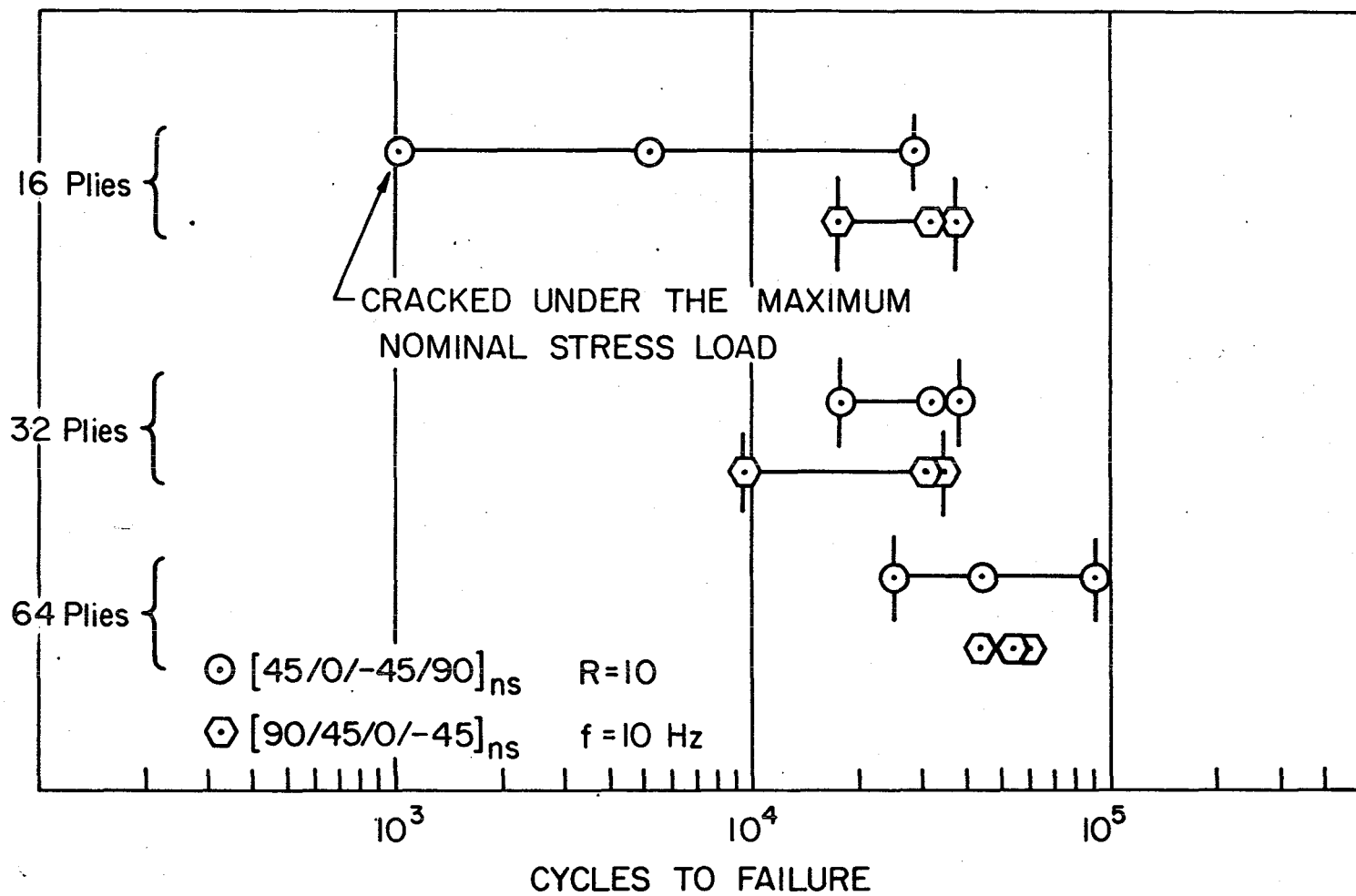
Figure 13   Fatigue Data for the Notched Specimens
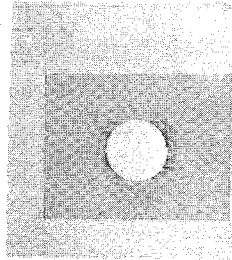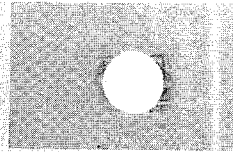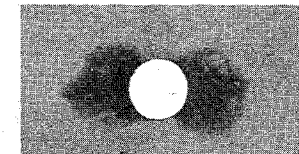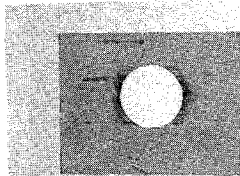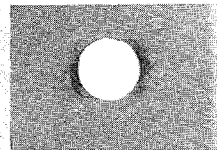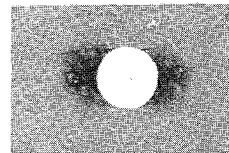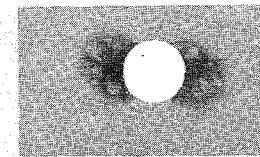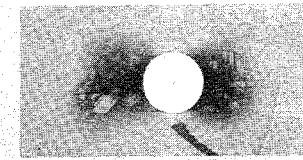
Figure 14 Progression of Damage in Two Specimens With Similar Lives
F20(31360 cycles) and F21(30850) 32 Plies 90/45/0/-45
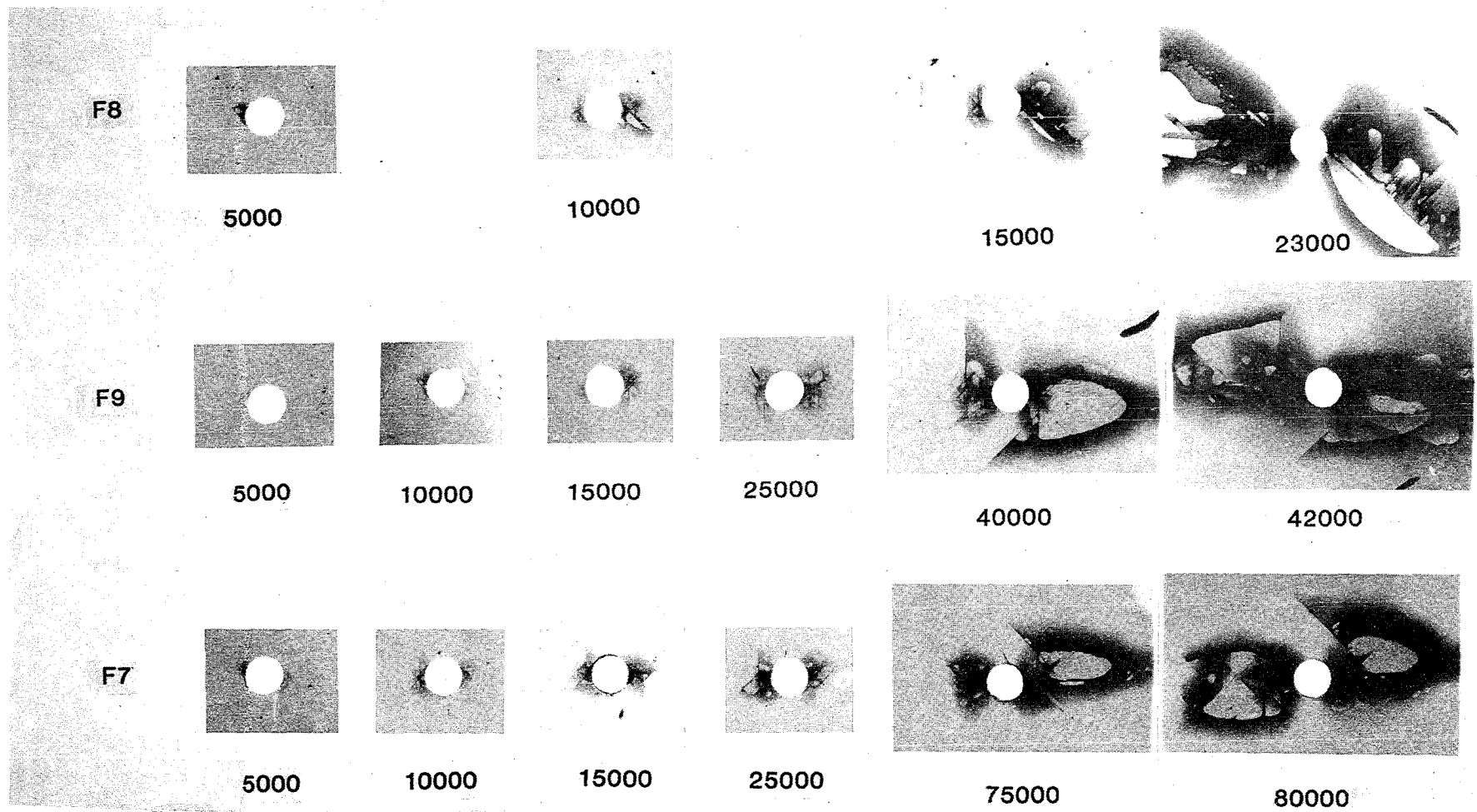
Figure 15 Progression of Damage in Three Specimens With Different Lives,
F8(25110) F9(44120) and F7(90850) 64 Plies 45/0/-45/90
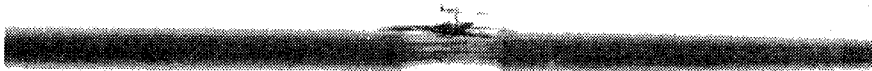
F20

F21

Figure 16   Edge View X-ray photographs of specimens F20 and F21
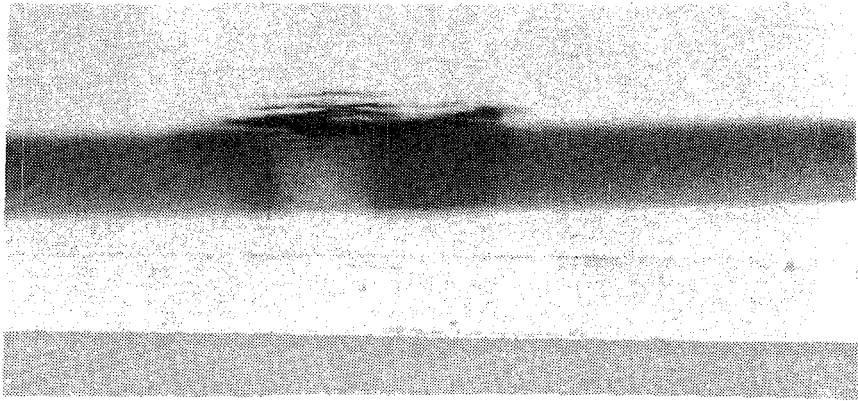
F7
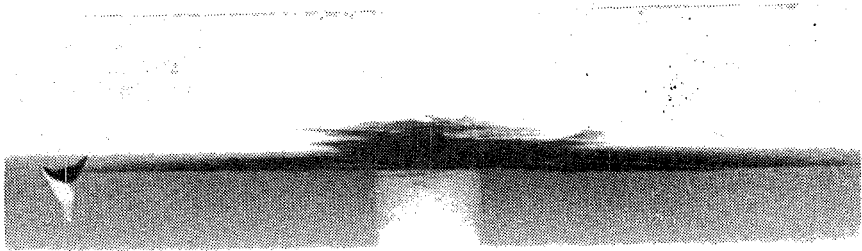
F9

Figure 17   Edge View X-ray photographs of specimens F7 and F9
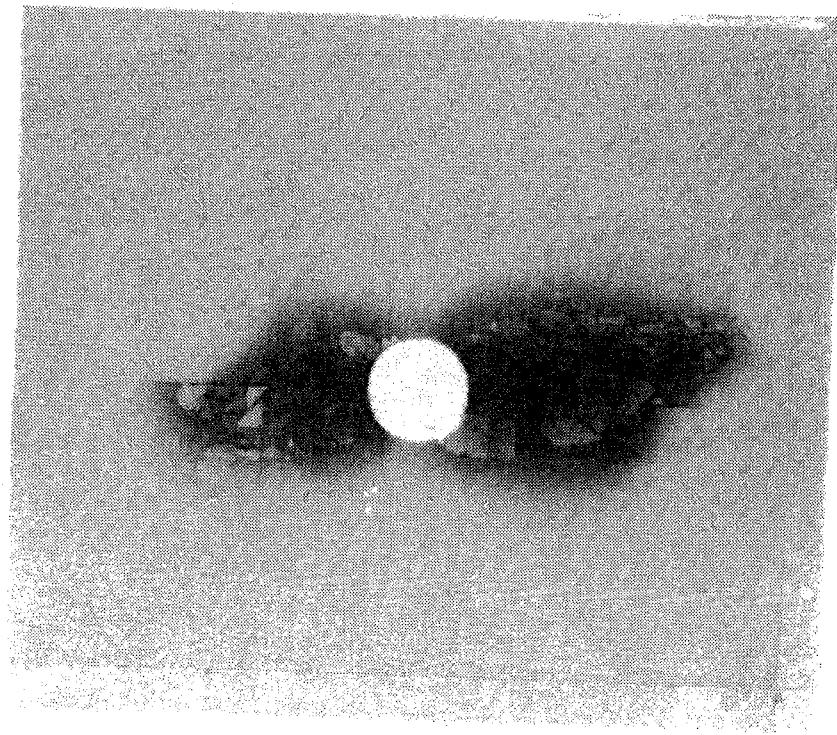
Figure 18 Damage in Specimen F17 at 98.9% of Life

$[45/0/-45/90]_{ns}$

$[90/45/0/-45]_{ns}$

$[90/45/0/-45]_{ns}$
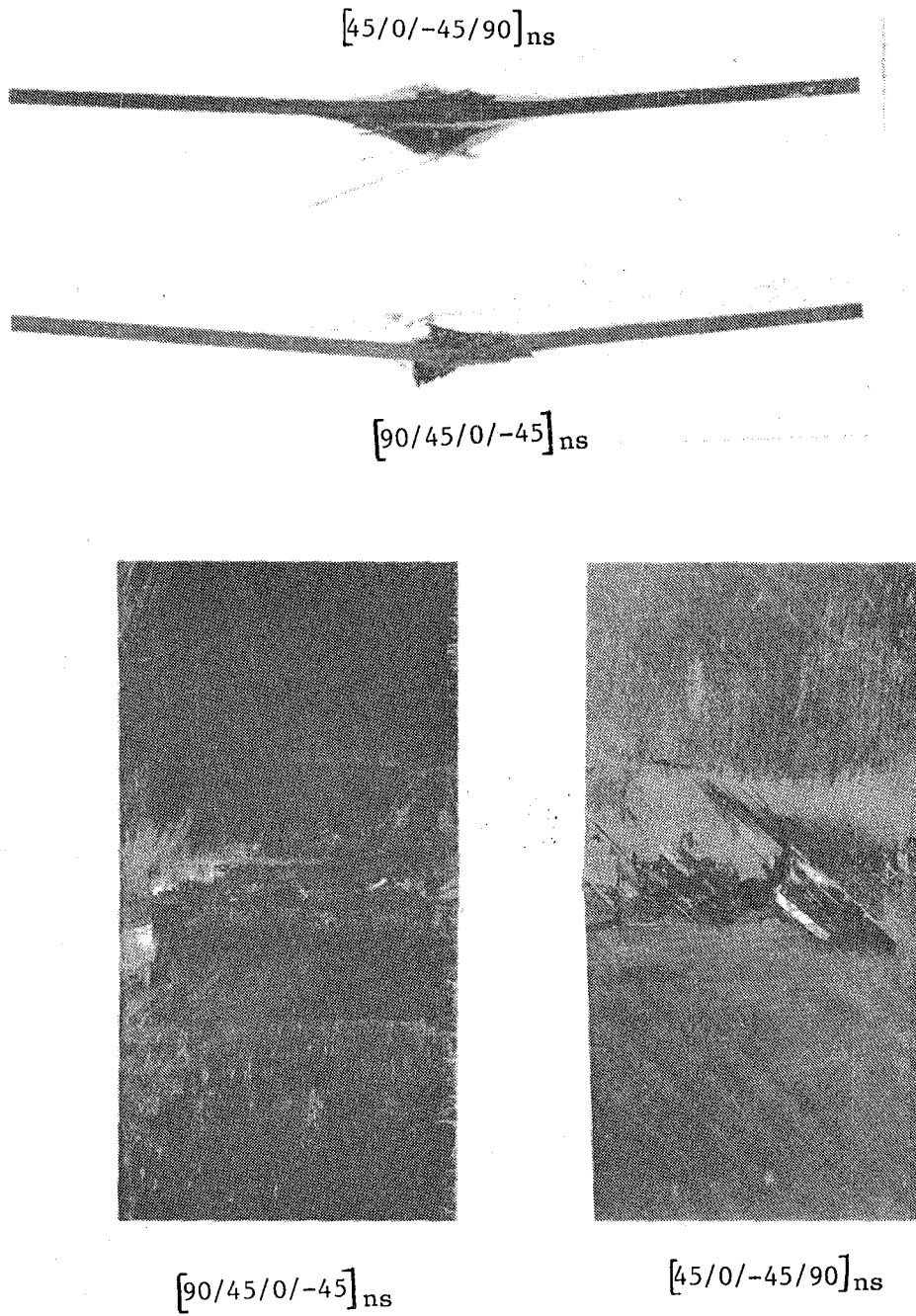
$[45/0/-45/90]_{ns}$

Figure 19   Failed 16 Ply Notched Specimens

$[90/45/0/-45]_{ns}$
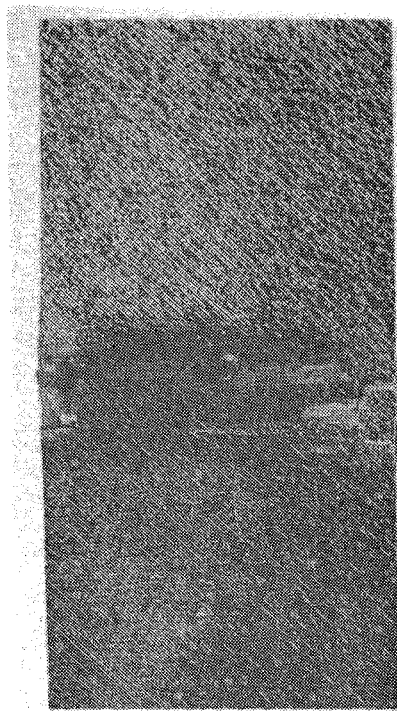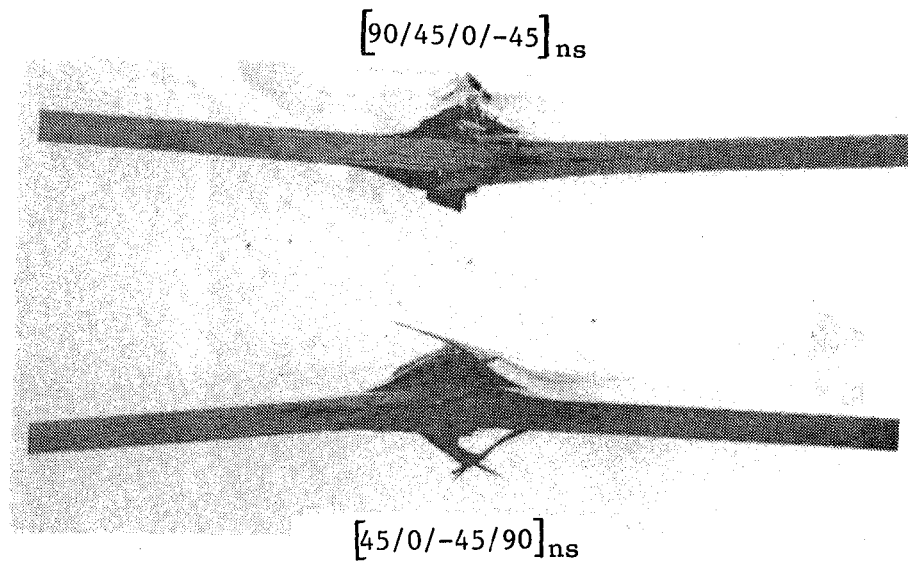
$[45/0/-45/90]_{ns}$
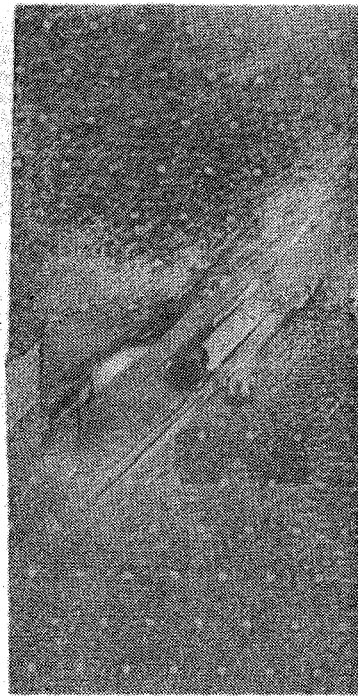
$[90/45/0/-45]_{ns}$　　　　　　$[45/0/-45/90]_{ns}$

Figure 20　Failed 32 Ply Notched Specimens
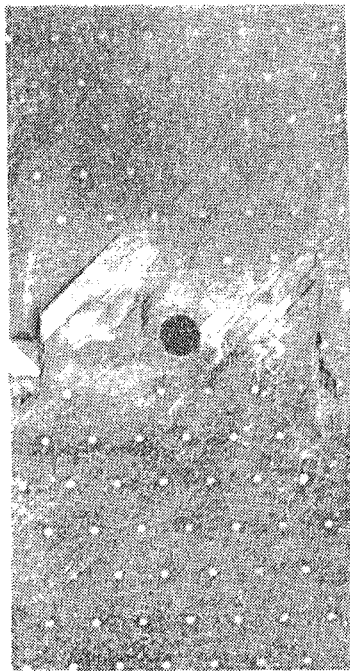
$[45/0/-45/90]_{ns}$ $[90/45/0/-45]_{ns}$

Figure 21   Failed 64 Ply Notched Specimens

$[45/0/-45/90]_{ns}$

$[90/45/0/-45]_{ns}$

$[90/45/0/-45]_{ns}$ $[45/0/-45/90]_{ns}$
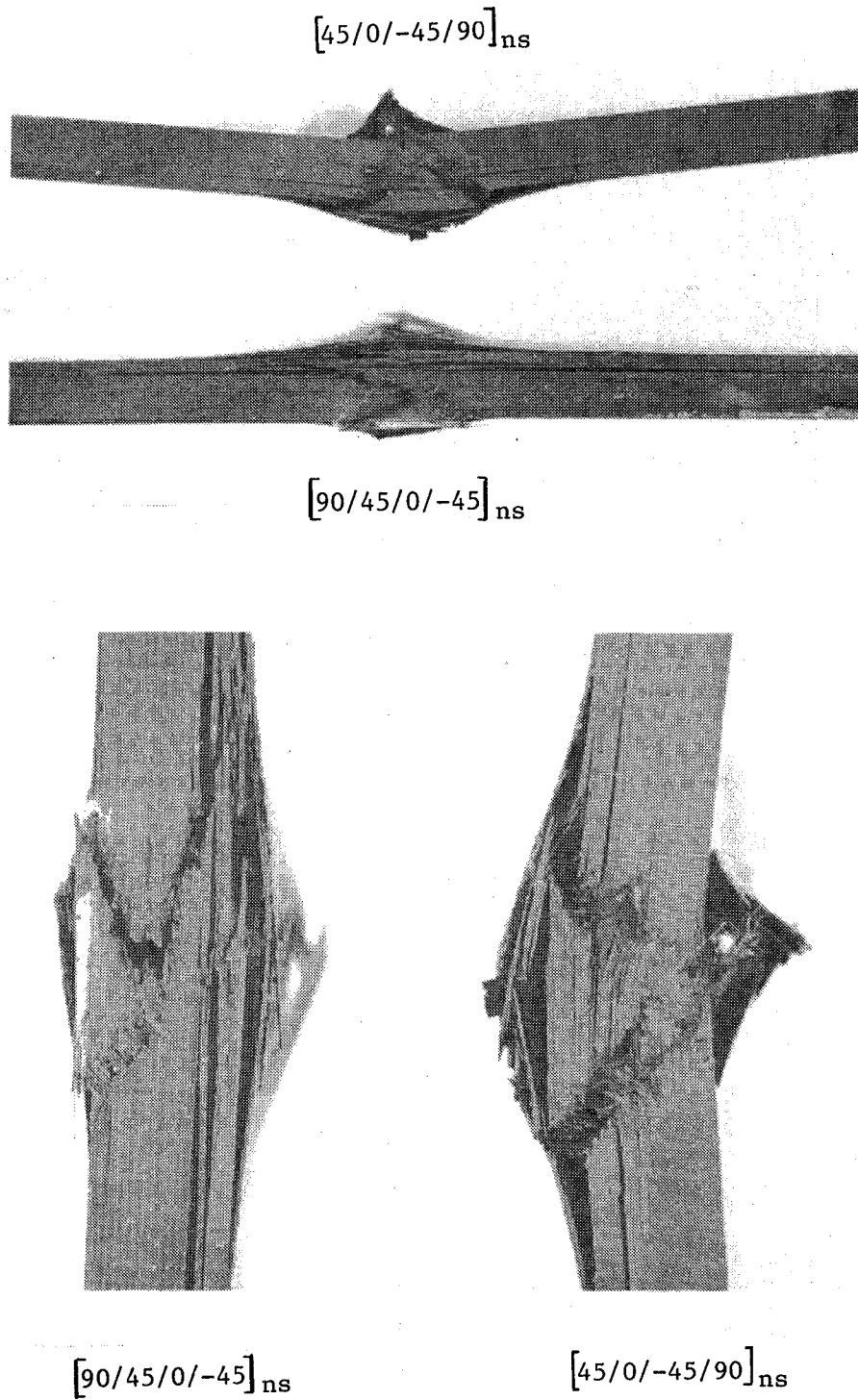
Figure 22   Failed 64 Ply Notched Specimens
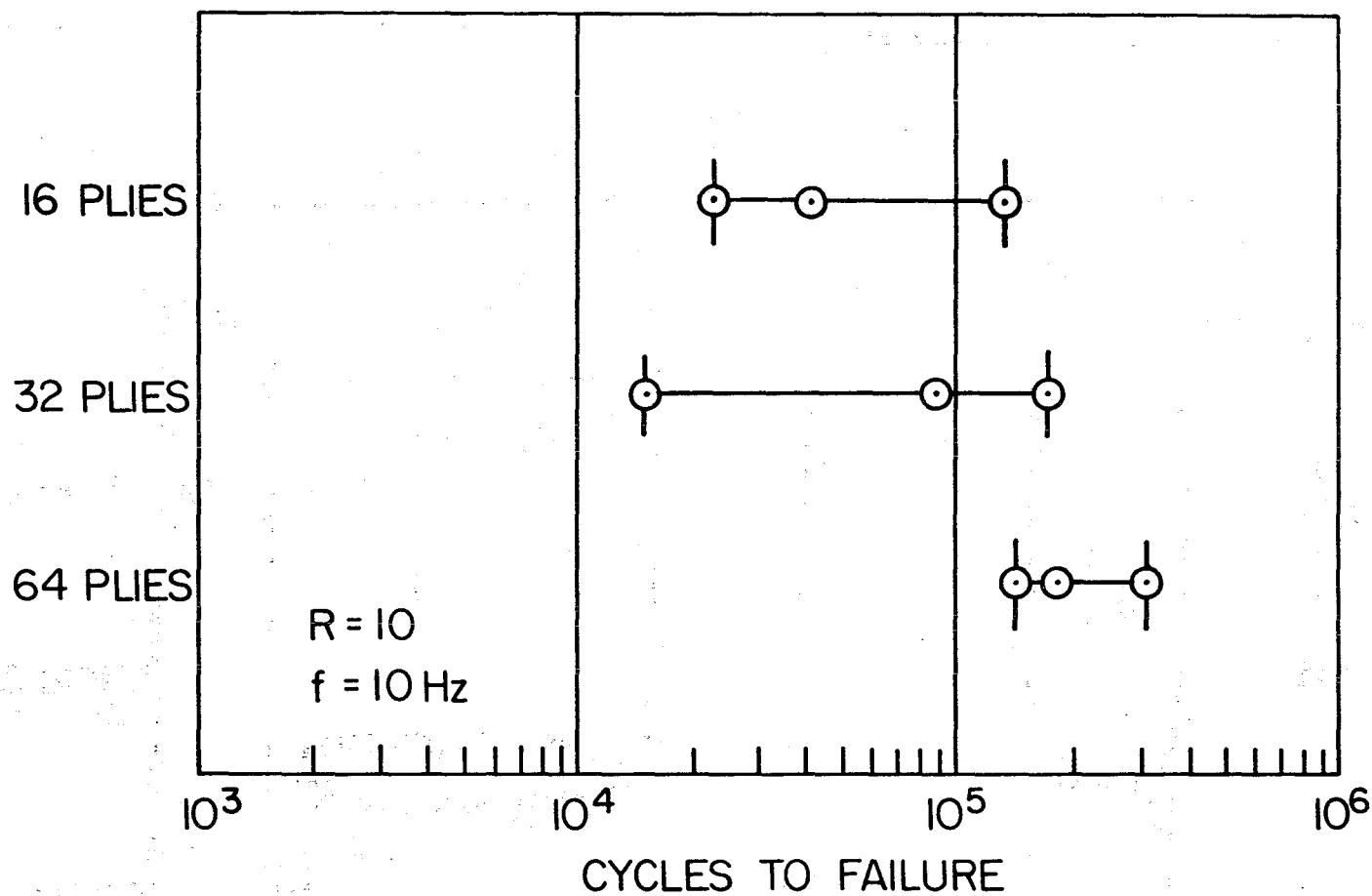
Figure 23   Data for the $[45/0/-45/90]_{ns}$ Laminate,
            Unnotched Specimens, σ = -60 ksi (-414 MPa)
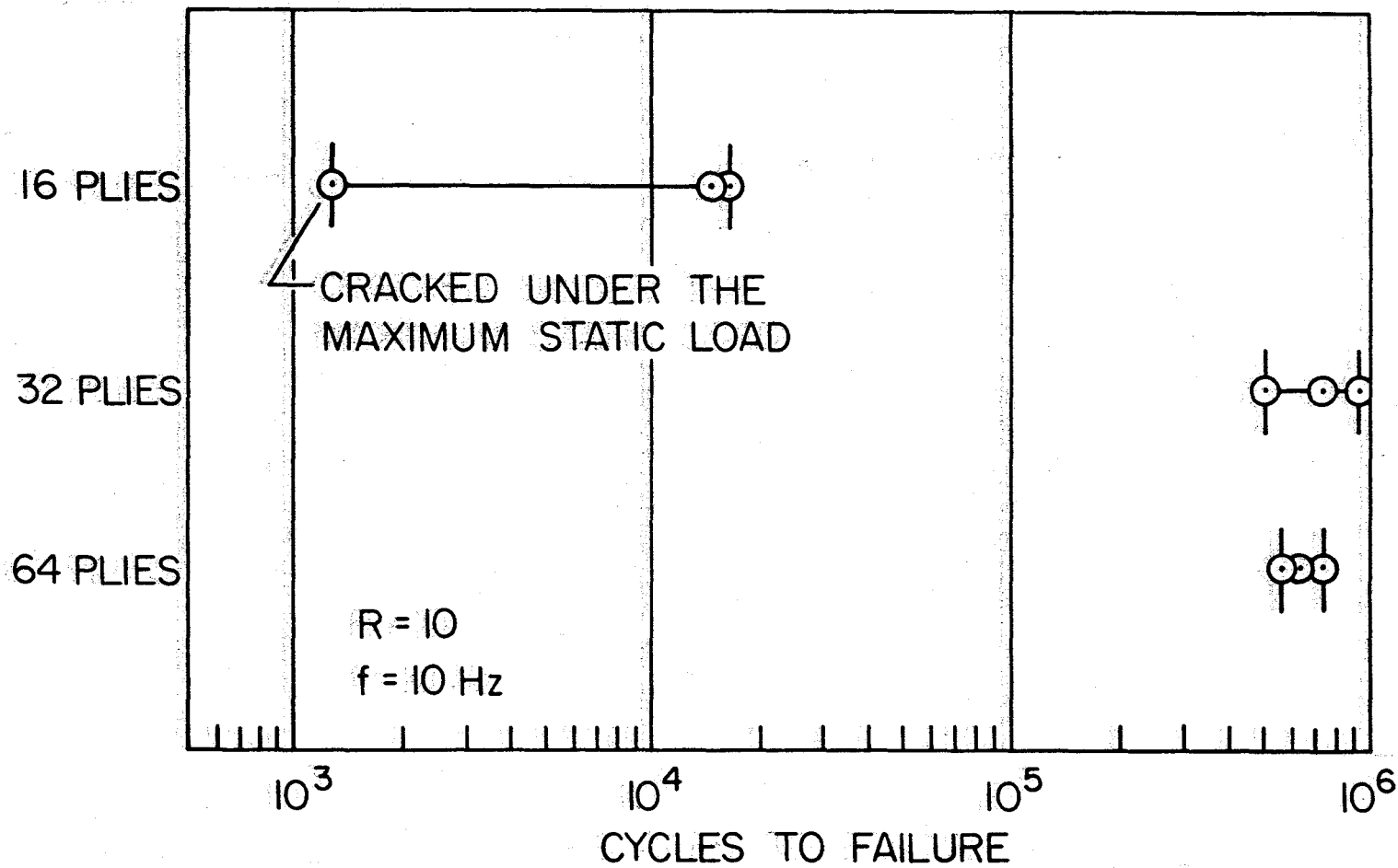
Figure 24 Data for the $[90/45/0/-45]_{ns}$ Laminate,
Unnotched Specimens, $\sigma = -48$ ksi (-330 MPa)

MATRIX CRACKS DUE TO LOCAL BUCKLING
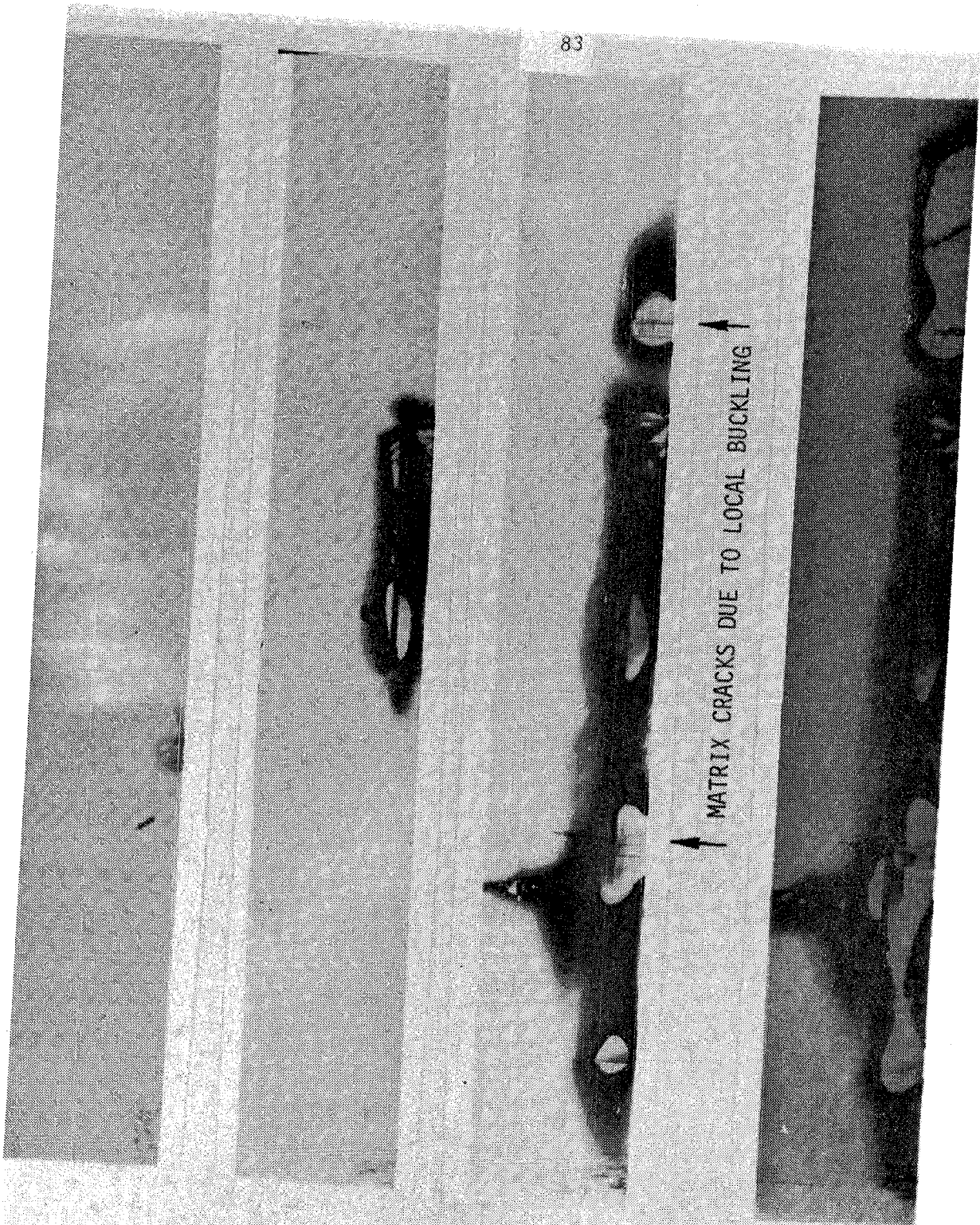
Figure 25 Progression of Delamination Damage in Specimen FU16
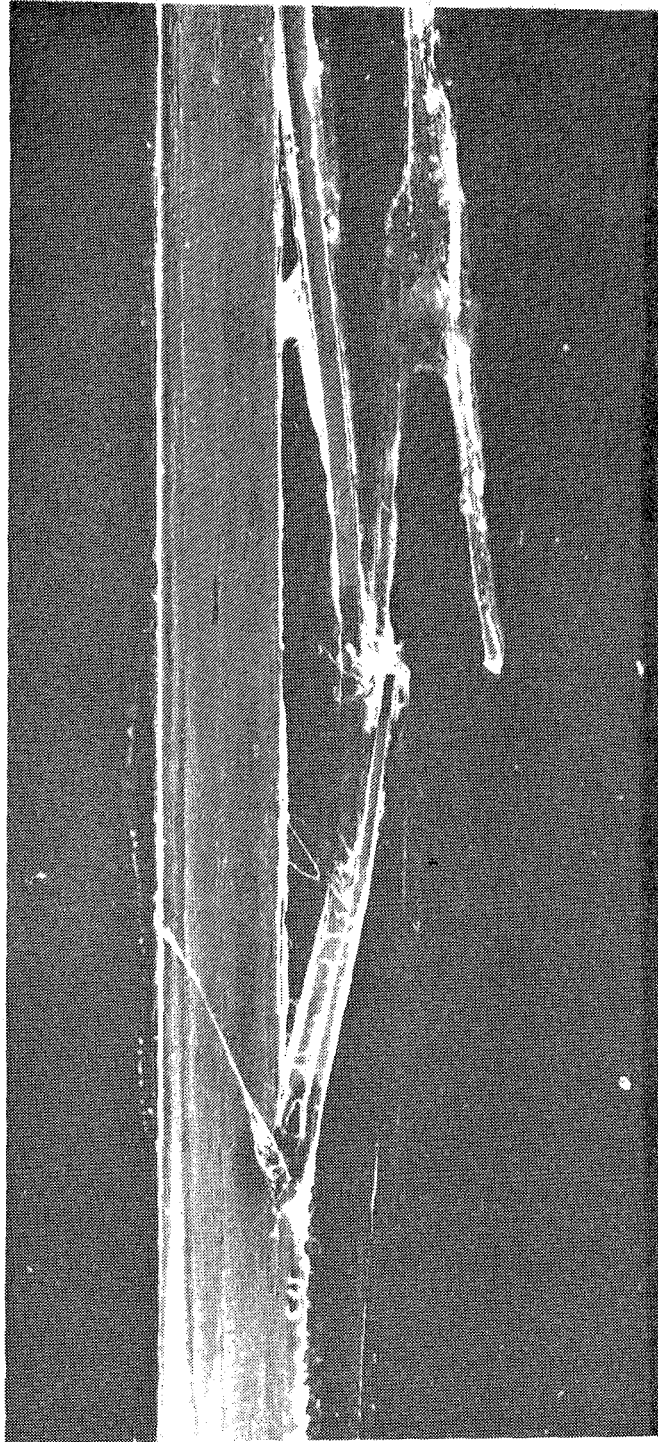
Figure 26 Edge Replica of FU7-16 Plies at 23,000 cycles,
$[45/0/-45/90]_{ns}$
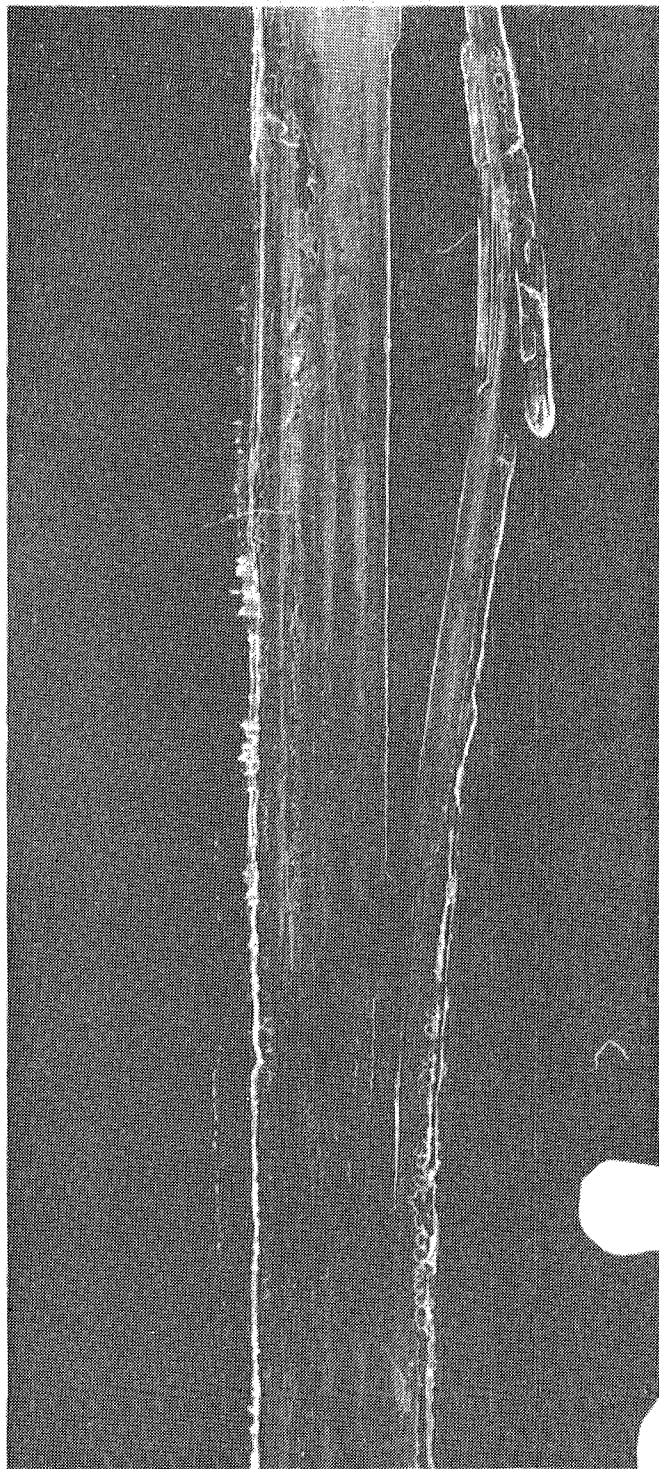
Figure 27   Edge Replica of FU17-16 plies at 15,000 cycles,
[90/45/0/-45]$_{ns}$
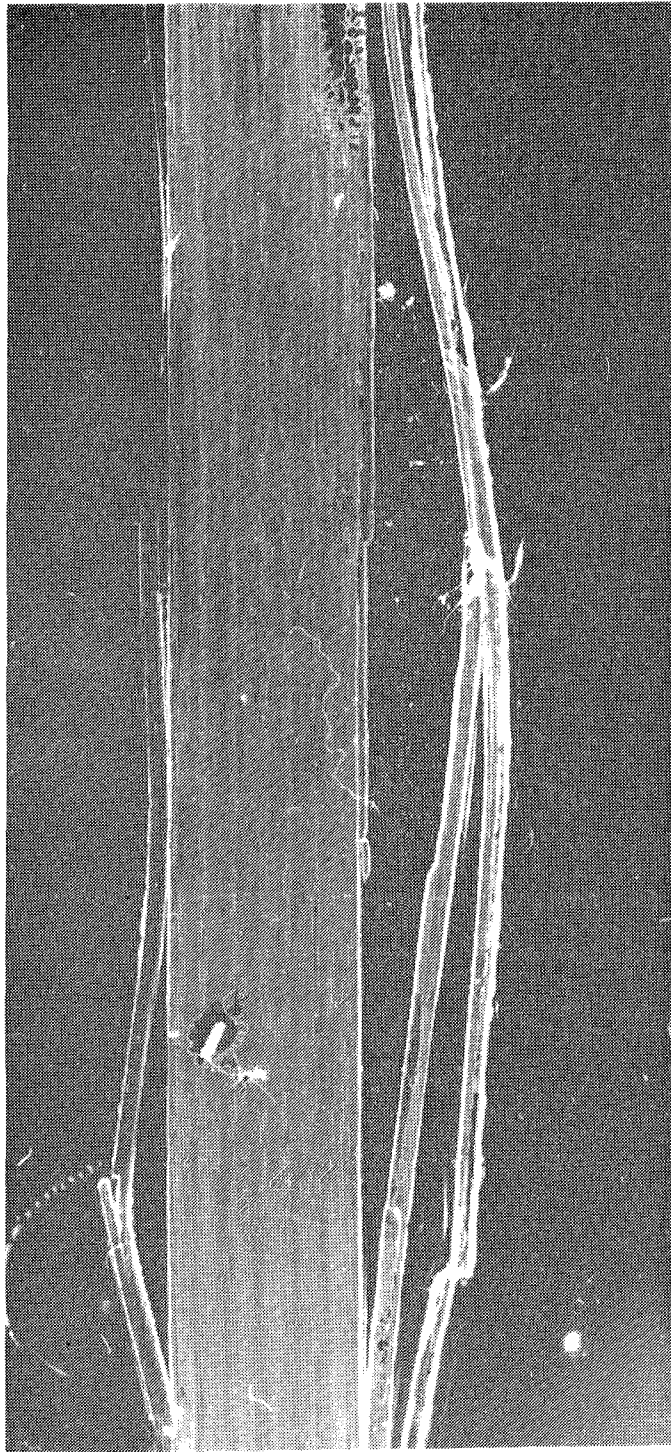
Figure 28   Edge Replica of FU17-32 plies at 681,000 cycles, [90/45/0/-45]$_{ns}$
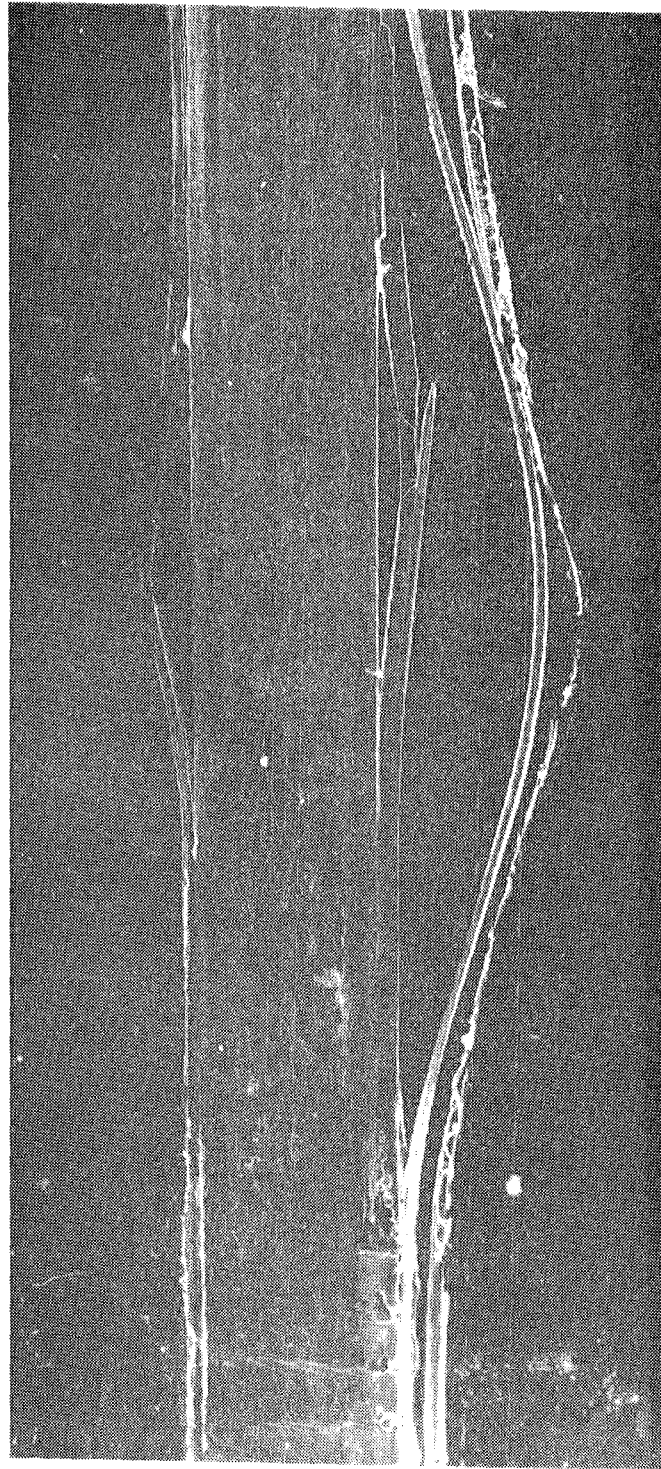
Figure 29   Edge Replica of FU18-32 plies at 700,000 cycles, $[90/45/0/-45]_{ns}$
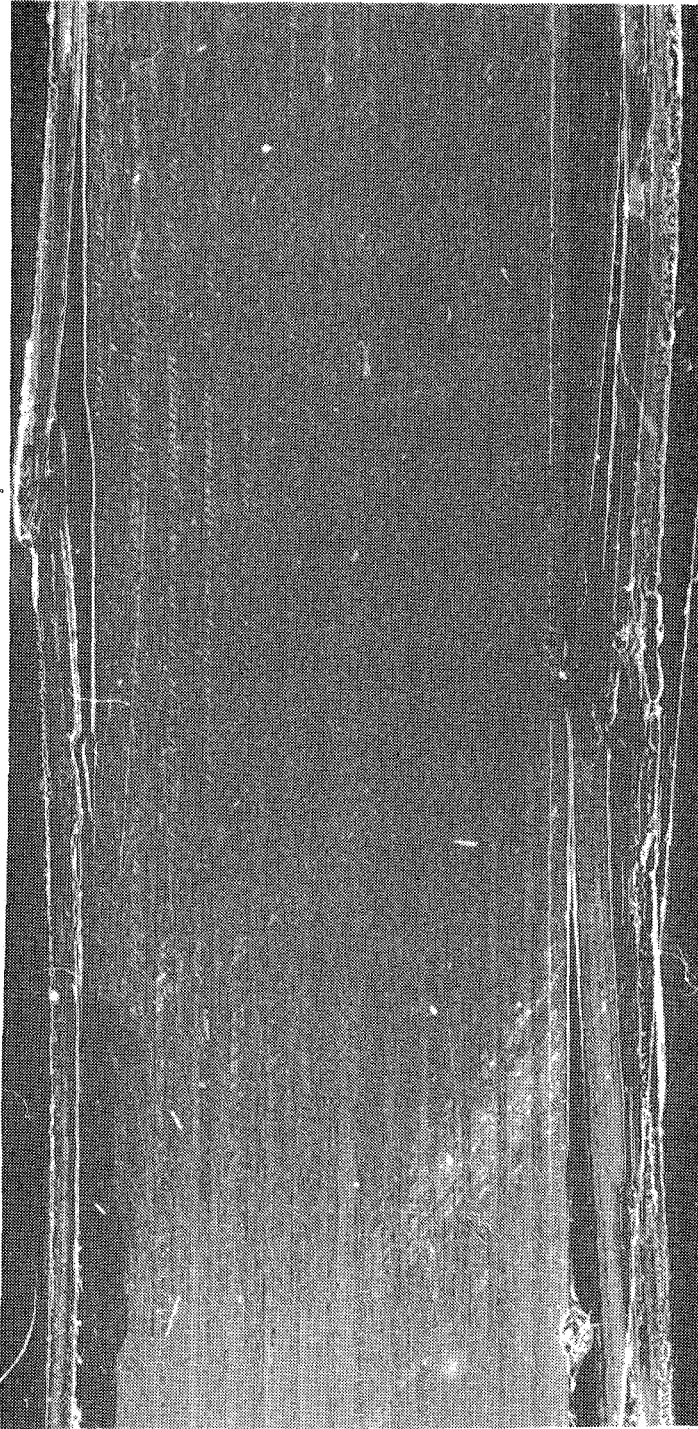
Figure 30   Edge Replica of FU19-64 plies at 342,000 cycles
[90/45/0/-45]$_{ns}$
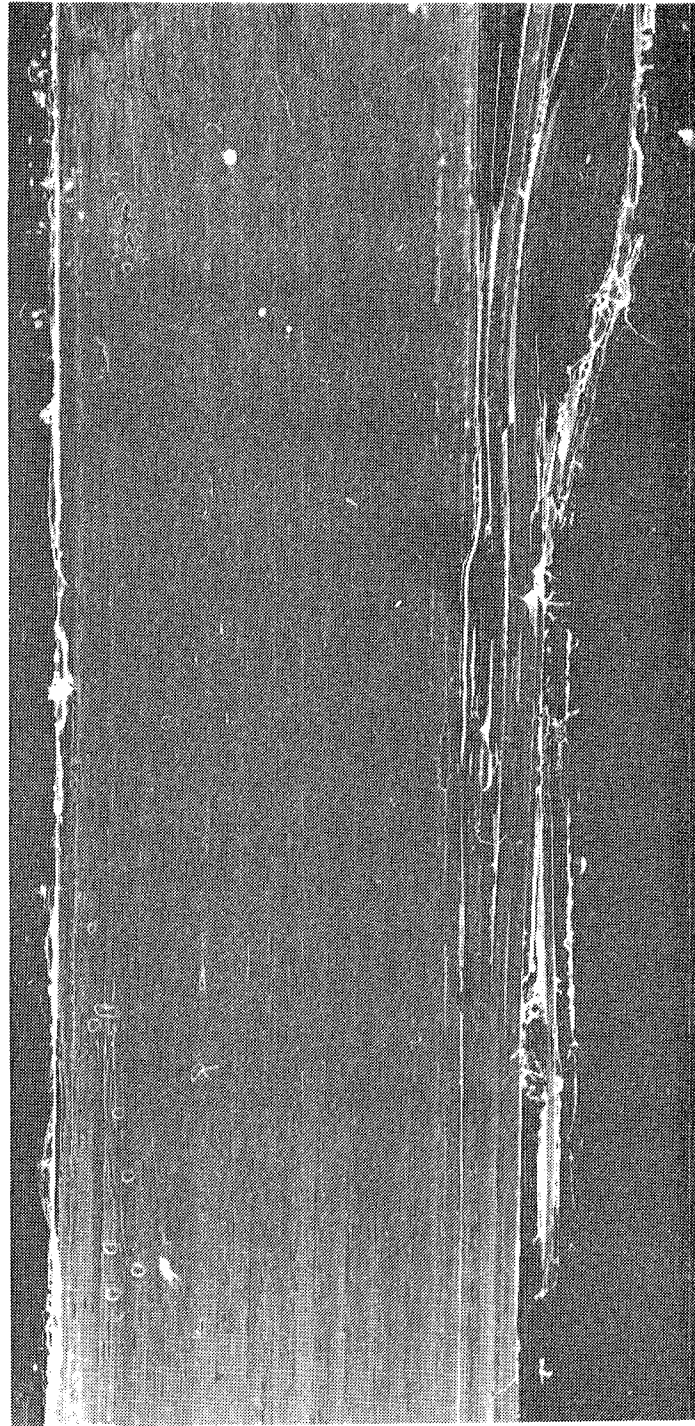
Figure 31   Edge Replica of FU17-64 Plies at 618,000 cycles, $[90/45/0-45]_{ns}$

$[45/0/-45/90]_{ns}$

$[90/45/0/-45]_{ns}$

$[90/45/0/-45]_{ns}$
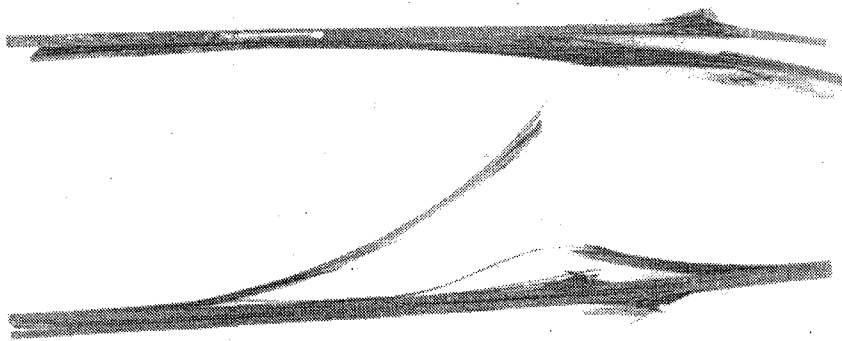
$[45/0/-45/90]_{ns}$

Figure 32   16 and 32 ply Failed, Unnotched Specimens

$[45/0/-45/90]_{ns}$

$[90/45/0/-45]_{ns}$

$[90/45/0/-45]_{ns}$
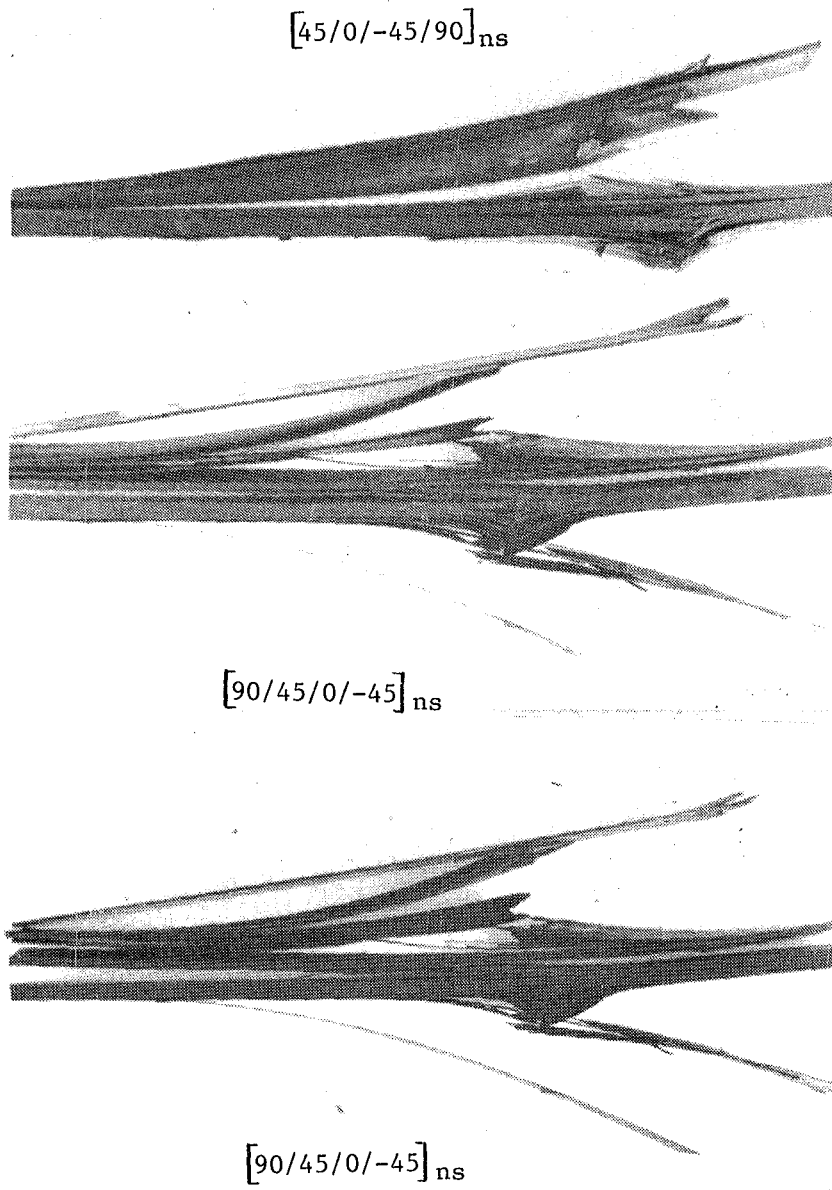
Figure 33   64 ply Failed, Unnotched Specimens
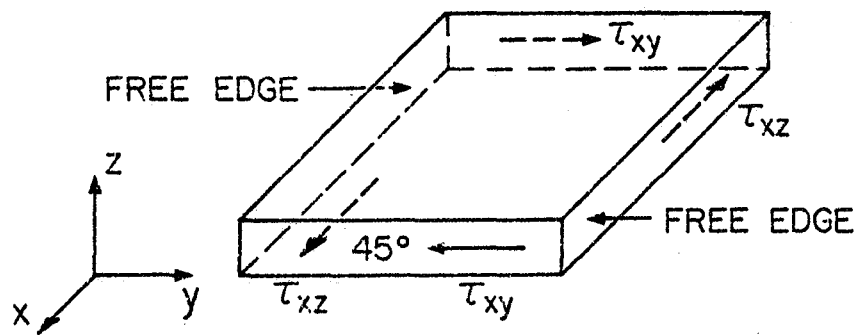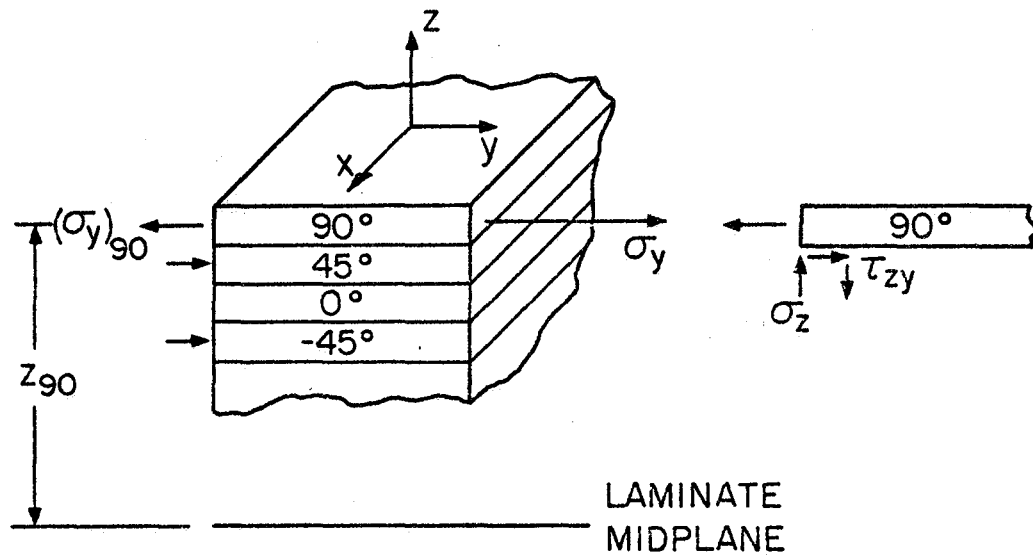
Figure 34   Laminate, Lamina Interlaminar Stress Diagrams
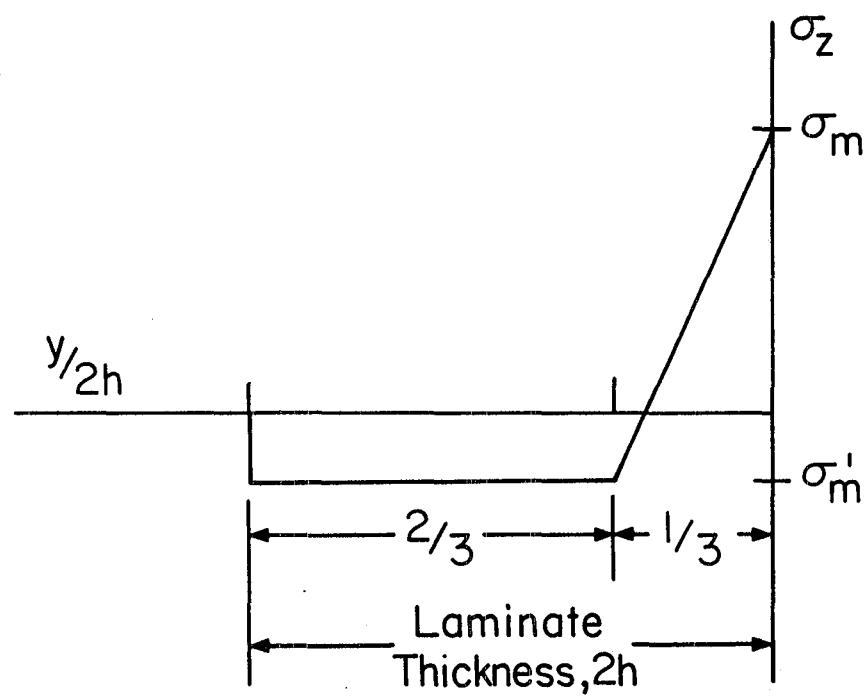
Figure 35   Pipes and Pagano [1] Approximation Model of the
Interlaminar Normal Stress Distribution
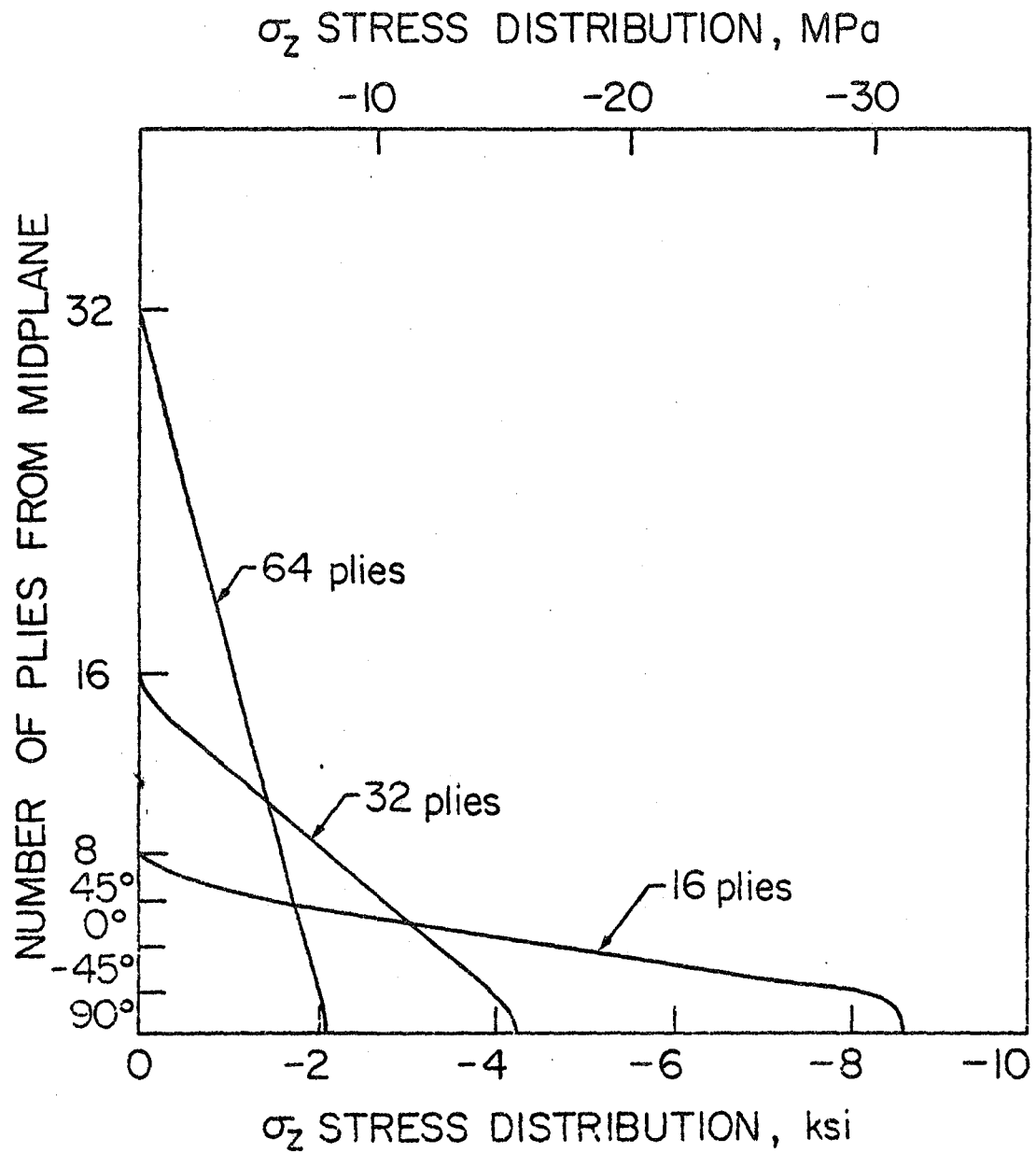
Figure 36 Plot of the Interlaminar Normal Stress at the Free Edge of Laminate $[45/0/-45/90]_{ns}$ for a Nominal Laminate Stress of -60 ksi (-414 MPa)
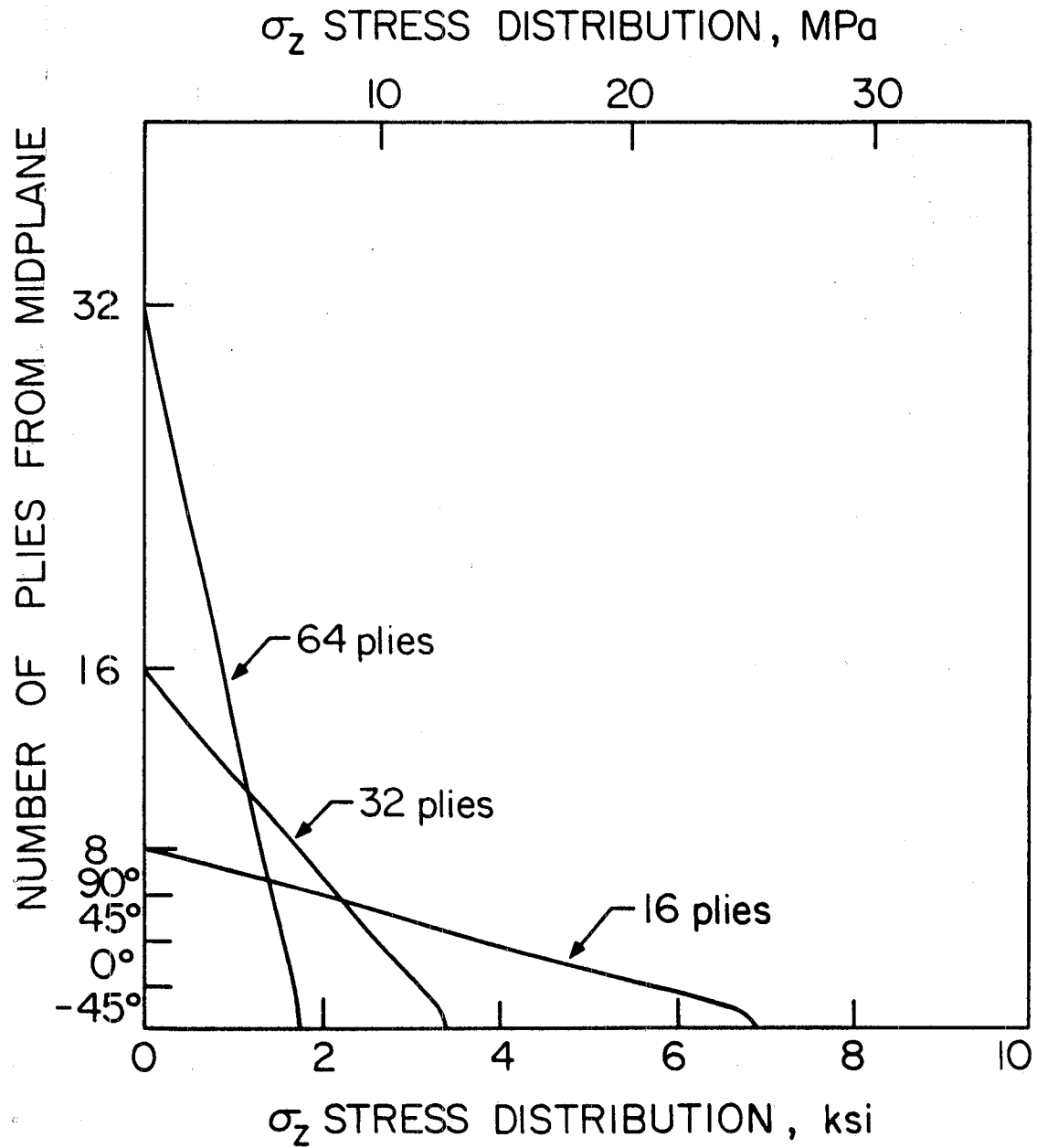
Figure 37 Plot of the Interlaminar Normal Stress at the Free
Edge of Laminate [90/45/0/-45] for a Nominal Laminate
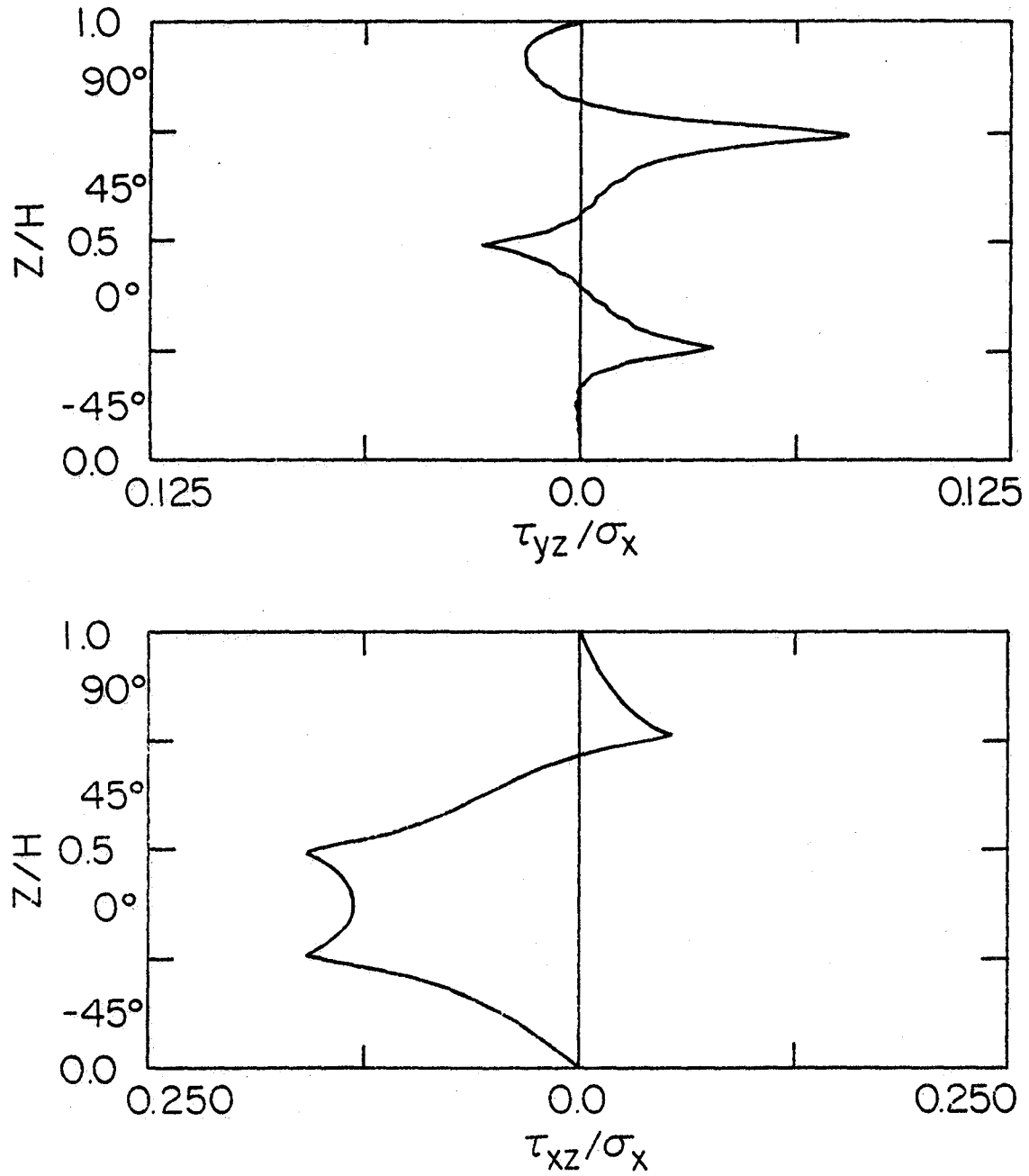Stress of -48 ksi (-331 MPa)

Figure 38   Interlaminar shear stress distributions in a
[90/45/0/-45]$_s$ laminate, graphite-epoxy, by
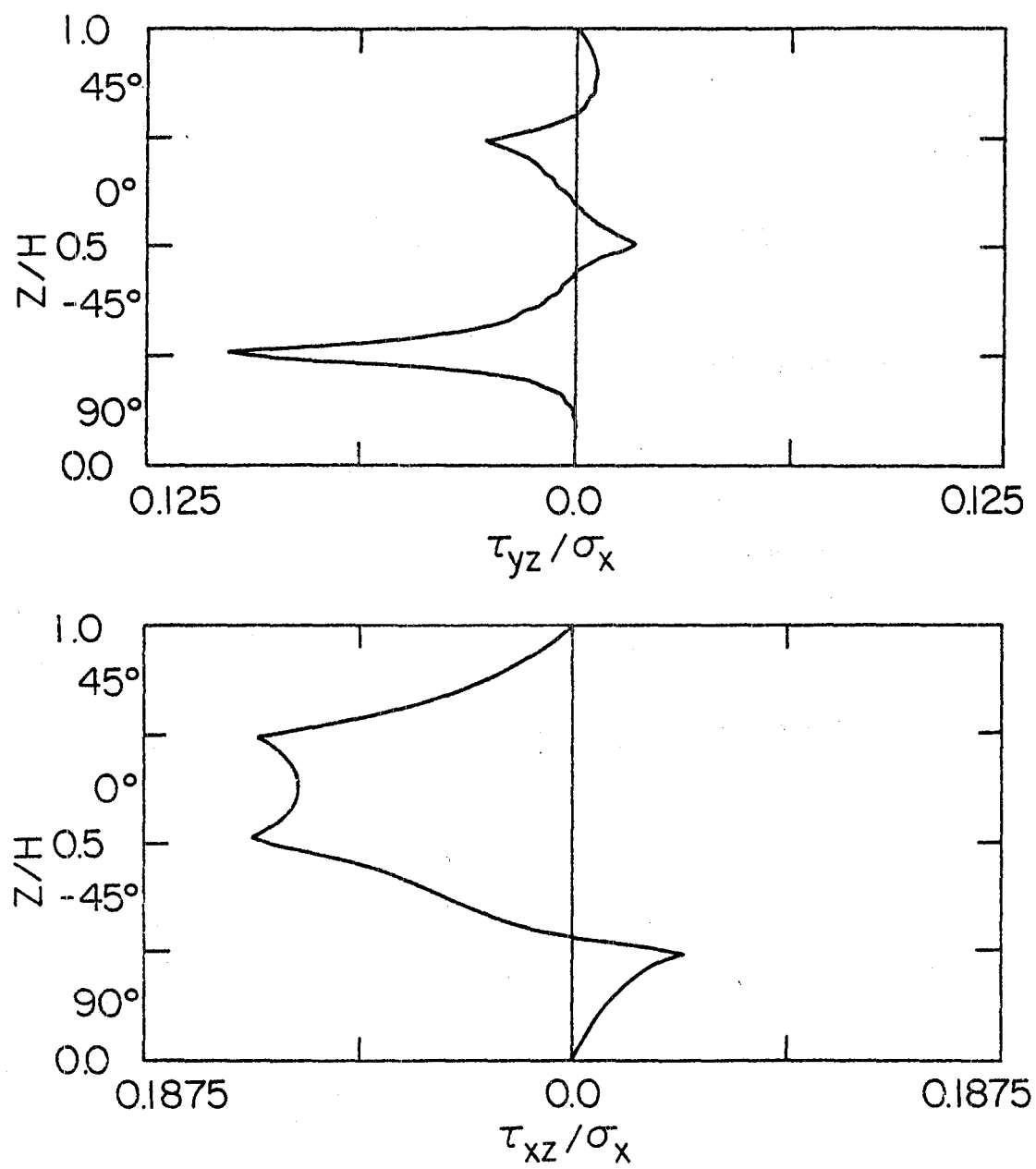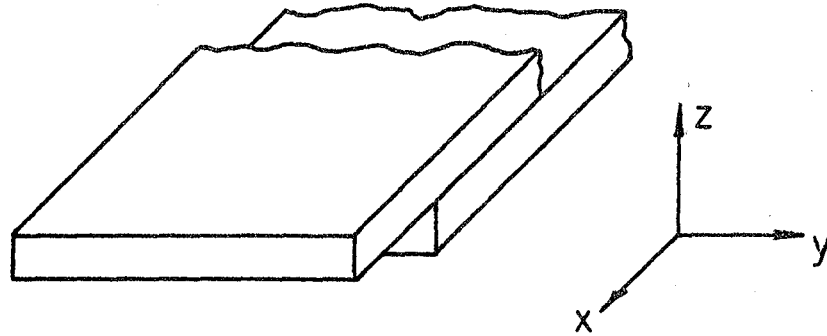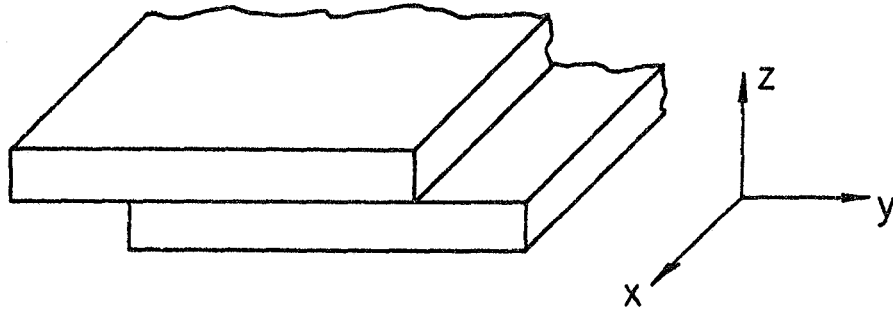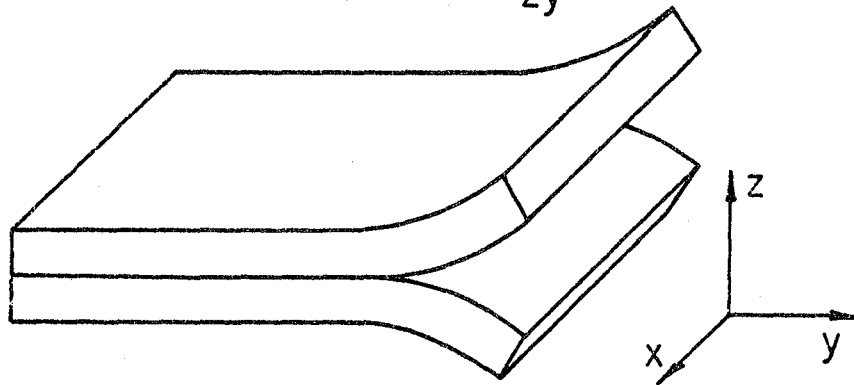Herakovich [2]

Figure 39 Interlaminar shear stress distributions in a
[45/0/-45/90]$_s$ laminate, graphite-epoxy, by
Herakovich [2]

(a) DELAMINATION DUE TO τ_{zx}

(b) DELAMINATION DUE TO τ_{zy}

(c) DELAMINATION DUE TO σ_{zz}

Figure 40   Schematic of the Type of Damage Produced by
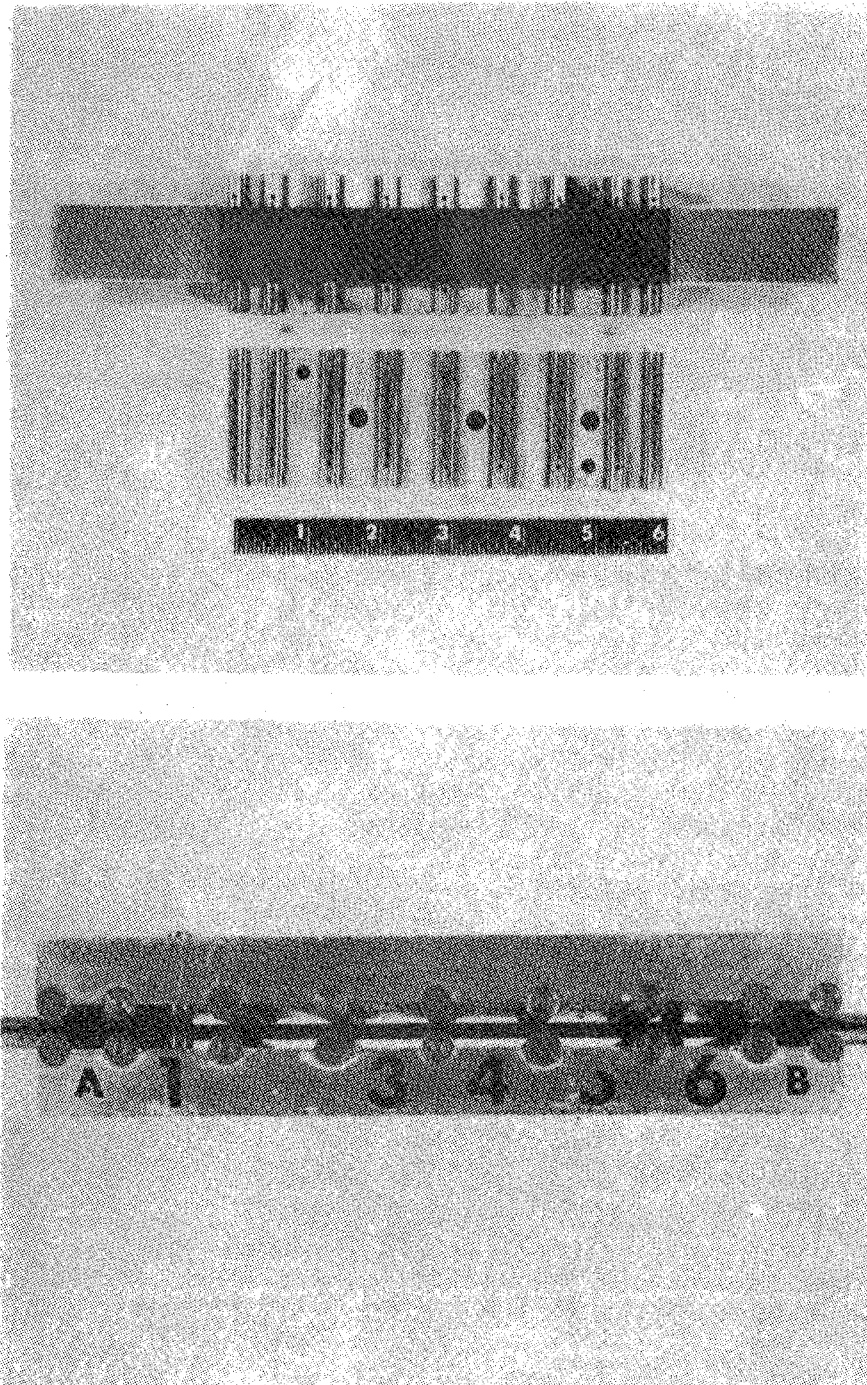Interlaminar stresses.

Figure 41   Fixture Used for Compression-Compression
            Fatigue Loading by Ryder and Lauraitis [8]

1. Report No. NASA CR-172169	2. Government Accession No.	3. Recipient's Catalog No.
4. Title and Subtitle AN EVALUATION OF THE EFFECTS OF STACKING SEQUENCE AND THICKNESS ON THE FATIGUE LIFE OF QUASI-ISOTROPIC GRAPHITE/EPOXY LAMINATES		5. Report Date April 1983
		6. Performing Organization Code
7. Author(s) C. E. Harris and D. H. Morris		8. Performing Organization Report No. VPI-E-83-16
		10. Work Unit No.
9. Performing Organization Name and Address Virginia Polytechnic Institute and State University College of Engineering Blacksburg, VA 24061		11. Contract or Grant No. NAG1-264
		13. Type of Report and Period Covered Contractor Report
12. Sponsoring Agency Name and Address National Aeronautics and Space Administration Washington, DC 20546		14. Sponsoring Agency Code

15. Supplementary Notes

Langley technical monitor: E. P. Phillips

16. Abstract

A test program has been conducted in which the effect of specimen thickness on the fatigue lives of quasi-isotropic, graphite/epoxy laminates was investigated. Notched and unnotched geometries at 16, 32, and 64 ply thicknesses of a $[90/45/0/-45]_{ns}$ laminate and a $[45/0/-45/90]_{ns}$ laminate were tested in compression-compression fatigue. The fatigue life and the initiation, type, and progression of damage were determined in each test. Specially designed antibuckling fixtures were utilized to prevent specimen out-of-plane motion. Interlaminar stresses were generated at straight, free edges of axially loaded laminates; these stresses were used to interpret the test results.

The fatigue lives of the notched specimens did not appear to be a strong function of laminate stacking sequence or specimen thickness. The stress concentration at the hole dominated over the interlaminar stresses at the straight free edge. The unnotched specimens of the $[90/45/0/-45]_{ns}$ laminate with tensile interlaminar normal stresses delaminated more readily than did the $[45/0/-45/90]_{ns}$ laminate with compressive interlaminar normal stress. The life of the 16 ply unnotched specimens was lower than was the life of the 32 and 64 ply specimens. Delaminations were located at the interface where the maximum τ_{xz} shear stress occurred regardless of the sense or magnitude of the interlaminar normal stress. Finally, the antibuckling fixture was found to be effective in preventing out-of-plane motion without overconstraining the specimen.

17. Key Words (Suggested by Author(s)) Composite Fatigue Thickness Stacking sequence Graphite/epoxy	18. Distribution Statement Unclassified - Unlimited Subject Category 39

19. Security Classif. (of this report) Unclassified	20. Security Classif. (of this page) Unclassified	21. No. of Pages 111	22. Price A06

End of Document